Accept-reject decision-making revealed via a quantitative and ethological study of *C. elegans* foraging

Authors: Jessica A. Haley[1,2], Tianyi Chen[2], Mikio Aoi[3,4]*, and Sreekanth H. Chalasani[2]**[Lead Contact]

Affiliations:

[1] Neurosciences Graduate Program, University of California San Diego, La Jolla, CA, USA.

[2] Molecular Neurobiology Laboratory, Salk Institute for Biological Studies, La Jolla, CA, USA.

[3] Halıcıoğlu Data Science Institute, University of California San Diego, La Jolla, CA, USA.

[4] Department of Neurobiology, University of California San Diego, La Jolla, CA, USA.

*Correspondence: maoi@ucsd.edu

**Correspondence: schalasani@salk.edu

ORCID: 0000-0001-6282-7124 (J.A.H), 0009-0003-7572-2155 (T.C.), 0000-0002-7052-880X (M.A.), 0000-0003-2522-8338 (S.H.C.)

Abstract

Decision-making is a ubiquitous component of animal behavior that is often studied in the context of foraging. Foragers make a series of decisions while locating food (food search), choosing between food types (diet or patch choice), and allocating time spent within patches of food (patch-leaving). Here, we introduce a framework for investigating foraging decisions using detailed analysis of individual behavior and quantitative modeling in the nematode *Caenorhabditis elegans*. We demonstrate that *C. elegans* make *accept-reject* patch choice decisions upon encounter with food. Specifically, we show that when foraging amongst small, dispersed, and dilute patches of bacteria, *C. elegans* initially *reject* several bacterial patches, opting to prioritize exploration of the environment, before switching to a more exploitatory foraging strategy during subsequent encounters. Observed across a range of bacterial patch densities, sizes, and distributions, we use a quantitative model to show that this decision to *explore* or *exploit* is guided by available sensory information, internal satiety signals, and learned environmental statistics related to the bacterial density of recently encountered and *exploited* patches. We behaviorally validated model predictions on animals that had been food-

deprived, animals foraging in environments with multiple patch densities, and null mutants with defective sensory modalities. Broadly, we present a framework to study ecologically relevant foraging decisions that could guide future investigations into the cellular and molecular mechanisms underlying decision-making.

Keywords

decision-making, foraging, exploration, exploitation, dietary choice, *C. elegans*, quantitative modeling

Introduction

Decision-making is frequently defined as the selection of a course of action among several alternatives. The ubiquity and importance of decision-making has led to its use in describing a broad range of behaviors from taxes of unicellular organisms to economics and politics in human society [1, 2]. In decision neuroscience, laboratory experiments have investigated the behavioral choices of animals in well-controlled environments or tasks [3]. While these experiments have led to key insights into mechanisms underlying decision-making and related cognitive processes [4], a comprehensive understanding of decision-making remains elusive. Many researchers have advocated for a more neuroethological approach – suggesting that experiments designed to understand problems the brain evolved to solve offer a more rigorous framework for investigation [3, 5, 6]. Thus, one approach to enrich our understanding of decision-making is to look at the decisions made by animals foraging in naturalistic environments.

Foraging animals make a hierarchy of decisions to locate food (food search), choose between different food types (diet or patch choice), and allocate time spent within patches of food items (patch-leaving) [5, 7-10]. These foraging decisions often require that an animal *exploit* an environment for known resources or *explore* it for potentially better opportunities elsewhere [9, 11]. This exploration-exploitation trade-off requires cognitive computations such as learning the spatiotemporal distribution of food, route planning, estimation of food availability, and decision-making [12, 13]. According to optimal foraging theory, foragers may seek to maximize their rate of net energy gained over time [8, 9, 14] by using internal and external information to guide decision-making, especially in environments where resources are sparsely distributed or fluctuating. Although many studies have provided insight into the motivations, behavioral implementations, and genes associated with foraging decisions [9, 10], a more rigorous framework for exploring the neuronal mechanisms underlying foraging decisions is essential to establish a comprehensive understanding of decision-making.

The microscopic nematode *Caenorhabditis elegans* is well suited for investigating the cellular and molecular basis of foraging decisions [15]. A myriad of genetic tools, behavioral assays, and neuronal imaging techniques have been developed to take advantage of the species' quick reproductive cycle, isogeneity, optical transparency, and ease of maintenance [16-18]. While *C. elegans* typically feed upon a diversity of bacterial types in the wild [19], they are commonly maintained in the laboratory on agar plates containing large patches of the bacteria *Escherichia coli* as a food source

[16]. However, even in these simplified laboratory conditions and despite having a numerically simple nervous system of only 302 neurons [16, 20], *C. elegans* display complex and robust species-typical behaviors [21] involving learning and memory [22-25], and decision-making [26-31]. Recent studies have demonstrated that ecologically focused environmental enrichment permits identification of novel behaviors and gene functions in *C. elegans* and other animals [32-35].

Foraging animals often must make one of two types of decisions: *stay-switch* or *accept-reject*. *Stay-switch* decisions refer to scenarios where an individual experiences diminishing returns with the current action and must decide when to switch to a new action (e.g., patch-leaving and area-restricted search) [5, 7-10]. In contrast, *accept-reject* decisions refer to situations where an individual must decide between engaging with an option or ignoring it in search of a better one (e.g., diet or patch choice) [5, 8, 9]. *Stay-switch* decisions have been well described in *C. elegans* [25, 26, 36-41] and enable them to successfully explore an environment and exploit the bacteria within [28, 42-44]. However, to our knowledge, *accept-reject* decisions have not yet been demonstrated in *C. elegans*. While *C. elegans* have been shown to alter food preferences in a diet choice assay, this behavior has only been described by a set of *stay-switch* decisions [31, 36, 44]. The ability to make *accept-reject* decisions is likely advantageous for foraging in fluctuating or variable environments as rejecting an encountered food item of low quality creates the opportunity for a subsequent encounter with preferred food. Thus, while *C. elegans* can successfully forage in patchily distributed environments, it is not known whether *C. elegans* make decisions to *exploit* a patch of food upon encounter and how this decision-making process changes over a series of patch encounters.

In this study, we aimed to identify if *C. elegans* make *accept-reject* decisions upon encounter with bacterial patches. To answer this question, we performed a detailed analysis of the behavior of individual animals foraging in an ecologically inspired environment where bacterial patches were dilute and dispersed. In conditions where the bacterial density was much lower than that of previously visited patches, animals first explored the environment before *accepting* patches for exploitation. This explore-then-exploit strategy persists even when only one bacterial patch is present in the environment. Using a theoretical framework, we found that this initial exploration reflects a series of *accept-reject* decisions guided by signals related to the bacterial density of current and recently *explored* and *exploited* patches as well as the animal's state of satiety.

Results

103 ***C. elegans* forage in patchy environments with an explore-then-exploit strategy**

104 To investigate whether *C. elegans* make *accept-reject* decisions upon encounter with bacterial
105 patches, we observed the behavior of animals foraging on an agar surface containing an isometric
106 grid of small, low density bacterial patches (Figure 1A, Video 1-2). Animals were confined to an
107 arena where their behavior was recorded and tracked for 60 minutes (Figure 1A, Figure 1 –
108 supplement 1, Video 3). During this time, animals were observed to move about the arena (Figure
109 1A-C, Figure 1 – supplement 2, Video 4) with each animal encountering, on average, ~8.4 total
110 patches and ~5.3 unique patches during the one-hour recording (Figure 1D). These patch
111 encounters ranged in duration from seconds to tens of minutes and could be classified as either
112 short or long (2+ minutes) using a Gaussian mixture model (Figure 1E, Figure 1 – supplement 3).
113 Notably, animals were significantly more likely to stay on patch for longer durations at later time
114 points (Figure 1F) which corresponded to an overall increase in their probability of residing on
115 patch (Figure 1G, Figure 1 – supplement 4). Specifically, we found that while animals initially resided
116 on bacterial patches at levels close to those predicted by chance, an animal's probability of residing
117 on a bacterial patch increased significantly after ~10 minutes. These findings, that patch duration
118 and residence increased over time, suggest that animals are more likely to exploit an encountered
119 patch as time goes on.

120 Given that the bacterial density of the experimental patches was approximately 20 times
121 more dilute than that of conditions animals experienced during development and immediately
122 preceding the assay, it was possible that the initial delay in exploitation could be due to animals'
123 inability to detect the presence of bacteria in these more dilute patches. We therefore set out to
124 determine if animals detected patches at all time points. Previous studies have shown that *C. elegans*
125 display an immediate and marked slowdown upon encounter with the edge of a food patch and
126 sustain these slower speeds on food [28, 45]. Therefore, velocity can be used as a proxy for an
127 animal's ability to sense a bacterial patch. Following this precedent, we quantified the instantaneous
128 velocity of individuals in our assay (Figure 1H). We observed significant deceleration of an animal's
129 instantaneous velocity upon encounter with the patch edge (Figure 1I), with no obvious difference
130 between short duration, early time point (Figure 1J) and long duration, late time point (Figure 1K)
131 encounters. Animals consistently displayed marked slowdown when approaching the patch edge
132 (Figure 1L), achieving an average deceleration of -19.5 $\mu m/s^2$ upon encounter with the bacterial
133 patch (Figure 1M, Figure 1 – supplement 5). This slowdown was statistically significant for both long
134 and short duration encounters (Figure 1M). Further, consistent with *C. elegans* behavior on larger and

135 more densely seeded patches in other studies [46], animals in our assay maintained significantly lower
136 average velocities on patch (~52 μm/s) compared to off patch (~198 μm/s) (Figure 1N,O). These
137 results suggest that, despite detecting the availability of food during early patch encounters, *C. elegans*
138 opt to initially prioritize exploration of the environment before switching to a more exploitatory
139 foraging strategy during subsequent patch encounters.
140

141 **The timing of the switch from exploration to exploitation varies with bacterial density**

142 To determine whether this explore-then-exploit foraging strategy is dependent upon food-
143 related characteristics of the environment, we varied the density of the bacterial patches. By diluting
144 bacterial stocks and controlling growth time, we created 12 bacterial density conditions with relative
145 density ranging from 0 to ~200 (Figure 2A, Figure 2 – supplement 1-3). At the low end of this range
146 (densities less than ~0.5), animals do not appear to detect bacterial patches as indicated by on-patch
147 velocities matching those of animals foraging on bacteria-free (density 0) patches (Figure 2B,C). At
148 the high end of the range (density ~200), bacterial density is comparable to the environments
149 animals experienced during development and immediately prior to the assay (Figure 2 – supplement
150 2-3).

151 Previous studies have shown that in diet choice assays where animals are given the option
152 between patches of varying quality or density, animals spend more time on preferred patches [31, 36,
153 44]. We hypothesized that even when all patches in the environment are of equal density, an efficient
154 forager should still modulate the amount of time spent on the bacterial patches in a density-
155 dependent manner. To test this, behavior was recorded and tracked for one hour as animals foraged
156 in patchy environments matching one of the bacterial density conditions (Figure 2D, Figure 2 –
157 supplement 4). Consistent with our hypothesis, we found that the total time animals spent on
158 bacterial patches increased monotonically with increasing bacterial density following a sigmoidal
159 trend (Figure 2E). Further, the probability of an animal residing on patch as a function of time was
160 highly dependent on the bacterial density (Figure 2F, Figure 2 – supplement 5). At the highest
161 densities (50 and 200), animals spent nearly 100% of time in the assay on bacterial patches, while at
162 the lowest densities (0 to 0.3), animals spent chance levels of time on patch for the duration of the
163 experiment. At intermediate densities (0.5 to 10) animals initially resided on patches at rates
164 predicted by chance, later transitioning to more time spent on patch. Notably, this delayed increase
165 in patch residence is density dependent with animals switching earlier in environments with patches
166 of greater density.

167 Consistent with our previous observation that animals reside on patches for either short or
168 long durations (Figure 1E), we observed two distinct patch encounter types: 1) short (less than 2
169 minute) patch visits and 2) long (often tens of minutes) patch visits (Figure 2G). We validated the
170 existence of two patch types using Silverman's test [47, 48] for bi-modality (Figure 2 – supplement
171 6) and then, using a two-component Gaussian mixture model (GMM), classified all encounters
172 based on the duration of these patch visits and animals' average velocity during the encounter
173 (Figure 2H, Figure 2 – supplement 6). We identified two behaviorally distinct clusters: 1) short
174 duration and fast velocity (*explore*), and 2) long duration and slow velocity (*exploit*) encounters. The
175 *explore* encounters suggest that an animal has *rejected* a patch, opting to continue exploration of the
176 environment. In contrast, the *exploit* encounters suggest that an animal has *accepted* a patch and is
177 consuming the bacteria within.
178 While we previously found that animals consistently slowed down upon encounter with the
179 patch edge when foraging in relative density ~10 (Figure 1J-M), we observed that a large portion of
180 short duration, exploratory encounters were not accompanied by this slow down (Figure 2 –
181 supplement 7A-B), especially for the lowest bacterial densities tested. Therefore, to determine which
182 exploratory encounters displayed evidence that the patch was detected by the animal, we further
183 classified encounters by an animal's minimum velocity on patch, deceleration upon patch entry, and
184 maximum change in the animal's velocity upon encounter (i.e., the difference between the peak
185 velocity immediately before the patch encounter and the minimum velocity achieved during the
186 patch encounter) (Figure 2I, Figure 2 – supplement 7). We again observed two behaviorally distinct
187 clusters: 1) large slow-down and slow on-patch velocity, and 2) small slow-down and fast on-patch
188 velocity. We validated the existence of these two clusters using Silverman's test [47, 48] for bi-
189 modality (Figure 2 – supplement 7) and then classified these encounters as *sensing* or *non-responding*,
190 respectively, using a semi-supervised quadratic discriminant analysis (QDA) approach (Figure 2 –
191 supplement 8, Video 5). The presence of a slowdown and the subsequent continuation of slower
192 on-patch velocity suggest that an animal sensed the bacteria, while the absence of a slowdown
193 response suggests that the animal either did not perceive the encounter or chose to ignore it. For
194 simplicity, we define: 1) *non-responding* encounters as *searching* (i.e., on-patch behavior that matches
195 off-patch behavior where an animal appears to be searching for food); 2) *sensing*, short duration
196 encounters as *sampling* (i.e., evaluating a patch's suitability as a food source, but ultimately *rejecting* the
197 patch and continuing to explore the environment); and 3) *sensing*, long duration encounters as
198 *exploiting* (i.e., *accepting* a patch and consuming its bacteria) (Figure 2J). Consistent with our

interpretation of *searching* encounters, the average velocities that animals achieved during *search* on (~200 μm/s) and off (~207 μm/s) patch were similar, especially when compared to markedly slower on-patch velocities during *sample* (~114 μm/s) and *exploit* (~57 μm/s) encounters (Figure 2K). In summary, we have identified three distinct patch encounter types: encounters lacking a slowdown that were either not detected or ignored (*search*) and encounters that were detected with the animal subsequently deciding to *reject* (*sample*) or *accept* (*exploit*) the patch.

We next characterized how the frequency of encounter types varied as a function of time and patch density. The behavior of 443 animals (20-50 worms per condition) was tracked and classified at each time point (Figure 2L, Video 6). In low density conditions (0 to 0.3), animals spent nearly all of their time *searching* on or off patch. With increasing bacterial patch density, animals spent less time *searching* and more time *sampling* and *exploiting*. Animals foraging in medium density patches (0.5 to 10) initially spent most of their time *sampling* patches upon encounter. However, animals eventually switched to mostly *exploiting* patches. Animals foraging on high density patches (50 and 200) almost exclusively *exploited*. Classification of on-patch behavior across all densities tested revealed a consistent switch from *exploratory* behaviors (*searching* and *sampling*) to *exploitation* (Figure 2M) with the timing of the switch occurring earlier for animals foraging in environments with higher bacterial patch density (Figure 2N). The delay in exploitation corresponded to a comparatively large number of initial exploratory encounters with animals on medium density conditions (0.5 to 10) *exploiting* after an average of 4.8 to 18.7 exploratory encounters (Figure 2O). To summarize, for densities similar to those experienced immediately preceding the experiment (50 and 200), animals immediately *exploit* available bacteria. On the other hand, for bacterial densities that appear to be below an animal's sensory threshold (0 to 0.3), animals never *exploit* patches and spend the entire 60-minute assay *searching* for food. When foraging in medium density patches (0.5 to 10), animals initially explore the environment via a combination of *searching* and *sampling* encounters and eventually switch to *exploiting*. Notably, the timing of this switch is density-dependent with animals switching earlier when foraging on higher density patches.

Animals explore before exploiting even when only one patch is available

Given that bacterial patches within an environment were relatively invariable and that bacterial growth during the experiment was negligible (Figure 2 – supplement 3), it was surprising that animals were often willing to *reject* 10+ patches before *exploiting* a patch of the same density as those previously *rejected* (Figure 2O). This *sampling* behavior may be beneficial when food is patchily

231 distributed in the environment as exploiting a dilute patch may result in a lost opportunity for future
232 encounter with a higher quality patch. Thus, we hypothesized that an animal's willingness to *accept* a
233 patch whose density matched that of a previously *rejected* patch could be a specific feature of a
234 patchily distributed environment where numerous observations of individual patches could
235 contribute to learning the features of a changing environment. To address this, we observed whether
236 animals were willing to *reject* a patch numerous times before *accepting* it even when only one patch is
237 available in the environment. We created environments with single large (~8.3 mm) or small (~1.8
238 mm) diameter patches with relative density ranging from 0 to ~400 (Figure 3A-C). Behavior was
239 tracked for 60 minutes as animals foraged in these environments (Figure 3D-E, Figure 3 –
240 supplement 1-2). We found that even in these single patch environments, animals initially *explore*
241 (*search* and *sample*) before *exploiting* (Figure 3F-G) in a density-dependent manner. Just as when
242 foraging in a patchily distributed environment (Figure 2N), animals *explored* (*search* and *sample*) the
243 small and large single patches numerous times prior to *exploiting* with the timing of this switch
244 occurring significantly earlier with increasing bacterial density (Figure 3H-I). These results suggest
245 that the explore-then-exploit strategy employed by *C. elegans* is not specific to a patchily distributed
246 environment. Rather, animals may *sample* the same patch numerous times before deciding to *exploit*,
247 especially when foraging on dilute patches. The decision of when to stop *exploring* and start *exploiting*
248 is highly dependent upon the density of bacteria within a patch with the switch occurring earlier
249 when animals encounter patches of higher density.
250

251 **External and internal sensory information guide the decision to explore or exploit**

252 While our behavioral analysis demonstrated that *C. elegans* modulate their decision to *explore*
253 or *exploit* in a density-dependent manner, it remains unclear whether these animals use more
254 complex cognitive processes such as learning and memory to guide their foraging decision. It is
255 plausible that animals are making decisions using simple heuristics given only available sensory
256 information about the current patch. However, previous studies have shown that food-related
257 behaviors in *C. elegans* can be driven by internal states [31] as well as memories of the environment
258 [25, 36, 42]. Thus, to better understand the factors driving the exploitation decision, we implemented
259 a generalized linear model (GLM) to test how foraging decisions are influenced by the density of the
260 current patch as well as additional food-related factors such as an animal's level of satiety and prior
261 experience (Figure 4A).

We considered that the probability of exploiting a patch upon any given encounter can be described by a logistic function:

$$p(y_k = 1|\boldsymbol{\beta} \cdot \boldsymbol{x}_k) = \frac{1}{1 + e^{-\boldsymbol{\beta} \cdot \boldsymbol{x}_k}}$$

where $p(y_k = 1|\boldsymbol{\beta} \cdot \boldsymbol{x}_k)$ represents the conditional probability that an animal exploited during patch encounter k; $\boldsymbol{x}_k \in R^n$ is a vector of covariates; and $\boldsymbol{\beta} \in R^n$ is a vector of weights that describes how much each covariate influences the animal's choice. In models compared here, $\boldsymbol{x}_k$ includes a combination of a constant element and covariates that may empirically influence the decision to *exploit*. We considered the simplest model where every encounter is independent with fixed probability of *exploiting* (i.e., $p(y_k = 1|\beta_0)$) where β_0 represents the average animal's propensity to *exploit*. We compared this null model against a set of nested models containing covariates that vary from encounter to encounter and relate to: 1) the relative density of the encountered patch k (ρ_k), 2) the duration of time spent off food since departing the last *exploited* patch (τ_s), 3) the relative density of the patch encountered immediately before encounter k (ρ_h), and 4) the relative density of the last *exploited* patch (ρ_e). Using this model design (i.e., $\boldsymbol{\beta} \cdot \boldsymbol{x}_k = \beta_0 + \beta_k \rho_k + \beta_s \tau_s + \beta_h \rho_h + \beta_e \rho_e$), we assessed how each of these covariates influences the probability of *exploitation* at each patch encounter k (Figure 4A).

Given that our aim is to understand what factors influence an animal's decision to *explore* or *exploit*, we rationalized that encounters where the animal did not detect the presence of bacteria were unlikely to contribute to decision-making. Therefore, we excluded *searching* encounters from our analysis where animals did *not respond* to the bacterial patch. To account for the uncertainty in our classification of *sensing*, we probabilistically included patch encounters with frequency equal to the probability that the bacterial patch was *sensed* (Figure 4B) as previously estimated by semi-supervised QDA (Figure 2I, Figure 2 – supplement 8). In doing so, we simulated sets of observations of *sensed* (*sample* and *exploit*) encounters. Further, to account for the uncertainty in our classification of patch encounters as *exploration* or *exploitation*, we fit our GLM to the probability of *exploiting* $p(y_k = 1|\boldsymbol{z}_k)$ as previously estimated by GMM (Figure 2H, Figure 2 – supplement 6) rather than fitting to direct observations of exploitation y_k (see Models of exploitation probability).

When selecting covariates for our model, we calculated the Bayesian information criterion (BIC) – a model selection test to avoid overfitting by penalizing increases in the number of parameters – and observed the best model performance when all covariates were included (Figure 4

– supplement 1A-B). Further, we found that all covariates (i.e., ρ_k, τ_s, ρ_h, and ρ_e) significantly contribute to the decision to *exploit* $p(y_k = 1|\boldsymbol{\beta} \cdot \boldsymbol{x}_k)$ as indicated by coefficient values significantly greater than or less than zero (Figure 4C, Figure 4 – supplement 1C). Specifically, we found that β_k and β_s are significantly greater than zero which suggests that animals are more likely to *exploit* patches with increasing patch density ρ_k and duration of food-deprivation τ_s. On the other hand, β_h and β_e are significantly negative, which suggests that the greater the density of a recently encountered or *exploited* patch, ρ_h and ρ_e, the less likely an animal should be willing to *exploit* the current patch.

In order to better understand how each of the covariates in our model affect the *exploitation* decision, we examined the probability of observing *exploitation* for the first time as a function of the cumulative number of patches an animal encountered. Exploitation events were simulated from a Bernoulli distribution with probability estimated by the model (i.e., $y_k|\boldsymbol{x}_k \sim \mathrm{Bern}\big(p(y_k = 1|\boldsymbol{\beta} \cdot \boldsymbol{x}_k)\big)$) or observed from our classification of *exploitation* (i.e., $y_k|\boldsymbol{z}_k \sim \mathrm{Bern}\big(p(y_k = 1|\boldsymbol{z}_k)\big)$). Although the probability of *exploiting* for the first time was not expressly fit by our model, this derived metric highlights the model's ability to predict the delay in *exploitation* observed for animals foraging on low to medium density bacterial patches in our experiments (Figure 4D, Figure 4 – supplement 2). For the simplest model where every encounter is independent with fixed probability of *exploiting* $p(y_k = 1|\beta_0)$, we find that the probability of *exploiting* for the first time is greatest for the first encounter and decreases for every subsequent encounter (Figure 4D, Figure 4 – supplement 2), fitting a geometric distribution.

We next considered whether the observed delay in *exploitation* could be explained by a simple density-dependent model (i.e., $p(y_k = 1|\beta_0 + \beta_k \rho_k)$). This model predicts that animals are more likely to *exploit* bacterial patches of greater density with probability proportional to the relative density of the current patch ρ_k. While this density-dependent model accurately predicted that the first *exploitation* occurs earlier on average for higher density patches, it also predicted that, regardless of patch density, the first *exploitation* is most frequently observed on the first encounter which did not match the observed distribution (Figure 4D, Figure 4 – supplement 2). We subsequently considered that the onset of food-deprivation during *exploration* of these low-density environments could drive the observed time-dependent delay in *exploitation*. We assume that animals become satiated during *exploitation* and use the duration of time an animal spent searching off-food since the last *exploitation* event (i.e., τ_s) as a proxy for the animal's likely decrease in satiety. With the addition

322 of this satiety-related signal (i.e., $p(y_k = 1|\beta_0 + \beta_k\rho_k + \beta_s\tau_s)$), we observed a slight delay in when
323 animals are predicted to first *exploit* for the lowest density conditions tested (Figure 4D, Figure 4 –
324 supplement 2). To validate our finding that animals use a satiety-related signal to inform decision
325 making, we applied our model to observations of animals foraging in patchily distributed
326 environments following 3 hours of food-deprivation (Figure 4 – supplement 3A-B). We found that
327 only with the inclusion of a satiety-related covariate in our model, were we able to reliably predict
328 the immediate *exploitation* that food-deprived animals exhibit (Figure 4 – supplement 3C).
329 We next considered the alternative possibility that this time-dependent signal could actually
330 be related to the physical stress induced by the process of moving animals into the experimental
331 arena rather than the onset of food-deprivation. While we used an agar plug method to mitigate the
332 stress of moving (see Nematode cultures); we sought to examine the impact of satiety as compared
333 to transfer-induced stress on the *exploitation* decision. We quantified both τ_s, the duration of time an
334 animal spent searching off-food since the last *exploitation* event, and τ_t, the duration of time since
335 transfer (i.e., the time elapsed in the experiment). However, as our initial experiments were only one
336 hour, we typically observed only one *exploitation* event. Resultantly, τ_s and τ_t were highly correlated
337 and their individual contributions to the model could not be easily parsed. Therefore, we ran
338 additional experiments with animals foraging in environments with multiple patch densities over two
339 hours (Figure 4E, Figure 4 – supplement 4A-C) which led to observations containing multiple
340 *exploitation* events and a resultant decorrelation of τ_s and τ_t. When the model was re-fit to this two-
341 hour data set using both τ_s and τ_t covariates (i.e.,
342 $p(y_k = 1|\beta_0 + \beta_k\rho_k + \beta_s\tau_s + \beta_t\tau_t + \beta_h\rho_h + \beta_e\rho_e)$), only the satiety-related covariate τ_s was
343 statistically significant (Figure 4 – supplement 4D). This result suggests that the time-dependent
344 change in *exploitation* is likely due to a satiety-related signal rather than a stress-related signal.
345 Altogether, these results suggest that animals use available external and internal sensory information
346 to guide the decision to *exploit*.
347
348 **Prior experience guides the decision to *explore* or *exploit***
349 Although the current patch density and satiety covariates significantly influence the decision
350 to *exploit*, this model (i.e., $p(y_k = 1|\beta_0 + \beta_k\rho_k + \beta_s\tau_s)$) does not accurately predict the extent that
351 *exploitation* was delayed. We hypothesized that because animals had experienced very densely seeded
352 bacterial patches immediately prior to the assay, animals may have built an expectation that high

353 density bacterial patches are available in the new environment. We would therefore expect an initial
354 suppression in the probability of *exploiting* while animals updated their expectation using information
355 learned from *sampling* patches in the current environment. To test whether the decision to *exploit*
356 could be influenced by prior experience, we added a history-dependent covariate to our model (i.e.,
357 $p(y_k = 1|\beta_0 + \beta_k\rho_k + \beta_s\tau_s + \beta_h\rho_h)$ where ρ_h is the relative density of the patch encountered
358 immediately before encounter k). We find that inclusion of the density of the most recently
359 encountered patch significantly improves our prediction of *exploitation* (Figure 4D, Figure 4 –
360 supplement 2). We then considered whether the animal's expectation of bacterial density in the
361 environment might be a longer lasting memory. Specifically, we considered if the relative density of
362 the most recently *exploited* patch ρ_e could have influenced the animal's decision to *exploit*. The
363 addition of this second history-dependent term to our model (i.e.,
364 $p(y_k = 1|\beta_0 + \beta_k\rho_k + \beta_s\tau_s + \beta_h\rho_h + \beta_e\rho_e)$) further improved the fit of our model (Figure 4D,
365 Figure 4 – supplement 2) suggesting that *C. elegans* use recent experiences of encountered and
366 *exploited* patches to guide their decision to *exploit*. Animals may use this learned information to create
367 and update an expectation for the relative density of bacterial patches available in their environment
368 and compare that estimate against the density of a subsequently encountered patch. Altogether,
369 these results suggest that animals use recent experiences to estimate available resources and
370 modulate their decision to *explore* or *exploit*, a strategy that is highly beneficial for behavioral
371 adaptation in a changing environment.

372 To validate the role of prior experience in guiding foraging decisions, we observed animals
373 foraging in environments with multiple patch densities (Figure 4E, Figure 4 – supplement 4A-C).
374 Our model predicts that the lower the density of recently encountered and/or *exploited* patches, the
375 more likely an animal should be to *exploit* a subsequent patch. Without the history-dependent terms
376 ρ_h and ρ_e, our model predicts that no relationship should exist between prior experience and the
377 probability of *exploiting* the current patch. To test which model best fit the animals' behavior, we
378 calculated the conditional probabilities of *exploiting* $p(y_k = 1|\boldsymbol{\beta} \cdot \boldsymbol{x}_k)$ for this new multi-density,
379 multi-patch data set with more nuanced combinations of current (ρ_k) and recent patch (ρ_h and ρ_e)
380 density using the coefficients $\boldsymbol{\beta}$ learned previously (Figure 4C). We observed significantly better
381 predictions of *exploitation* probability for the model including prior experience as compared to the
382 model without the terms ρ_h and ρ_e (Figure 4F, Figure 4 – supplement 4E) as confirmed by a
383 likelihood-ratio test. We observed an augmentation in *exploitation* when animals move from low to

384 high density (e.g., 1 to 4 or 1 to 7) as predicted by the model with history-dependence, but not the
385 model without. It is important to note, that this improvement in prediction was achieved without
386 fitting the model to this new multi-density data set. In summary, our modeling results suggest that
387 animals evaluate bacterial density, monitor internal signals of satiety, and leverage recent experiences
388 to drive their decision to *exploit* a bacterial patch upon encounter.
389
390 **Ciliated sensory neurons are required for the evaluation of patch density**
391 The quantitative modeling applied in this study provides a useful framework for testing the
392 influence of behaviorally relevant features on decision-making. To validate this approach and further
393 elucidate how animals evaluate current and recent patch density, we assessed the foraging behavior
394 of mutants with sensory deficiencies (Figure 4 – supplement 5). We found that animals with reduced
395 function of non-ciliated mechanoreceptor neurons due to a null mutation in the *mec-4* gene behave
396 similarly to wild-type N2 animals, displaying increasingly delayed *exploitation* as patch density
397 decreases (Figure 4G, Figure 4 – supplement 5). Contrastingly, animals with reduced function of
398 ciliated chemoreceptor and mechanoreceptor neurons due to a null mutation in the *osm-6* gene
399 displayed immediate *exploitation* even while foraging on low density patches (Figure 4G, Figure 4 –
400 supplement 5). These results indicate altered decision-making in the *osm-6* mutants. Specifically, it
401 appears that the influence of patch density on the *exploitation* decision is reduced in *osm-6* mutants
402 and that these animals are more likely to *accept* a patch by default.
403 To further elaborate on these findings, we fit our GLM to each of the three data sets (i.e.,
404 N2, *mec-4*, *osm-6*) and assessed the difference in the estimated distributions of coefficients $\boldsymbol{\beta}$ between
405 mutant and wild-type models (Figure 4H). We hypothesized that the density-related covariates (ρ_k,
406 ρ_h, and ρ_e) would have smaller magnitude (i.e., less influence on decision-making) for animals with
407 reduced sensation of bacterial density. Consistent with this hypothesis, we found a significant
408 reduction in the magnitude of the influence of current patch density (i.e., β_k) on the decision to
409 exploit in *osm-6* mutants. Further, we found a significant increase in the intercept β_0 in *osm-6* mutants
410 which corresponds to the overall increase in *exploitation* observed in these animals (Figure 4G, Figure
411 4 – supplement 5). These results suggest that the ciliated sensory neurons play an important role in
412 evaluating the density of the current patch and that when sensation is impaired, animals modify their
413 default behavioral strategy to prioritize *exploitation*. We also observed a marginal increase in our
414 estimate of the influence of recently *exploited* patches (i.e., β_e) in *osm-6* mutants which suggests that

415 reduced efficacy in the evaluation of current patch density also affects learning and memory of
416 patch density. No significant changes were detected in the *mec-4* mutants. Although we cannot rule
417 out a role for non-ciliated mechanoreceptor neurons in contributing to the assessment of patch
418 density, this modality likely provides less salient information. Altogether, these results suggest that
419 ciliated sensory neurons are necessary for the evaluation of patch density and that when the
420 function of these neurons is impaired, animals prioritize *exploitation*. Further, these results
421 demonstrate that this quantitative modeling approach can be used to probe mechanisms underlying
422 decision-making.
423

424 Discussion

425

426 Like all foraging animals, *C. elegans* must choose between *exploiting* an environment for known
427 resources and *exploring* it for potentially better opportunities elsewhere [5, 7-11]. Previous studies
428 have shown that *C. elegans* use *stay-switch* decisions to efficiently explore a patchily distributed
429 environment and exploit the bacteria within [28, 42-44]. In this study, we show that *C. elegans* also
430 make *accept-reject* decisions while foraging. Specifically, we observe that animals often initially *reject* low
431 density bacterial patches, opting to prioritize exploration of the environment, before switching to a
432 more exploitatory foraging strategy during subsequent encounters. This explore-then-exploit
433 strategy was consistent across a range of bacterial patch densities, sizes, and distributions. In order
434 to better understand this phenomenon and identify the factors that contribute to the decision to
435 *exploit*, we leveraged a quantitative modeling approach to hypothesis testing. We found that animals
436 do not employ a default explore-then-exploit strategy; rather, this behavior reflects a series of *accept-*
437 *reject* decisions guided by multimodal information related to an animal's environment and internal
438 state. Specifically, we show that each decision to *explore* or *exploit* is informed by available sensory
439 information, internal satiety signals, and learned environmental statistics related to the bacterial
440 density of recently encountered and *exploited* patches.
441

442 *C. elegans* make *accept-reject* foraging decisions

443 While *C. elegans* have been shown to alter food preferences in a diet choice assay, this
444 behavior has only been described by a set of *stay-switch* decisions [31, 36, 44]. Specifically, *C. elegans*
445 were found to modulate their patch-leaving frequency to *stay* on high quality bacterial patches and
446 *switch* with declining food quality and quantity [26, 36, 40, 41]. The overall effect of leaving low

447 quality patches more frequently is that animals are more likely to reside on high quality patches.
448 Thus, *stay-switch* decision-making enables *C. elegans* to allocate time spent between exploring or
449 exploiting in a manner consistent with optimal foraging theory [5, 7-11]. However, optimal foraging
450 theory also predicts that an animal should never exploit (i.e., always *reject*) a low density patch if
451 higher density patches are sufficiently abundant as inclusion of the low density patch type in the
452 animals' diet decreases the overall rate of energy gained [5, 9]. Thus, while leaving low density
453 patches more frequently drives an overall increase in the rate of energy gained, it can still result in
454 sub-optimal foraging behavior.

455 Here, we demonstrate that *C. elegans* are capable of making *accept-reject* decisions upon
456 encounter with bacterial patches. We employed quantitative methods – GMM and semi-supervised
457 QDA – to estimate whether animals *sensed* a patch and, if they did, whether they *accepted* or *rejected* it.
458 We found that when transferred from high to low density bacterial patches, animals initially *rejected*
459 several patches, opting to continue exploration of the environment, and that this *reject* decision did
460 not reflect an animal's inability to detect the presence of bacteria in these dilute patches. Further, we
461 found that the decision to *explore* or *exploit* is density-dependent and robust across a range of
462 bacterial densities, distributions, and sizes. The initial preference for *exploration* during foraging on
463 low density patches suggests that animals may be *searching* for denser bacterial patches such as those
464 experienced immediately preceding the assay and throughout development. This explore-then-
465 exploit strategy is advantageous for animals when bacterial patch density is low or variable. On the
466 other hand, we observed immediate *exploitation* of high density patches. In these environments, an
467 explore-then-exploit strategy is disadvantageous, as delaying *exploitation* when patch density is already
468 high results in spending more energy on food search with no expected increase in energy gained
469 during *exploitation* of a subsequently encountered patch. Thus, consistent with an energy maximizing
470 optimal forager, *C. elegans* initially *explores* when bacterial patch density is low but immediately *exploits*
471 when bacterial patch density is sufficiently high. Altogether, our results demonstrate that *C. elegans*
472 make a distinct decision to either *explore* or *exploit* a patch upon encounter and that the density-
473 dependence of this decision is consistent with predictions from optimal foraging theory.

474 The concepts of *accept-reject* and *stay-switch* decision-making are well described in foraging
475 theory literature (see Pyke, Pulliam & Charnov 1977 [8] for a review on the subject) and represent
476 the questions "Do you want to eat it?" and, if so, "How long do you want to eat it for?". These
477 concepts are easily distinguishable for animals that forage using the following framework: 1) search
478 for prey, 2) encounter prey from a distance, 3) identify prey type, 4) decide to pursue (*accept-reject*

479 decision), 5) pursue and capture the prey, 6) exploit prey, and 7) decide to stop exploiting and start
480 searching again (*stay-switch* decision). However, in some scenarios, animals must physically encounter
481 prey prior to identification. In these cases where pursuit and capture are not visualized, it is harder to
482 distinguish between *accept-reject* and *stay-switch* decisions. In our experiments, *C. elegans* do not appear
483 to detect the presence of bacterial patches prior to encounter as slow-down only occurs within one
484 body-length of the patch edge (Figure 2B). Further, we find significant bimodality in encounter
485 duration (Figure 2H) where short duration (*exploratory*) encounters appear to represent a lower
486 bound where animals spend the minimum amount of time possible on a patch (less than 2 minutes),
487 which we interpret as a *rejection* of the patch. On the other hand, *exploitatory* encounters span a large
488 range of durations from 2 to 60+ minutes which we interpret as an initial *acceptance* of the patch
489 followed by a series of *stay-switch* decisions which determine the overall duration of the encounter.
490 While we could certainly model our data using only *stay-switch* decision-making, we ascertain that an
491 encounter of minimal duration is better interpreted ethologically as a *rejection* rather than as an
492 immediate *switch* decision. In accordance with this interpretation, we hypothesize that if *C. elegans*
493 were able to detect the presence of a bacterial patch prior to encountering it, it's possible that
494 animals may be observed to navigate towards (*accept*) or away from (*reject*) a patch. However, it could
495 be the case that, for *C. elegans*, *sampling* the patch is prerequisite to an *accept-reject* decision which would
496 suggest that gustation, mechanosensation, and/or post-ingestive feedback may guide *C. elegans*
497 foraging decisions.

498 Our finding that *C. elegans* are willing to *reject* numerous encountered patches is somewhat
499 surprising, especially given that *C. elegans* likely possess limited spatial memory [25] and are likely
500 unaware of how many patches are in the environment as evidenced by their willingness to *reject* a
501 patch even when only one patch is available (Figure 3). Taken together, this suggests that animals are
502 "knowingly" passing up an opportunity to *exploit* an immediately available food source for the
503 potential opportunity to *exploit* preferred food later. This type of behavior has been described in
504 humans and other animals in the context of delayed gratification [49, 50], intertemporal choice [49,
505 51, 52], self-control [53, 54], and optimal stopping [55, 56]. Notably, few animals display the capacity
506 for delayed gratification when given the option between eating an immediately available but less
507 preferred food item and waiting for a preferred food item [57-60]. Even fewer animals are willing to
508 wait if the delayed reward is not visible or increases in quantity rather than quality [61, 62]. Our
509 observation that *C. elegans* can exhibit delayed gratification suggests that this and similar processes

510 require less complex cognition than previously considered or that we may have underestimated the
511 cognitive capacity of *C. elegans*.
512
513 **External and internal sensory information guide foraging decision-making**
514 *Stay-switch* decisions in *C. elegans* are strongly modulated by a variety of internal and external
515 sensory cues over a range of behavioral timescales. For example, patch-leaving frequency can be
516 modulated by an animal's prior experience [25, 42], metabolic status, arousal state [31], as well as the
517 presence of pathogens [63, 64], chemorepellents [65], predators [66, 67], and varying levels of
518 environmental O_2 and CO_2 [40, 68].
519 Here, we used a quantitative framework to show that recent experiences (i.e., the density of
520 current and recently encountered and *exploited* bacterial patches) guide *accept-reject* decision-making. In
521 our study and others [44, 46], *C. elegans* appear to be able to detect the presence of and assess the
522 relative density of bacterial patches. When foraging in environments with low density bacterial
523 patches, we initially observed many *searching* encounters where animals did not appear to slowdown;
524 however, over time, the proportion of *searching* encounters decreased (Figure 2L,M). This increased
525 responsiveness to dilute patches over time could have resulted from small changes in bacterial
526 growth or a modulation of patch detection sensitivity. Contrastingly, animals with reduced function
527 of ciliated chemoreceptor and mechanoreceptor neurons due to a null mutation in the *osm-6* gene
528 almost never *searched*. Rather, they displayed immediate *exploitation* even while foraging on low density
529 patches. This suggests that *osm-6* mutants display an augmented ability to detect bacterial patches but
530 a diminished ability to assess the bacterial density of those patches. While this may seem
531 contradictory, it suggests that bacterial detection and density assessment are mediated by distinct
532 sensory mechanisms. Specifically, post-ingestive feedback or other non-ciliary sensory cues may
533 drive the initial detection of bacteria, while ciliated sensory neurons appear to be crucial for the
534 nuanced evaluation of bacterial patch density. This interplay allows for a flexible foraging strategy
535 where initial detection by one modality can trigger exploitation, which can then be modulated or
536 overridden by more detailed chemosensory and mechanosensory information. This framework may
537 explain why *osm-6* mutants, lacking the ability to finely assess bacterial density, prioritize exploitation;
538 if all patches appear effectively equivalent, further exploration is inefficient. Collectively, these results
539 suggest an important role for sensory modalities in the detection and assessment of bacterial patch
540 density and highlight a need to investigate the mechanisms behind these effects in future studies.

541 The difficulty in assessing bacterial patch density is more than just a sensory challenge.
542 Within-patch spatial inhomogeneity resulting from areas of active proliferation of bacteria [43, 69]
543 complicate an animal's ability to accurately assess the quantity of bacteria within a patch and,
544 consequently, our ability to accurately compute a metric related to our assumptions of what the
545 animal is sensing. In our study, we used the relative density of the patch edge where bacterial density
546 is highest as a proxy for an animal's assessment of bacterial patch density (Figure 2 – supplement 1).
547 This decision was based on a previous finding that the time spent on the edge of a bacterial patch
548 affected the dynamics of subsequent area-restricted search [25]. While within-patch spatial
549 inhomogeneity likely affects an animal's ability to assess patch density, we do not believe that this
550 qualitatively affects the results of our study. Both the patch densities tested (Figure 2 – supplement
551 3A) as well as our observations of time-dependent changes in *exploitation* (Figure 2E,N-O; Figure
552 3H-I) maintained a monotonic relationship. Therefore, alternative methods of patch density
553 estimation should yield similar results.
554 According to early models in optimal foraging theory, foragers behave as if they have *complete*
555 *information* about the environment (e.g., animals are assumed to know the average density of bacterial
556 patches) [9]. Later theoretical and empirical work expanded models of patch choice to accommodate
557 situations where animals have *incomplete information* (e.g., environments with fluctuating resources)
558 and, therefore, must both acquire information and forage [8, 10, 70]. This work suggests that
559 animals may continuously sample areas in their environment to keep track of resource availability.
560 Here, we found that animals initially choose to *sample* patches and that the duration of this period of
561 *sampling* is correlated with the degree of mismatch between current and recently experienced and
562 *exploited* patches (i.e., animals spend more time *sampling* as the magnitude of difference between the
563 patch density experienced immediately before and during the experiment increases). When there is
564 no difference between current and prior experience (i.e., animals foraging on patches of relative
565 density 200), animals rarely *sample*. These results suggest that *C. elegans* use *sampling* as a way of re-
566 evaluating the overall quality of patches available in the environment when a change is detected.
567 Further, the results of our model suggest that animals likely use the information learned during
568 *sampling* encounters to guide their decision to *explore* or *exploit* on subsequent patch encounters. We
569 behaviorally validated this hypothesis by applying our model predictions to animals foraging in
570 environments with multiple patch densities. Consistent with our predictions, we observed that the
571 lower the density of recently encountered or *exploited* patches and the higher the density of the
572 current patch, the more likely an animal would be to *exploit* (Figure 4F). These results suggest that *C.*

573 *elegans* can learn and remember features of recent experiences and use that learned information to
574 guide efficient decision-making. Incorporating prior experience into the decision to *explore* or *exploit*
575 currently available food is highly beneficial when foraging in a fluctuating environment. *C. elegans*
576 thus may have evolved this ability to maximize foraging in the wild where animals experience a
577 boom-and-bust environment [71]. Future studies investigating the effects of varying patch density
578 during animal development could provide additional insights into the effects of more distant
579 experiences on the *explore-exploit* decision. However, testing this is non-trivial as maintaining stable
580 bacterial density conditions over long timescales requires matching the rate of bacterial growth with
581 the rate of bacterial consumption.
582 In addition to external sensory information, internal state signals serve a critical role in
583 modifying decision-making in *C. elegans* [31, 72]. For example, food-deprived animals are more likely
584 to cross an aversive barrier (e.g., copper, primaquine, glycerol) in search of food as compared to
585 well-fed controls [72, 73]. Here, we find that a satiety-related signal likely drives the decision to
586 *exploit*. Specifically, our model suggests that as animals' satiety decreases, their willingness to accept a
587 lower quality patch increases. We confirmed this prediction by analyzing the behavior of food-
588 deprived animals, which immediately *exploit* even when bacterial patches are very dilute (Figure 4 –
589 supplement 3). Further, we showed that this temporal signal was not likely to have been caused by
590 transfer-induced stress (Figure 4 – supplement 4D). Combined with the effect of prior experience,
591 these results suggest that the decision to *explore* or *exploit* likely requires integration of food-related
592 internal and external cues. Future studies should probe if additional factors related to the animal's
593 biotic and abiotic environment [35, 74-77] as well as alternative motivations (e.g., reproduction and
594 predatory avoidance) [78-81] further modify these foraging decisions.
595
596 **Quantitative and ethological approach to investigating decision-making**
597 Naturalistic observations of *C. elegans* behavior are necessary to achieve a more complete
598 cellular, molecular, and genetic understanding of how the nervous system has evolved to drive
599 animal behavior. For example, large patches of densely seeded bacteria have primarily been used in
600 experiments assessing *C. elegans* foraging [20, 21, 82-84]. However, wild nematodes experience a
601 boom-and-bust environment [71] that may be more consistent with sparse, patchily distributed
602 bacteria [28]. Thus, just as quiescence is only observed on high quality bacterial patches [85],
603 additional behavioral states may be discovered when assessing foraging in dilute patchy
604 environments. By conducting detailed analyses of ecologically inspired foraging behaviors in

605 individual animals, we discovered that *C. elegans* make *accept-reject* decisions upon encounter with
606 bacterial patches. By studying foraging in these environments containing small, dilute bacterial
607 patches, we increased the frequency of opportunities for *accept-reject* decision-making (i.e., patch
608 encounters and patch-leaving events are more frequent) and decreased the condition-specific bias
609 towards *accept* decisions (i.e., animals are less likely to *accept* patches when moved between
610 environments of differing bacterial density). We expect that further investigation into naturalistic
611 behaviors could reveal additional insights into more complex behaviors and decision-making in *C.*
612 *elegans* and other animals.

613 In this study, we developed an assay that enables observation of ecologically relevant
614 decision-making in freely moving animals. We posit that future studies can leverage this assay to
615 investigate the neuronal mechanisms underlying decision-making. The frequency of decision-making
616 opportunities (i.e., numerous *accept-reject* decisions could be observed in the span of minutes) and
617 consistency of patch choice decisions across hundreds of animals and a range of environmental
618 conditions tested supports this claim. Further, we anticipate that the *accept-reject* decision occurs
619 during a narrow time window – possibly at the time of encounter with the patch edge or shortly
620 thereafter. Therefore, we expect that this assay could be adapted for experiments utilizing calcium
621 imaging in freely-moving animals [17, 30, 86-90] to monitor neuronal activity as animals make these
622 decisions. Additionally, the foraging task used here could be leveraged as an accumulation of
623 evidence paradigm, which has been predominantly studied using mammalian animal models [91].

624 Finally, we used simple quantitative models to dissect and validate the components
625 underlying decision-making. Specifically, we employed a logistic regression GLM which we adapted
626 to accommodate our uncertainty in classification of *sensing* and *exploitation* for each encounter. While
627 alternative models may provide more mechanistic predictions, the GLM enabled us to conduct a
628 sequence of hypothesis tests probing the influence of food-related signals on the decision to *exploit*.
629 Indeed, we conducted a great number of analyses involving model selection and optimization.
630 Ultimately, we focused our study on asking whether a set of simple covariates could be used to
631 predict foraging decisions. The GLM enabled us to identify the simplest model that could explain
632 the observed delay in *exploitation*. While even the null model predicted that, on average, numerous
633 *exploratory* encounters were likely to occur before the first *exploitation*, models including satiety and
634 prior experience significantly better predicted the extent of this delay. Further, we demonstrated that
635 we could validate these model predictions in food-deprived animals, animals exploring multiple
636 patch densities, and animals with sensory deficiencies. We regard our study as an initial foray into

637 demonstrating *accept-reject* decision-making in nematodes and, while our model is a useful tool for
638 testing the effects of past experiences, our results do not imply that *C. elegans* discretize their
639 experiences into the parameters used in our model. The exact mechanisms and, consequently, the
640 best model design require further investigation. For example, it is possible that the density of
641 recently *exploited* patches is predictive of subsequent *exploitation* because post-ingestive feedback is
642 required for the memory and/or because more distant experiences are remembered (i.e., long-term
643 memory is involved). Future studies should seek to differentiate between these possibilities and
644 characterize the time window of the memory. Altogether, we suggest that this quantitative and
645 ecologically inspired approach to investigating behavior and decision-making is incredibly powerful
646 for refining hypotheses and enables subsequent investigation into the underlying cellular, molecular
647 and circuit pathways in *C. elegans*, a strategy that could be adopted across species.
648

649 ## Abbreviations

650 Bayesian information criterion (BIC), Gaussian mixture model (GMM), generalized linear model
651 (GLM), kernel density estimate (KDE), Kullback-Leibler (KL) divergence, lysogeny broth (LB),
652 nematode growth medium (NGM), optical density at 600 nm (OD_{600}), first principal component
653 (PC1), quadratic discriminant analysis (QDA)
654

655 ## Acknowledgements

656 We thank members of the Chalasani lab for comments on the manuscript and James Fitzgerald for
657 advice on modeling. This research was funded by grants from the National Science Foundation
658 (J.A.H.), UCSD Undergraduate Summer Research Award (T.C.), NIH RO1 MH096881, Dorsett
659 Brown Foundation, and Salk Innovation Grant (S.H.C.).
660

661 ## Author Contributions

662 **Jessica Haley:** Conceptualization, Methodology, Software, Validation, Formal analysis,
663 Investigation, Resources, Data Curation, Writing – Original Draft, Writing – Reviewing & Editing,
664 Visualization, Supervision, Project administration, Funding acquisition. **Tianyi Chen:** Investigation,
665 Data Curation, Writing – Reviewing & Editing. **Mikio Aoi:** Methodology, Formal analysis, Writing –
666 Reviewing & Editing, Visualization, Supervision. **Sreekanth Chalasani:** Conceptualization,
667 Resources, Writing – Reviewing & Editing, Supervision, Funding acquisition.

Declaration of Interests

The authors declare no competing interests.

671 ## Materials and Methods

672

673 ### Key Resources Table

Reagent type (species) or resource	Designation	Source or reference	Identifier
bacterial strain (*Escherichia coli*)	OP50	Caenorhabditis Genetics Center	WBStrain00041969
bacterial strain (*Escherichia coli*)	OP50-GFP	Caenorhabditis Genetics Center	WBStrain00041972
organism/strain (*Caenorhabditis elegans*)	N2: wild isolate	Caenorhabditis Genetics Center	WBStrain00000001
organism/strain (*Caenorhabditis elegans*)	PR811: [osm-6(p811) V]	Caenorhabditis Genetics Center	WBStrain00030796
organism/strain (*Caenorhabditis elegans*)	TU253: [mec-4(u253) X]	Caenorhabditis Genetics Center	WBStrain00035037
software, algorithm	StreamPix 8	NorPix	RRID:SCR_015773
software, algorithm	WormLab	MBF Bioscience	RRID:SCR_017669
software, algorithm	MATLAB 2024a	Mathworks	RRID:SCR_001622
software, algorithm	Photoshop 2024	Adobe	RRID:SCR_014199
software, algorithm	Illustrator 2024	Adobe	RRID:SCR_010279
software, algorithm	Code for analysis	https://github.com/shreklab/Haley-et-al-2024	

674

675 ### Data and Code Availability

676 Source data files containing summarized data have been provided for all figures. All
677 processed data (e.g. animal and bacterial patch locations over time) reported in this paper is publicly
678 available at NDI-Cloud (https://doi.org/10.63884/ndic.2025.pb77mj2s). Raw data (e.g. videos) can
679 be shared by the lead contact upon request. All original code is publicly available at GitHub
680 (https://github.com/shreklab/Haley-et-al-2024).

681

682 ### Bacterial cultures

683 Stock liquid cultures of the OP50 strain of *Escherichia coli* were prepared via inoculation of a
684 single colony in sterile lysogeny broth (LB) grown overnight at room temperature. Stock liquid
685 cultures were subsequently stored at 4°C for up to 6 weeks.

686 Solutions of OP50 for each experiment were prepared via a series of dilutions in LB (Figure
687 1 – supplement 1A). 50 mL of OP50 stock solution was centrifuged at 3000 rpm for 5 minutes.
688 After removal of supernatant, approximately 500 to 1000 μL of saturated liquid culture remained.

689 The bacterial density of this saturated solution was estimated by measuring the optical density at 600
690 nm (OD_{600}) of a 1:50 dilution of the homogenized solution on a spectrophotometer (Molecular
691 Devices SpectraMax Plus 384). The saturated solution was subsequently diluted to achieve an OD_{600}
692 of ~10 (μ = 10.22, σ = 0.31). Measurements of the number of colony forming units in the "10"
693 solution estimated 13.1×10^9 cells per mL on average. Additional densities (OD_{600} = {0.05, 0.1, 0.5, 1,
694 2, 3, 4, 5}) were prepared via dilution of the "10" solution with LB and kept on ice to prevent
695 bacterial growth. A "0" density solution was prepared with just LB.
696 For all experiments, these density solutions were seeded onto cold, low-moisture nematode
697 growth medium (NGM) plates (3% agar) to facilitate pipetting of small, circular, quick-drying
698 patches. Unless otherwise noted, seeded plates were immediately returned to 4°C after patches dried
699 to prevent bacterial growth. Plates were stored at 4°C for an average of 6 days before
700 experimentation.
701 For experiments using an OP50 strain expressing green fluorescent protein (OP50-GFP)
702 [92], cultures were prepared as above, but with the addition of 100 μg/mL of carbenicillin to the
703 liquid LB. All bacterial strains used in this study are listed in the Key Resources table.
704
705 **Nematode cultures**
706 *Caenorhabditis elegans* strains were maintained under standard conditions at 20°C on NGM
707 plates (1.7% agar) seeded with stock liquid culture of OP50 [16]. All experiments were performed
708 on young adult hermaphrodites, picked as L4 larvae the day before the experiment (μ= 24.6 hours, σ
709 = 3.4). Unless otherwise indicated, well-fed animals of the standard *C. elegans* strain N2 Bristol were
710 used for experiments. Transgenic strains were always compared to matched controls tested in parallel
711 on the same days. All *C. elegans* strains used in this study are listed in the Key Resources table.
712
713 **Assay preparation and recording**
714 ***Single-density, multi-patch assay***
715 Several days before the experiment, condition and acclimation plates were prepared (Figure 1
716 – supplement 1A). For the condition plates, a large circular arena (30 mm in diameter) made of clear
717 transparency film (6 mil, PET) was cut using a computer-controlled cutting machine (Cricut Maker
718 3) and placed in the center of a 10 cm petri dish filled with 25 mL of NGM (3% agar). These arenas
719 function to corral animals with a low probability of escape [93]. A pipetting template made of the
720 same material was designed and cut with an isometric grid consisting of 19 circular holes spaced 6

721 mm apart from center-to-center. The pipetting template was overlaid on top of the arena and 0.5 μL
722 of OP50 solution (OD_{600} = {0, 0.05, 0.1, 0.5, 1, 2, 3, 4, 5, 10}) was pipetted into each hole. After
723 drying, the template was immediately removed, and the petri dish lid replaced to prevent
724 contamination and dehydration. For two conditions ("1 (12H)" and "1 (48H)"), plates were seeded
725 with OD_{600} = 1 and then left at room temperature for 12 or 24 hours, respectively, prior to storage at
726 4°C. For all other conditions, plates were immediately stored at 4°C after drying. Acclimation plates
727 were prepared by seeding NGM (3% agar) plates with one large patch of 200 μL of OD_{600} = 1
728 grown for 24 hours at room temperature.

729 Approximately 24 hours before the experiment, acclimation plates and "1 (48H)" condition
730 plates were transferred from 4°C to room temperature. After plates warmed to room temperature
731 (~1 hour), 30-60 L4 animals were picked onto the acclimation plates. Plates were then stored at
732 20°C until the experiment for a combined bacterial growth time of approximately 48 hours (24
733 hours from freshly seeded to 4°C; 24 hours from 4°C to experiment). The combined bacterial
734 growth time for all condition plates was approximately 1 hour (μ= 1.16 hours, σ = 0.23) unless
735 otherwise noted as "12" (μ= 13.63 hours, σ = 0.50) or "48" hours (μ= 49.28 hours, σ = 2.94).

736 On the day of the experiment, each set of condition plates was transferred from 4°C to
737 room temperature. After one hour, 4 young adult animals were gently transferred to an empty NGM
738 plate to limit the spread of bacteria from acclimation to condition plates. Animals were then quickly
739 transferred to a condition plate. Animals were transferred using the flat surface of cylindrical plugs
740 excised from clean 3% agar [66, 93]. Importantly, the use of agar as a medium to transfer animals
741 provides minimal disruption to their environment as all physical properties (e.g. temperature,
742 humidity, surface tension) are maintained. Qualitatively, we observe no marked change in behavior
743 from before to after transfer with the agar plug method, especially as compared to the often drastic
744 changes observed when using a metal or eyelash pick.

745 Condition plates were subsequently placed face down on a piece of glass suspended above
746 an edge-lit backlight (Advanced Illumination). Recordings were acquired using PixeLink cameras
747 (PL-B741F) combined with Navitar lenses (1-60135 and 1-6044) and Streampix 8 software. Behavior
748 was recorded for one hour at 1024x1024 pixels and 3 frames per second (fps) with spatial resolution
749 of ~33 pixels per mm (μ= 32.68 pixels/mm, σ = 1.70).

750 The assay was repeated over numerous days with every condition assayed on each day when
751 possible. The order of seeding assay plates and recording behavior was randomized for each day to
752 compensate for the potential effects of time on animal age and bacterial density. Further, the average

753 temperature (μ= 21.99°C, σ = 0.95) and humidity (μ= 51.39%, σ = 11.67) during each experiment
754 were recorded. As a result of randomization, animal age, bacterial growth time, temperature, and
755 humidity did not significantly vary between density conditions. Replication of the assay was
756 constrained by the set-up (~4 hours per day), recording (1-2 hours per animal), and analysis (0.5-1
757 hours per animal) time required. A maximum of 24 animals (2 cameras run for 12 hours) could be
758 assayed per day. Given these resource constraints, we collected replicates until saturation of
759 qualitative observations (i.e., new animals merely replicated earlier observations without adding new
760 information) [94] resulting in sample sizes comparable to similar studies [28, 42].
761
762 ***Large, single-patch assay***
763 Plates were prepared as described for the single-density, multi-patch assay with the exception
764 that only one large patch was created by pipetting 20 μL of OP50 solution (OD_{600} = {0, 0.05, 0.1,
765 0.5, 1, 2, 3, 4, 5, 10}) into the center of the 30 mm diameter arena.
766
767 ***Small, single-patch assay***
768 Plates were prepared as described for the single-density, multi-patch assay with the exception
769 that only one small patch was created by pipetting 0.5 μL of OP50 solution (OD_{600} = {0, 0.5, 1, 5,
770 10}) into the center of a 9 mm diameter arena. Given the smaller arena size, only one young adult
771 animal was transferred into the arena. Behavior was recorded for one hour at higher spatial (μ=
772 104.76 pixels/mm, σ = 17.6) and temporal resolution (8 fps). The acquisition set-up was otherwise
773 unaltered except for the removal of a 0.25x Navitar lens (1-6044) from the light path.
774
775 ***Multi-density, multi-patch assay***
776 Plates were prepared as described for the single-density, multi-patch assay with the exception
777 that varying combinations of OD_{600} = {1, 5, 10} (i.e., OD_{600} = {1, 5, 10, 1+5, 1+10, 1+5+10}) were
778 pipetted onto each assay plate in a patterned isometric grid of 18 0.5 μL droplets. Behavior was
779 recorded for two hours. To compensate for the longer duration recordings, NGM agar plates were
780 poured without Bacto™ peptone (BD 211677) to prevent bacterial growth. The result of this
781 change was that the relative density of bacterial patches was ~30% lower as compared to
782 comparable 0.5 μL patches in the single-density, multi-patch assay and the small, single-patch assay
783 (Figure 2 – supplement 2-3). Further, to prevent censorship of our data at the beginning of the
784 recording, we formed a small droplet of S-Complete solution [95] in the middle of the arena where

785 no bacterial patch was placed. Animals were transferred to this droplet using an eyelash pick
786 immediately prior to the assay plate being placed on the imaging set-up. The recording was started
787 once the droplet evaporated and animals were free to crawl about the arena. This process ensured
788 that recordings began prior to an animal's first patch encounter.
789
790 **Bacterial patch location detection**
791 Most bacterial densities tested in these experiments were too dilute to be visible under
792 normal imaging conditions. Therefore, several strategies were employed to accurately detect the
793 location of bacterial patches. First, a small reference dot was cut into the arena and pipetting
794 templates enabling consistent and traceable patch placement. Further, prior to each behavior
795 recording, a "contrast" video was acquired wherein a piece of dark cardstock was passed between
796 the light source and the condition plate (Figure 1 – supplement 1B-D, Video 2). This produced an
797 effect where diffraction of light through the patches provided enough contrast to view the patches.
798 Binary masks of the circular arena and patches were extracted from these videos in MATLAB using
799 the Image Processing Toolbox and further refined manually in Photoshop (Adobe, 2024). Arena
800 masks were used to calculate the scale (pixels/mm) of each image. In early experiments, the
801 "contrast" video was acquired prior to worms being added to the condition plate, which resulted in
802 displacement of the arena within the camera's field-of-view. Image registration using MATLAB's
803 Computer Vision Toolbox was performed to accurately map the patches detected in the "contrast"
804 video onto the behavioral recording.
805
806 **Bacterial patch density estimation**
807 As described above (see Assay preparation and recording), we varied the relative density of
808 bacterial solutions by diluting OP50 in LB and growing patches for different lengths of time. As a
809 result of these procedures, the relative bacterial density throughout the assay was not known and
810 needed to be estimated. To determine the relative density of these bacterial patches, we seeded
811 plates with fluorescently labeled OP50-GFP under identical conditions as in our assays (Figure 2 –
812 supplement 1A). We imaged these bacterial patches for several hours using a Zeiss Axio Zoom.V16.
813 Images were analyzed using the Image Processing Toolbox in MATLAB. After correcting for
814 inconsistent illumination across the field-of-view and normalizing images using matched controls
815 (Figure 2 – supplement 1B-C), we detected the location of each bacterial patch and extracted a
816 fluorescence intensity profile along each patch's radius (Figure 2 – supplement 1D). Consistent with

817 previous studies, we found that even in extremely dilute conditions, bacterial density was greater at
818 the patch edge where actively proliferating bacteria are concentrated [43, 69]. Therefore, we detected
819 the patch edge and computed the peak amplitude of each bacterial patch at all time points assayed
820 (Figure 2 – supplement 1E). We then performed linear regression on the values for each condition
821 to create models of peak amplitude as a function of time. For low density conditions (i.e., OD_{600} =
822 {0.05, 0.1}) of small patches, fluorescent signals could not be detected. We therefore estimated these
823 functions from a multinomial regression of values taken from OD_{600} = {0.5, 1, 2}. Through this
824 process, we used the total time that bacteria were allowed to grow at room temperature for each
825 condition plate to estimate the peak amplitude at each time point (Figure 2 – supplement 3). Finally,
826 to minimize confusion about density conditions between experiments, we computed values for
827 relative density by linearly scaling estimated peak amplitude values so that 0.5 μL patches seeded
828 with OD_{600} = 10 and grown for 1 hour at room temperature would have relative density equal to 10.
829 We labeled each condition using the relative density rounded to one significant digit.
830
831 **Behavioral tracking**
832 WormLab® (MBF Bioscience) was used for tracking animal behavior (Figure 1 – supplement
833 1E-G, Video 3). For each video, we adjusted thresholds for pixel intensity and worm dimensions to
834 enable automatic tracking. WormLab then fit the worm's body at every frame and stitched together a
835 track of each worm across frames. Subsequent manual corrections were required for instances
836 where the software created new worm tracks. This occurred most frequently when animals: 1)
837 encountered the arena border, 2) collided with each other, or 3) overlapped with bubbles or dust
838 particles embedded in the agar. To correct for these discontinuities, we manually "stitched" worm
839 tracks together enabling us to keep track of each animal's location throughout the duration of the
840 experiment. We exported the location of each animal's midpoint for further analysis in MATLAB
841 (Mathworks, 2024a). For small, single-patch assays where higher spatial resolution enabled reliable
842 distinction between the head and tail of the animal, we manually confirmed the head-tail and
843 exported 25 points along the animal's midline (Figure 1 – supplement 2A-C).
844 Animals were excluded from analyses when 1) the animal's location could only be tracked for
845 less than 75% of the video due to the animal escaping the arena and when 2) the location of
846 bacterial patches could not be reliably assessed due to missing or low-quality "contrast" videos (see
847 Bacterial patch location detection).
848

849 **Patch encounter detection**

850 As the head position of animals in our experiments was difficult to track due to low spatial
851 resolution and limited automated detection of head position using WormLab, we instead tracked the
852 midpoint position of the worm's body and estimated patch encounters using a set of measured
853 criteria. To do this, we tracked the behavior of worms in higher resolution (~105 pixels/mm
854 compared to ~33 pixels/mm and 8 fps compared to 3 fps), single patch assays (Figure 1 –
855 supplement 2A-C). We found that when the head of the animal was in contact (i.e., within 1 pixel)
856 with the patch edge (see Bacterial patch location detection), the animal's midpoint was on average
857 0.46024 mm away (Figure 1 – supplement 2D). We therefore defined a patch encounter as the time
858 when an animal's midpoint came within 0.46024 mm of the patch edge. However, this definition led
859 to two types of errors: 1) putative entry events where the animal merely passed by the patch and 2)
860 putative leaving events where the animal did not fully leave the patch.

861 To remove putative entry events where the animal nearly passed by the patch, we defined an
862 additional distance threshold based on the distance between the animal's midpoint and the patch
863 edge for all time points when the head was within the patch (Figure 1 – supplement 2E). The
864 midpoint was almost always (99% of time) within 0.28758 mm of the patch edge. Therefore, we
865 removed patch encounters where the midpoint never got closer than 0.28758 mm from the patch
866 edge. Although this criterion removes most "near miss" events, some events remain where the
867 animal approached the patch, but its head never entered. Further decreasing this threshold (e.g.,
868 midpoint must be on patch) would result in real events being excluded due to the animal taking on
869 specific postures where the midpoint remains outside the patch while feeding within the patch.
870 Therefore, we chose to be more liberal (i.e., more false positive patch encounters than false
871 negatives) in our detection of patch encounters. Subsequent analysis of these putative patch
872 encounters removed the majority of remaining false positives (see Patch encounter classification as
873 sensing or non-responding).

874 To address putative leaving events and avoid splitting a single patch encounter into multiple
875 encounters, we considered that a lawn leaving event is most frequently defined as an event where all
876 body parts have left the patch [31]. When tracking only the midpoint, it is not possible to ensure that
877 the worm's entire body has exited the patch. Using the criterion that an animal exits a patch when it's
878 midpoint exceeds 0.46024 mm from the patch edge accurately predicts exit events most of the time,
879 but under certain scenarios (e.g., animals maintain an outstretched feeding posture [66]) false leaving
880 events were detected. To exclude these leaving events, we analyzed the variability in the distance

881 from the midpoint to the patch edge during on- and off-patch events (Figure 1 – supplement 2F).
882 We found that on-patch events had low distance variability while off-patch events displayed a
883 bimodal distribution, with some events having high variability as expected, and some events having
884 low variability. We fit a two-component Gaussian mixture model to the off-patch distance variability
885 and found that low variability leaving events could be reliably excluded when the standard deviation
886 of off patch distances was less than 0.22221. We subsequently combined putative patch encounters
887 where variability was below this threshold, resulting in fewer overall encounters.
888
889 **Patch encounter classification as exploration or exploitation**
890 To classify patch encounters as *exploration* or *exploitation* events, patch encounters were
891 detected (see Patch encounter detection) and two features were computed: 1) duration of patch
892 encounter and 2) average on-patch velocity. Both the duration and velocity features displayed a
893 bimodal distribution with two visible clusters: one with short duration encounters and high on-patch
894 velocity and one with long duration encounters and low on-patch velocity (Figure 2 – supplement
895 6A). To confirm the existence of two clusters, we conducted a modified version of Silverman's test
896 for bimodality [47, 48]. Broadly, Silverman's test uses kernel density estimation (KDE) to investigate
897 the number of modes in a distribution. By solving for a critical bandwidth at which the KDE
898 switches modality from j to $j + 1$ modes, one is able to test the null hypothesis that a distribution
899 has j modes, versus the alternative that it has more than j modes. Following a previously described
900 protocol [47, 48], we tested the null hypothesis that our data set was unimodal (i.e. $j = 1$). We first
901 mean-centered the matrix $\boldsymbol{z}_k$ containing the log transforms of the duration and average velocity of
902 each patch encounter k. We then calculated the projection of each data point onto the first principal
903 component (PC1) of the data to get a one-dimensional distribution representing the data in $\boldsymbol{z}_k$
904 (Figure 2 – supplement 6B). The use of principal *components* instead of principle *curves* as described
905 previously was justified as both methods are indistinguishable when $j = 1$ [47]. Two modes are
906 visible in both the histogram and KDE of the distribution of PC1 projected data when the KDE is
907 computed using a Gaussian kernel and Silverman's rule of thumb for bandwidth [96] defined as
908 $\hat{h} = \sigma\left(\frac{4}{(d+2)\,n}\right)^{\frac{1}{d+4}}$ where, for this data set, σ is the standard deviation, $d = 1$ is the dimensionality,
909 and $n = 6560$ is the number of observations. To test the significance of this distribution being
910 bimodal rather than unimodal, we computed the critical bandwidth h^* defined as the minimum

bandwidth for which the KDE has only one mode. Following Silverman's test procedure, we computed a smoothed bootstrap across 2000 replicates by sampling the data with replacement and adding noise such that for any data point z_i and bootstrap resample b, we make noisy $\tilde{z}_{i,b} = \frac{z_i + h^* \epsilon_{i,b}}{\sqrt{1+\left(\frac{h^*}{\sigma}\right)^2}}$ where $\epsilon_{i,b}$ is a standard normal random variable independently drawn for each i and b. We found that the critical bandwidth h^* of our data set was significantly ($p < 0.001$) greater than that of the bootstrapped data sets which allows us to reject the null hypothesis that the distribution of $\boldsymbol{z}_k$ is unimodal and justifies the use of a two-cluster model in classifying these data (Figure 2 – supplement 6C).

After confirming the bimodality of the data set, we classified patch encounters using a two-component Gaussian mixture model (GMM) to estimate $p(y_k = 1|\boldsymbol{z}_k)$ where for each encounter k, $\boldsymbol{z}_k$ are the log transforms of the duration and average velocity of the patch encounter, $y_k = 1$ indicates an *exploitation*, and $y_k = 0$ indicates an *exploration* (Figure 2 – supplement 6D). We optimized the GMM across cross-validated replicates with respect to the regularization value α to minimize the posterior variance given by

$$\sum_k p(y_k = 1|\boldsymbol{z}_k)\, p(y_k = 0|\boldsymbol{z}_k)$$

We found that $\alpha = 0.025$ best separated the *exploration* and *exploitation* clusters (Figure 2 – supplement 6E). The posterior probability of *exploitation* $p(y_k = 1|\boldsymbol{z}_k)$ was subsequently estimated for all encounters (Figure 2 – supplement 6F-G).

Patch encounter classification as sensing or non-responding

To classify patch encounters as *sensing* or *non-responding* events, we computed animals' 1) deceleration upon encounter with the patch edge, 2) minimum velocity during the patch encounter, and 3) maximum change in velocity between the peak velocity immediately prior to the start of the patch encounter and the minimum velocity during the encounter (Figure 2 – supplement 7A-B). Deceleration was defined as the slope of the line fit on an animal's velocity between -1.5 seconds before and 6.5 seconds after the start of an encounter. Minimum velocity was defined as the absolute minimum velocity observed during the duration of the patch encounter. The maximum change in velocity was computed by subtracting the minimum velocity from the peak velocity within 10 seconds of the patch encounter. The combination of these three metrics reveals two non-

Gaussian clusters confirmed by Silverman's test (p = 0.003) as described in the previous section (Figure 2 – supplement 7C-F). These clusters represent encounters where animals sensed the patch (i.e., slow minimum velocity, large changes in velocity) or did not respond to it (i.e., maintained fast minimum velocity, with little to no change).

We estimated the probability of *sensing* $p(v_k = 1|\boldsymbol{w}_k)$ where for each encounter k, $\boldsymbol{w}_k = (s_k, t_k, u_k)$ are the three velocity-related features, $v_k = 1$ indicates an encounter that was *sensed*, and $v_k = 0$ indicates an encounter where *no response* was detected. Using a semi-supervised approach to quadratic discriminant analysis (QDA), we labeled a subset of all encounters and iteratively estimated labels on the remaining unlabeled data (Figure 2 – supplement 8A-C, Video 5). To label the data, we made two simple assumptions: 1) animals must have sensed the patch if they exploited it and 2) animals must not have sensed the patch if there was no bacteria to sense. Therefore, all encounters with bacteria-free patches (i.e., LB only, relative density 0) were labeled as true negatives $v_k = 0$ and, across 1000 replicates, we probabilistically included *exploitation* encounters $y_k = 1$ estimated from the distribution $y_k|\boldsymbol{z}_k \sim \mathrm{Bern}\big(p(y_k = 1|\boldsymbol{z}_k)\big)$ as true positives $v_k = 1$. The semi-supervised QDA method then used these initial labels to iteratively fit a paraboloid that best separated the labeled data, by minimizing the posterior variance of classification. Using this approach, the conditional probability of *sensing* $p(v_k = 1|\boldsymbol{w}_k)$ was estimated for all encounters using QDA and averaged across replicates (Figure 2 – supplement 8D-E).

Although we found that the two clusters were successfully discriminated by this semi-supervised QDA approach, a small subset of encounters (252 of 20109 encounters) could not be reliably classified in this manner as the onset of the patch encounter was not observed. This type of data censoring occurred when the behavioral recording was started after the animal had already entered the patch. Although we could compute deceleration-related metrics for these encounters with the assumption that the animal entered the patch at the first frame, these measurements are censored with a bias towards lower magnitudes of deceleration. Therefore, to better predict the conditional probabilities of *sensing* for these 252 encounters, we assumed that the minimum velocity on-patch s_k was a reliable metric and marginalized the conditional probabilities over the other two metrics (t_k and u_k) as defined by

$$p(v_k = 1|s_k) = \int_{-\infty}^{\infty}\int_{-\infty}^{\infty} p(v_k = 1 \mid s_k, t_k, u_k)\, p(t_k, u_k \mid s_k)\; dt\, du$$

We numerically integrated using an adaptive quadrature method over the product of the QDA estimated conditional probability distribution and the kernel density estimate of the joint probability distribution. This procedure resulted in a slight increase ($\mu = +0.0615$, $\sigma = 0.1832$) in our estimation of the probability of *sensing* (Figure 2 – supplement 8F).

Altogether, this classification approach resulted in low false positive and false negative rates. Specifically, 3.35% of the time encounters with bacteria-free patches were incorrectly identified as *sensing* while 2.92% of the time *exploitatory* encounters were incorrectly identified as *non-responding*. Further, this classification removed many of the remaining near miss patch encounters in which animals came close to but did not truly enter the patch (see Patch encounter detection). For all analyses, we excluded near miss encounters where the animal's midpoint never entered the patch and the probability of *sensing* was less than 5% (i.e., $p(v_k = 1|\boldsymbol{w}_k) < 0.05$).

Models of exploitation probability

We consider that the probability of *exploiting* a patch upon any given encounter can be described by a logistic function:

$$p(y_k = 1|\boldsymbol{\beta} \cdot \boldsymbol{x}_k) = \frac{1}{1 + e^{-\boldsymbol{\beta} \cdot \boldsymbol{x}_k}}$$

where $p(y_k = 1|\boldsymbol{\beta} \cdot \boldsymbol{x}_k)$ represents the conditional probability that an animal exploited during patch encounter k; $\boldsymbol{x}_k \in R^n$ is a vector of covariates; and $\boldsymbol{\beta} \in R^n$ is a vector of weights that describes how much each covariate influences the animal's choice. In models compared here, $\boldsymbol{x}_k$ includes a combination of a constant element as well as covariates that may empirically influence the decision to exploit: 1) the log-transformed relative density of the encountered patch k (ρ_k), 2) the duration of time spent off food since departing the last *exploited* patch (τ_s), 3) the log-transformed relative density of the patch encountered immediately before encounter k (ρ_h), and 4) the log-transformed relative density of the last *exploited* patch (ρ_e).

The observations of *exploitation* and *sensation* for our data are derived predictions from classification models rather than direct measurements (see Patch encounter classification as exploration or exploitation and Patch encounter classification as sensing or non-responding). As such, the labels for both whether a patch encounter was *sensed* by the animal $p(v_k = 1|\boldsymbol{w}_k)$ and whether the animal *exploited* the patch $p(y_k = 1|\boldsymbol{z}_k)$, are both reported as probabilities rather than binary, deterministic variables.

To account for uncertainty in *sensation*, we produced 100 sets of "encounter sampled" observations wherein we probabilistically included *sensed* encounters $v_k = 1$ estimated from the distribution $v_k|\boldsymbol{w}_k \sim \mathrm{Bern}\big(p(v_k = 1|\boldsymbol{w}_k)\big)$. In doing so, we assume that only patch encounters recognized by the animal guide the decision to *exploit* (Figure 4B). After removing *non-responding* encounters where $v_k = 0$, we defined observations of all covariates (i.e., ρ_k, τ_s, ρ_h, and ρ_e) using only *sensed* encounters.

To account for uncertainty in *exploitation* we modified the standard maximum likelihood. To understand our approach, consider that standard logistic regression models binary observations as realizations of the Bernoulli distribution $y_k|\boldsymbol{x}_k \sim \mathrm{Bern}\big(p(y_k = 1|\boldsymbol{\beta}\cdot\boldsymbol{x}_k)\big)$ and that the likelihood for this model is given by

$$\prod_k p(y_k = 1|\boldsymbol{\beta}\cdot\boldsymbol{x}_k)^{y_k}\left(1 - p(y_k = 1|\boldsymbol{\beta}\cdot\boldsymbol{x}_k)\right)^{1-y_k}$$

However, we do not have direct observations of y_k and cannot evaluate the logistic likelihood directly. Rather, we have posterior probabilities of *exploitation* determined by a classifier, denoted by $p(y_k = 1|\boldsymbol{z}_k)$, where $\boldsymbol{z}_k$ are a set of velocity-related features that are distinct from $\boldsymbol{x}_k$ (see Patch encounter classification as exploration or exploitation). Thus, rather than maximizing the Bernoulli likelihood, we accommodate our uncertainty about y_k by learning the regression parameters that minimize the Kullback-Leibler (KL) divergence between $p(y_k|\boldsymbol{\beta}\cdot\boldsymbol{x}_k)$ and the reference probability distribution $p(y_k|\boldsymbol{z}_k)$ as given by

$$\begin{aligned}
\mathcal{D}_{KL}[p(y_k|\boldsymbol{z}_k)||p(y_k|\boldsymbol{\beta}\cdot\boldsymbol{x}_k)] &\equiv \sum_{y_k} p(y_k|\boldsymbol{z}_k)\log\left[\frac{p(y_k|\boldsymbol{z}_k)}{p(y_k|\boldsymbol{\beta}\cdot\boldsymbol{x}_k)}\right] \\
&= C_{\boldsymbol{\beta}} - \sum_{y_k} p(y_k|\boldsymbol{z}_k)\log[p(y_k|\boldsymbol{\beta}\cdot\boldsymbol{x}_k)] \\
&= C_{\boldsymbol{\beta}} - \sum_{y_k} p(y_k|\boldsymbol{z}_k)\log\left[p(y_k|\boldsymbol{\beta}\cdot\boldsymbol{x}_k)^{y_k}\left(1 - p(y_k|\boldsymbol{\beta}\cdot\boldsymbol{x}_k)\right)^{1-y_k}\right] \\
&= C_{\boldsymbol{\beta}} - p(y_k = 1|\boldsymbol{z}_k)\log[p(y_k|\boldsymbol{\beta}\cdot\boldsymbol{x}_k)] \\
&\quad -\big(1 - p(y_k = 1|\boldsymbol{z}_k)\big)\log[1 - p(y_k|\boldsymbol{\beta}\cdot\boldsymbol{x}_k)] \\
&= C_{\boldsymbol{\beta}} \\
&\quad - \log\left[p(y_k|\boldsymbol{\beta}\cdot\boldsymbol{x}_k)^{p(y_k=1|\boldsymbol{z}_k)}\big(1 - p(y_k|\boldsymbol{\beta}\cdot\boldsymbol{x}_k)\big)^{1-p(y_k=1|\boldsymbol{z}_k)}\right]
\end{aligned}$$

1014 where C_β is a term that is constant with respect to $\boldsymbol{\beta}$, and the second term is equivalent to the
1015 logarithm of the logistic likelihood with $p(y_k = 1|\boldsymbol{z}_k)$ replacing y_k. Put plainly, minimizing the sum
1016 of the KL divergence between our classifier probabilities and logistic regression probabilities over all
1017 encounters k is equivalent to maximizing the logistic likelihood with our classifier-based *exploitation*
1018 probabilities $p(y_k = 1|\boldsymbol{z}_k)$ as observations instead of direct measurements of *exploitation* y_k as
1019 given by

$$\sum_k \log\left[p(y_k|\boldsymbol{\beta}\cdot\boldsymbol{x}_k)^{p(y_k=1|\boldsymbol{z}_k)}\left(1-p(y_k|\boldsymbol{\beta}\cdot\boldsymbol{x}_k)\right)^{1-p(y_k=1|\boldsymbol{z}_k)}\right]$$

1020 Notably, when there is no observation uncertainty $p(y_k = 1|\boldsymbol{z}_k)$ collapses to a delta function on
1021 $y_k = 1$ and we recover the standard likelihood function. Thus, our method is a generalization of
1022 maximum likelihood. To train our model, we therefore fit a standard logistic regression GLM where
1023 we provided sets of observations of covariates $\boldsymbol{x}_k$ and response variables $p(y_k = 1|\boldsymbol{z}_k)$ for *sensed*
1024 encounters.

1025 The covariates $\boldsymbol{x}_k$ included the relative density of the encountered patch k (ρ_k), the duration
1026 of time spent off food since departing the last *exploited* patch (τ_s), the relative density of the patch
1027 encountered immediately before encounter k (ρ_h), and the relative density of the last *exploited* patch
1028 (ρ_e). For every encounter k, ρ_k is the log-transformed relative density of the encounter patch as
1029 estimated from experiments using fluorescent bacteria OP50-GFP (as described in Bacterial patch
1030 density estimation). τ_s is the duration of time spent off food since the beginning of the recorded
1031 experiment (i.e., total time elapsed minus duration of time on patch). For the first patch encounter
1032 (i.e., $k = 1$), this is equivalent to the total time elapsed. ρ_h is the log-transformed relative density of
1033 the patch encountered immediately before encounter k. For the first patch encounter, we initialized
1034 this parameter using the approximated relative density of the bacterial patch on the acclimation
1035 plates (see Assay preparation and recording in Methods). Acclimation plates contained one large 200
1036 μL patch seeded with OD_{600} = 1 and grown for a total of ~48 hours. The relative density of these
1037 acclimation plates was estimated using the same procedure used to estimate values of ρ_k (see
1038 Bacterial patch density estimation). ρ_e is the log-transformed relative density of the most recently
1039 *exploited* patch. For the first patch encounter as well as every encounter prior to the first observed
1040 *exploitation*, we assume that animals must have *exploited* within the last 24 hours while on the
1041 acclimation plates and thus initialized ρ_e using the approximated relative density of the bacterial
1042 patch on the acclimation plates.

Exploitation of single-density, multi-patch environments

As described above, we used an "encounter sampling" protocol to generate 100 replicate observations of only *sensed* encounters by removing all encounters where *sensing* could not be determined (i.e., $v_k = 0$) as randomly estimated from the distribution $v_k|\boldsymbol{w}_k \sim \text{Bern}\big(p(v_k = 1|\boldsymbol{w}_k)\big)$. For example, we can consider an animal foraging in the single-density, multi-patch environment (Figure 4B). Although we detected 10 total encounters $K = k_1, k_2, \ldots, k_{10}$, several of these encounters had low probabilities of *sensing* $p(v_k = 1|\boldsymbol{w}_k)$ (Figure 4B). We use our "encounter sampling" protocol to simulate *sensation* of the patch during each of these 10 encounters and find that $v_k = 0$ for k_1, k_3, k_6 and k_8. By removing these 4 no response encounters, we generate a new observation comprised of the 6 *sensed* encounters $K_1^* = k_2, k_4, k_5, k_7, k_9, k_{10} = k_{1*}, k_{2*}, \ldots, k_{6*}$. Using only the data related to this new sequence of encounters K_1^*, we generated a vector of covariates (i.e., ρ_k, τ_s, ρ_h, and ρ_e). Importantly, this procedure considers time spent during the *no response* encounters k_1, k_3, k_6 and k_7 the same as time spent searching off patch. We repeated this process 100 times to generate new observations of encounter sequences (i.e., $K_1^*, K_2^*, \ldots, K_{100}^*$). In doing so, we reduced the number of encounters from 6,560 total encounters (as defined in Patch encounter detection) to 2,604-2,698 (μ = 2659.8, σ = 15.9) *sensed* encounters for each of the 100 replicates.

Additionally, we used a "worm sampling" protocol to generate 500 hierarchically bootstrapped replicates [97]. Specifically, we took our vector of 443 animals $A = a_1, a_2, \ldots, a_{443}$ and resampled with replacement (e.g., $A_1^* = a_{317}, a_{88}, \ldots, a_{130} = a_{1*}, a_{2*}, \ldots, a_{443*}$) to generate 500 new samples $A_1^*, A_2^*, \ldots, A_{500}^*$. When combined, the "encounter sampling" and "worm sampling" protocols created 50,000 unique replicates of observations of the covariates $\boldsymbol{x}_k$ and response variables $p(y_k = 1|\boldsymbol{z}_k)$ which were used to estimate the coefficients $\boldsymbol{\beta}$ (Figure 4C). A null distribution of coefficients $\boldsymbol{\beta}^*$ was estimated by shuffling the response variable vector (Figure 4 – supplement 1C). A two-tailed, one-sample bootstrap hypothesis test was used to assess whether our covariate estimates were significantly greater than or less than 0 (i.e., $\boldsymbol{p} = 2 \times \min[P(\boldsymbol{\beta} \leq \boldsymbol{0}), P(\boldsymbol{\beta} \geq \boldsymbol{0})]$).

Exploitation of food-deprived animals in single-density, multi-patch environments

To validate model predictions related to the satiety signal covariate τ_s, a novel data set of well-fed and 3-hour food-deprived animals foraging in single-density, multi-patch environments of relative density 5 was generated (Figure 4 – supplement 3A-B). The "encounter sampling" protocol described above was used to generate 100 replicates of observations of the covariates $\boldsymbol{x}_k$ and response variables $p(y_k = 1|\boldsymbol{z}_k)$ for this data set. As a result of "encounter sampling", we reduced the number of encounters from 42 total encounters to 30-37 (μ = 34.6, σ = 1.3) *sensed* encounters for food-deprived animals and 235 total encounters to 94-107 (μ = 99.8, σ = 2.1) *sensed* encounters for well-fed animals. Coefficient values $\boldsymbol{\beta}$ were re-estimated in the absence of the satiety signal τ_s (Figure 4 – supplement 3C) using the original single-density, multi-patch data set. Using the mean coefficient values $\boldsymbol{\beta}$ for both models (with and without satiety), we predicted the conditional probabilities of exploiting $p(y_k = 1|\boldsymbol{\beta} \cdot \boldsymbol{x}_k)$ for the new data set for well-fed and food-deprived animals. We subsequently simulated a series of *exploitation* events from a Bernoulli distribution using the estimated (i.e., $y_k|\boldsymbol{x}_k \sim \mathrm{Bern}\big(p(y_k = 1|\boldsymbol{\beta} \cdot \boldsymbol{x}_k)\big)$) and observed (i.e., $y_k|\boldsymbol{z}_k \sim \mathrm{Bern}\big(p(y_k = 1|\boldsymbol{z}_k)\big)$) *exploitation* probabilities. These simulated *exploitations* were used to generate distributions of the probability of an *exploitation* occurring for the first time as a function of the number of encounters (Figure 4 – supplement 3D).

Exploitation of multi-density, multi-patch environments

To investigate the individual contributions of a satiety-related signal and transfer-induced stress, a novel data set of animals foraging on multi-density, multi-patch environments was generated (Figure 4E, Figure 4 - supplement 4A-C). The "encounter sampling" protocol described above was used to generate 100 replicates of observations of the covariates $\boldsymbol{x}_k$ and response variables $p(y_k = 1|\boldsymbol{z}_k)$ for this data set. As a result of "encounter sampling", we reduced the number of encounters from 4,296 total encounters (350-984 total encounters per condition) to 1,702-1,745 (μ = 1,724.6, σ = 9.9) *sensed* encounters. Coefficient values $\boldsymbol{\beta}$ were estimated for models including combinations of τ_s, the duration of time an animal spent searching off-food since the last *exploitation* event, and τ_t, the duration of time since transfer (i.e., the time elapsed in the experiment) (Figure 4 – supplement 4D) using the new multi-density, multi-patch data set. While all coefficients were significant in models containing only τ_s or τ_t, only τ_s was significant in a model containing both terms (i.e., $p(y_k = 1|\beta_0 + \beta_k\rho_k + \beta_s\tau_s + \beta_t\tau_t + \beta_h\rho_h + \beta_e\rho_e)$).

1103 Further, to validate model predictions related to the prior experience covariates ρ_h and ρ_e,
1104 coefficient values $\boldsymbol{\beta}$ were re-estimated in the absence of the recently encountered and *exploited* patch
1105 density terms ρ_h and ρ_e (Figure 4 – supplement 4E) using the original single-density, multi-patch
1106 data set. Using the mean coefficient values $\boldsymbol{\beta}$ for both models (with and without prior experience),
1107 we predicted the probabilities of *exploiting* $p(y_k = 1|\boldsymbol{\beta} \cdot \boldsymbol{x}_k)$ for the new data set. To generate the
1108 heat maps of predicted behavior (Figure 4F), we varied ρ_k and ρ_h as well as ρ_k and ρ_e across a
1109 range of values and set the remaining covariate terms to the average values observed in the data set.
1110 To generate the heat maps of observed behavior (Figure 4F), we averaged the observed probabilities
1111 of *exploiting* $p(y_k = 1|\boldsymbol{z}_k)$ for each pairing of ρ_k and ρ_h as well as ρ_k and ρ_e and linearly
1112 interpolated values between these 9 points.
1113

1114 ***Exploitation of sensory mutants in single-density, multi-patch environments***

1115 To test the utility of our model in identifying covariate-specific phenotypes in animals with
1116 varied genotypes, a novel data set of wild-type animals and sensory mutants foraging on single-
1117 density, multi-patch environments was generated (Figure 4 - supplement 5A-B). The "encounter
1118 sampling" and "worm sampling" protocols described above were used to generate 50,000 replicates
1119 of observations of the covariates $\boldsymbol{x}_k$ and response variables $p(y_k = 1|\boldsymbol{z}_k)$ for this data set. As a
1120 result of "encounter sampling", we reduced the number of encounters from 1,352 total encounters
1121 (27-193 total encounters per condition) to 862-894 (μ = 879.4, σ = 7.4) *sensed* encounters. As the
1122 number of encounters were significantly less in these data sets as compared to the original single-
1123 density, multi-patch data set, we used ridge regression to regularize the magnitude of the covariates.
1124 We optimized each model across cross-validated replicates by varying the regularization value λ. We
1125 found that $\lambda_{\mathrm{N2}} = 0.0175$, $\lambda_{mec-4} = 0.0223$, and $\lambda_{osm-6} = 0.0614$ maximized the mean log-
1126 likelihood of each model (Figure 4 – supplement 5E). Coefficient values $\boldsymbol{\beta}$ were estimated for each
1127 of the three strains tested using these values (Figure 4 – supplement 5D). To assess whether the
1128 magnitude of coefficients significantly differed between wild-type and mutant models, we conducted
1129 a two-sample test of the mean of differences as given by

$$Z = \frac{\mu_{\mathrm{mutant}} - \mu_{\mathrm{N2}}}{\sqrt{\sigma^2_{\mathrm{mutant}} + \sigma^2_{\mathrm{N2}}}}$$

1130 where μ and σ are the mean and standard deviation, respectively, of the distribution of a covariate
1131 across replicates. Statistical significance was calculated as a left-tailed test $\phi(Z)$ for the density

coefficients (β_k, β_h, and β_e) and a two-tailed test $\phi(-|Z|)$ for the other coefficients (β_0 and β_s) where ϕ is the standard normal cumulative distribution function.

References

1. Lee D (2013). Decision making: From neuroscience to psychiatry. *Neuron* **78** (2): 233-248. https://doi.org/10.1016/j.neuron.2013.04.008.

2. Budaev S, Jørgensen C, Mangel M, Sigrunn E, and Giske J (2019). Decision-making from the animal perspective: Bridging ecology and subjective cognition. *Frontiers in Ecology and Evolution* **7**, 164. https://doi.org/10.3389/fevo.2019.00164.

3. Mobbs D, Trimmer PC, Blumstein DT, and Dayan P (2018). Foraging for foundations in decision neuroscience: Insights from ethology. *Nature Reviews Neuroscience* **19** (7): 419-427. https://doi.org/10.1038/s41583-018-0010-7.

4. Gold JI, and Shadlen MN (2007). The neural basis of decision making. *Annual Review of Neuroscience* **30**: 535-574. https://doi.org/10.1146/annurev.neuro.29.051605.113038.

5. Stephens DW (2008). Decision ecology: Foraging and the ecology of animal decision making. *Cognitive, Affective, & Behavioral Neuroscience* **8** (4): 475-484. https://doi.org/10.3758/CABN.8.4.475.

6. Hall-McMaster S, and Luyckx F (2019). Revisiting foraging approaches in neuroscience. *Cognitive, Affective, & Behavioral Neuroscience* **19**: 225-230. https://doi.org/10.3758/s13415-018-00682-z.

7. Schoener TW (1971). Theory of feeding strategies. *Annual Review of Ecology and Systematics* **2**: 369-404. https://doi.org/10.1146/annurev.es.02.110171.002101.

8. Pyke GH, Pulliam HR, and Charnov EL (1977). Optimal foraging: A selective review of theory and tests. *The Quarterly Review of Biology* **52** (2): 137-154. https://doi.org/10.1086/409852.

9. Stephens DW, and Krebs JR. (1986). Foraging Theory (Princeton University Press).

10. Stephens DW, Brown JS, and Ydenberg RC. (2007). Foraging: Behavior and Ecology (University of Chicago Press). 10.7208/9780226772653.

11. Nonacs P (2000). State dependent behavior and the Marginal Value Theorem. *Behavioral Ecology* **12** (1): 71-83. https://doi.org/10.1093/oxfordjournals.beheco.a000381.

12. Hills TT (2010). Animal foraging and the evolution of goal-directed cognition. *Cognitive Science* **30** (1): 3-41. https://doi.org/10.1207/s15516709cog0000_50.

13. Calhoun AJ, and Hayden BY (2015). The foraging brain. *Current Opinion in Behavioral Sciences* **5**: 24-31. https://doi.org/10.1016/j.cobeha.2015.07.003.

14. Charnov EL (1976). Optimal foraging, the marginal value theorem. *Theoretical Population Biology* **9** (2): 129-136. https://doi.org/10.1016/0040-5809(76)90040-x.

1166 15. Haley JA, and Chalasani SH (2024). *C. elegans* foraging as a model for understanding the neuronal
1167 basis of decision-making. *Cellular and Molecular Life Sciences* **81**, 252.
1168 https://doi.org/10.1007/s00018-024-05223-1.

1169 16. Brenner S (1974). The genetics of *Caenorhabditis elegans*. *Genetics* **77** (1): 71-94.
1170 https://doi.org/10.1093/genetics/77.1.71.

1171 17. Faumont S, and Lockery SR (2006). The awake behaving worm: Simultaneous imaging of
1172 neuronal activity and behavior in intact animals at millimeter scale. *Journal of Neurophysiolovy*
1173 **95**: 1976-1981. https://doi.org/10.1152/jn.01050.2005.

1174 18. Boulin T, and Hobert O (2012). From genes to function: The *C. elegans* genetic toolbox. *Wiley*
1175 *Interdisciplinary Review Developmental Biology* **1** (1): 114-137. https://doi.org/10.1002/wdev.1.

1176 19. Samuel BS, Rowedder H, Braendle C, Félix M-A, and Ruvkun G (2016). *Caenorhabditis elegans*
1177 responses to bacteria from its natural habitats. *PNAS* **113** (27): E3941-E3949.
1178 https://doi.org/10.1073/pnas.1607183113.

1179 20. White JG, Southgate E, Thomson JN, and Brenner S (1986). The structure of the nervous
1180 system of the nematode *Caenorhabditis elegans*. *Philisophical Transactions of the Royal Society B* **314**
1181 (1165): 1-340. https://doi.org/10.1098/rstb.1986.0056.

1182 21. de Bono M, and Maricq AV (2005). Neuronal substrates of complex behaviors in *C. elegans*.
1183 *Annual Review of Neuroscience* **28**: 451-501.
1184 https://doi.org/10.1146/annurev.neuro.27.070203.144259.

1185 22. Colbert HA, and Bargmann CI (1995). Odorant-specific adaptation pathways generate olfactory
1186 plasticity in *C. elegans*. *Neuron* **14** (4): 803-812. https://doi.org/10.1016/0896-6273(95)90224-
1187 4.

1188 23. Zhang Y, Lu H, and Bargmann CI (2005). Pathogenic bacteria induce aversive olfactory learning
1189 in *Caenorhabditis elegans*. *Nature* **438**: 179-184. https://doi.org/10.1038/nature04216.

1190 24. Ardiel EL, and Rankin CH (2010). An elegant mind: Learning and memory in *Caenorhabditis*
1191 *elegans*. *Learning & Memory* **17**: 191-201. https://doi.org/10.1101/lm.960510.

1192 25. Calhoun AJ, Tong A, Sharpee TO, and Chalasani SH (2015). Neural mechanisms for evaluating
1193 environmental variability in *Caenorhabditis elegans*. *Neuron* **86**: 428-441.
1194 https://doi.org/10.1016/j.neuron.2015.03.026.

1195 26. Bendesky A, Tsunozaki M, Rockman MV, Kruglyak L, and Bargmann CI (2011). Catecholamine
1196 receptor polymorphisms affect decision-making in *C. elegans*. *Nature* **472** (7343): 313-318.
1197 https://doi.org/10.1038/nature09821.

1198 27. Faumont S, Lindsay TH, and Lockery SR (2012). Neuronal microcircuits for decision making in
1199 *C. elegans*. *Current Opinion in Neurobiology* **22** (4): 580-591.
1200 https://doi.org/10.1016/j.conb.2012.05.005.

1201 28. Iwanir S, Brown AS, Nagy S, Najjar D, Kazakov A, Lee KS, Zaslaver A, Levine E, and Biron D
1202 (2016). Serotonin promotes exploitation in complex environments by accelerating decision-
1203 making. *BMC Biology* **14** (9). https://doi.org/10.1186/s12915-016-0232-y.

1204 29. Tanimoto Y, Yamazoe-Umemoto A, Fujita K, Kawazoe Y, Miyanishi Y, Yamazaki SJ, Fei X,
1205 Busch KE, Gengyo-Ando K, Nakai J, Iino Y, Iwasaki Y, Hashimoto K, and Kimura KD
1206 (2017). Calcium dynamics regulating the timing of decision-making in *C. elegans*. *eLife* **6**:
1207 e21629. https://doi.org/10.7554/eLife.21629.

1208 30. Ji N, Madan GK, Fabre GI, Dayan A, Baker CM, Kramer TS, Nwabudike I, and Flavell SW
1209 (2021). A neural circuit for flexible control of persistent behavioral states. *eLife* **10**: e62889.
1210 https://doi.org/10.7554/eLife.62889.

1211 31. Scheer E, and Bargmann CI (2023). Sensory neurons couple arousal and foraging decisions in *C.*
1212 *elegans*. *eLife* **12**: RP88657. https://doi.org/10.7554/eLife.88657.3.

1213 32. Petersen C, Dirksen P, and Schulenburg H (2015). Why we need more ecology for genetic
1214 models such as *C. elegans*. *Trends in Genetics* **31** (3): 120-127.
1215 https://doi.org/10.1016/j.tig.2014.12.001.

1216 33. Volgin AD, Yakovlev OV, Demin KA, de Abreu MS, Rosemberg DB, Meshalkina DA,
1217 Alekseeva PA, Friend AJ, Amstislavskaya TG, and Kalueff AV (2018). Understanding the
1218 role of environmental enrichment in zebrafish neurobehavioral models. *Zebrafish* **15** (5): 425-
1219 432. https://doi.org/10.1089/zeb.2018.1592.

1220 34. Kempermann G (2019). Environmental enrichment, new neurons and the neurobiology of
1221 individuality. *Nature Reviews Neuroscience* **20** (4): 235-245. https://doi.org/10.1038/s41583-
1222 019-0120-x.

1223 35. Guisnet A, Maitra M, Pradhan S, and Hendricks M (2021). A three-dimensional habitat for *C.*
1224 *elegans* environmental enrichment. *PLoS One* **16** (1): e0245139.
1225 https://doi.org/10.1371/journal.pone.0245139.

1226 36. Shtonda BB, and Avery L (2006). Dietary choice behavior in *Caenorhabditis elegans*. *Journal of*
1227 *Experimental Biology* **209** (1): 89-102. https://doi.org/10.1242/jeb.01955.

1228 37. Hills T, Brockie PJ, and Maricq AV (2004). Dopamine and glutamate control area-restricted
1229 search behavior in *Caenorhabditis elegans*. *Journal of Neuroscience* **24** (5): 1217-1225.
1230 https://doi.org/10.1523/JNEUROSCI.1569-03.2004.

1231 38. Calhoun AJ, Chalasani SH, and Sharpee TO (2014). Maximally informative foraging by
1232 *Caenorhabditis elegans*. *eLife* **3**: e04220. https://doi.org/10.7554/eLife.04220.001.

1233 39. Gray JM, Hill JJ, and Bargmann CI (2005). A circuit for navigation in *Caenorhabditis elegans*. *PNAS*
1234 **102** (9): 3184-3191. https://doi.org/10.1073/pnas.0409009101.

1235 40. Milward K, Busch KE, Murphy RJ, de Bono M, and Olofsson B (2011). Neuronal and molecular
1236 substrates for optimal foraging in *Caenorhabditis elegans*. *PNAS* **108** (51): 20672-20677.
1237 https://doi.org/10.1073/pnas.1106134109.

41. Olofsson B (2014). The olfactory neuron AWC promotes avoidance of normally palatable food following chronic dietary restriction. *Journal of Experimental Biology* **217** (10): 1790-1798. https://doi.org/10.1242/jeb.099929.

42. Pradhan S, Quilez S, Homer K, and Hendricks M (2019). Environmental programming of adult foraging behavior in *C. elegans*. *Current Biology* **29**: 2867-2879. https://doi.org/10.1016/j.cub.2019.07.045.

43. Gloria-Soria A, and Azevedo RBR (2008). *npr-1* regulates foraging and dispersal strategies in *Caenorhabditis elegans*. *Current Biology* **18** (21): 1694-1699. https://doi.org/10.1016/j.cub.2008.09.043.

44. Madirolas G, Al-Asmar A, Gaouar L, Marie-Louise L, Garza-Enríquez A, Rodríguez-Rada V, Khona M, Dal Bello M, Ratzke C, Gore J, and Pérez-Escudero A (2023). *Caenorhabditis elegans* foraging patterns follow a simple rule of thumb. *Communications Biology* **6**, 841. https://doi.org/10.1038/s42003-023-05220-3.

45. Fujiwara M, Sengupta P, and McIntire SL (2002). Regulation of body size and behavioral state of *C. elegans* by sensory perception and the EGL-4 cGMP-dependent protein kinase. *Neuron* **36** (6): 1091-1102. https://doi.org/10.1016/s0896-6273(02)01093-0.

46. Sawin ER, Ranganathan R, and Horvitz HR (2000). *C. elegans* locomotory rate is modulated by the environment through a dopaminergic pathway and by experience through a serotonergic pathway. *Neuron* **26** (3): 619-631. https://doi.org/10.1016/S0896-6273(00)81199-X.

47. Ahmed MO, and Walther G (2012). Investigating the multimodality of multivariate data with principal curves. *Computational Statistics & Data Analysis* **56** (12): 4462-4469. https://doi.org/10.1016/j.csda.2012.02.020.

48. Silverman BW (1981). Using kernel density estimates to investigate multimodality. *Journal of the Royal Statistical Society: Series B (Methodological)* **43** (1): 97-99. https://doi.org/10.1111/j.2517-6161.1981.tb01155.x.

49. Fawcett TW, McNamara JM, and Houston AI (2012). When is it adaptive to be patient? A general framework for evaluating delayed rewards. *Behavioural Processes* **89** (2): 128-136. https://doi.org/10.1016/j.beproc.2011.08.015.

50. Susini I, Safryghin A, HIllemann F, and Wascher CAF (2021). Delay of gratification in non-human animals: A review of inter-specific variation in performance. *bioRxiv*. https://doi.org/10.1101/2020.05.05.078659.

51. Constantino SM, and Daw ND (2015). Learning the opportunity cost of time in a patch-foraging task. *Cognitive, Affective, & Behavioral Neuroscience* **15**: 837-853. https://doi.org/10.3758/s13415-015-0350-y.

52. Carter EC, Pedersen EJ, and McCullough ME (2015). Reassessing intertemporal choice: Human decision-making is more optimal in a foraging task than in a self-control task. *Frontiers in Psychology* **6**, 95. https://doi.org/10.3389/fpsyg.2015.00095.

1275 53. Hayden BY (2018). Why has evolution not selected for perfect self-control? *Philisophical*
1276 *Transactions of the Royal Society B* **374** (1766). https://doi.org/10.1098/rstb.2018.0139.

1277 54. Stephens DW, and Anderson D (2001). The adaptive value of preference for immediacy: When
1278 shortsighted rules have farsighted consequences. *Behavioral Ecology* **12** (3): 330-339.
1279 https://doi.org/10.1093/beheco/12.3.330.

1280 55. Ferguson TS (1967). Sequential Decision Problems. In Mathematical Statistics: A Decision
1281 Theoretic Approach, Z.W. Birnbaum, and E. Lukacs, eds. (Academic Press).

1282 56. Robbins H (1970). Optimal stopping. *The American Mathematical Monthly* **77** (4): 333-343.
1283 https://doi.org/10.2307/2316139.

1284 57. Mischel W, and Ebbesen EB (1970). Attention in delay of gratification. *Journal of Personality and*
1285 *Social Psychology* **16** (2): 329-337. https://doi.org/10.1037/h0029815.

1286 58. Rosati AG, Stevens JR, Hare B, and Hauser MD (2007). The evolutionary origins of human
1287 patience: Temporal preferences in chimpanzees, bonobos, and human adults. *Current Biology*
1288 **17** (19): 1663-1668. https://doi.org/10.1016/j.cub.2007.08.033.

1289 59. Schnell AK, Boeckle M, Rivera M, Clayton NS, and Hanlon RT (2021). Cuttlefish exert self-
1290 control in a delay of gratification task. *Proceedings of the Royal Society B: Biological Sciences* **288**,
1291 1946. https://doi.org/10.1098/rspb.2020.3161.

1292 60. Range F, Brucks D, and Virányi Z (2020). Dogs wait longer for better rewards than wolves in a
1293 delay of gratification task: But why? *Animal Cognition* **23** (3): 443-453.
1294 https://doi.org/10.1007/s10071-020-01346-7.

1295 61. Hillemann F, Bugnyar T, Kotrschal K, and Wascher CAF (2014). Waiting for better, not for
1296 more: Corvids respond to quality in two delay maintenance tasks. *Animal Behaviour* **90**: 1-10.
1297 https://doi.org/10.1016/j.anbehav.2014.01.007.

1298 62. Miller R, Frohnwieser A, Schiestl M, McCoy DE, Gray RD, Taylor AH, and Clayton NS (2020).
1299 Delayed gratification in New Caledonian crows and young children: Influence of reward type
1300 and visibility. *Animal Cognition* **23** (1): 71-85. https://doi.org/10.1007/s10071-019-01317-7.

1301 63. Pujol N, Link EM, Liu LX, Kurz CL, Alloing G, Tan M-W, Ray KP, Solari R, Johnson CD, and
1302 Ewbank JJ (2001). A reverse genetic analysis of components of the Toll signaling pathway in
1303 *Caenorhabditis elegans. Current Biology* **11** (11): 809-821. https://doi.org/10.1016/S0960-
1304 9822(01)00241-X.

1305 64. Melo JA, and Ruvkun G (2012). Inactivation of conserved *C. elegans* genes engages pathogen-
1306 and xenobiotic-associated defenses. *Cell* **149** (2): 452-466.
1307 https://doi.org/10.1016/j.cell.2012.02.050.

1308 65. Pradel E, Zhang Y, Pujol N, Matsuyama T, Bargmann CI, and Ewbank JJ (2007). Detection and
1309 avoidance of a natural product from the pathogenic bacterium *Serratia marcescens* by
1310 *Caenorhabditis elegans. PNAS* **104** (7): 2295-2300. https://doi.org/10.1073/pnas.0610281104.

1311 66. Quach KT, and Chalasani SH (2022). Flexible reprogramming of *Pristionchus pacificus* motivation
1312 for attacking *Caenorhabditis elegans* in predator-prey competition. *Current Biology* **32**: 1-14.
1313 https://doi.org/10.1016/j.cub.2022.02.033.

1314 67. Pribadi A, Rieger MA, Rosales K, Reddy KC, and Chalasani SH (2023). Dopamine signaling
1315 regulates predator-driven changes in *Caenorhabditis elegans'* egg laying behavior. *eLife* **12**:
1316 e83957. https://doi.org/10.7554/eLife.83957.

1317 68. Busch KE, and Olofsson B (2012). Should I stay or should I go? *Worm* **1** (3): 182-186.
1318 https://doi.org/10.4161/worm.20464.

1319 69. Hallatschek O, Hersen P, Ramanathan S, and Nelson DR (2007). Genetic drift at expanding
1320 frontiers promotes gene segregation. *PNAS* **104** (50): 19926-19930.
1321 https://doi.org/10.1073/pnas.0710150104.

1322 70. Krebs JR, and Inman AJ (1992). Learning and foraging: Individuals, groups, and populations. *The*
1323 *American Naturalist* **140**: S63-S84. https://doi.org/10.1086/285397.

1324 71. Frézal L, and Félix M-A (2015). *C. elegans* outside the Petri dish. *eLife* **4**: e05849.
1325 https://doi.org/10.7554/eLife.05849.

1326 72. Matty MA, Lau HE, Haley JA, Singh A, Chakraborty A, Kono K, Reddy KC, Hansen M, and
1327 Chalasani SH (2022). Intestine-to-neuronal signaling alters risk-taking behaviors in food-
1328 deprived *Caenorhabditis elegans*. *PLoS Genetics* **18** (5): e1010178.
1329 https://doi.org/10.1371/journal.pgen.1010178.

1330 73. Ezcurra M, Tanizawa Y, Swoboda P, and Schafer WR (2011). Food sensitizes *C. elegans*
1331 avoidance behaviors through acute dopamine signaling. *EMBO Journal* **30** (6): 1110-1122.
1332 https://doi.org/10.1038/emboj.2011.22.

1333 74. Anderson JL, Albergotti L, Ellebracht B, Huey RB, and Phillips PC (2011). Does
1334 thermoregulatory behavior maximize reproductive fitness of natural isolates of *Caenorhabditis*
1335 *elegans*. *BMC Evolutionary Biology* **11**, 157. https://doi.org/10.1186/1471-2148-11-157.

1336 75. Petersen C, Dirksen P, Prahl S, Strathmann EA, and Schulenburg H (2014). The prevalence of
1337 *Caenorhabditis elegans* across 1.5 years in selected North German locations: The importance of
1338 substrate type, abiotic parameters, and *Caenorhabditis* competitors. *BMC Ecology* **6** (14), 4.
1339 https://doi.org/10.1186/1472-6785-14-4.

1340 76. Fraune S, and Bosch TCG (2010). Why bacteria matter in animal development and evolution.
1341 *BioEssays* **32** (7): 571-580. https://doi.org/10.1002/bies.200900192.

1342 77. Dirksen P, Assié A, Zimmerman J, Zhang F, Tietje A-M, Marsh SA, Félix M-A, Shapira M,
1343 Kaleta C, Schulenburg H, and Samuel BS (2020). CeMbio - The *Caenorhabiditis elegans*
1344 microbiome resource. *G3 Genes|Genomes|Genetics* **10** (9): 3025-3039.
1345 https://doi.org/10.1534/g3.120.401309.

1346 78. Ding SS, Muhle LS, Brown AEX, Schumacher LJ, and Endres RG (2020). Comparison of
1347 solitary and collective foraging strategies of *Caenorhabditis elegans* in patchy food distributions.

1348 *Philosophical Transactions of the Royal Society B* **375**, 37520190382.
1349 https://doi.org/10.1098/rstb.2019.0382.

1350 79. Lipton J, Kleemann G, Ghosh R, Lints R, and Emmons SW (2004). Mate searching in
1351 *Caenorhabditis elegans*: A genetic model for sex drive in a simple invertebrate. *Journal of*
1352 *Neuroscience* **24** (34): 7427-7434. https://doi.org/10.1523/JNEUROSCI.1746-04.2004.

1353 80. Barrios A, Nurrish S, and Emmons SW (2008). Sensory regulation of *C. elegans* male mate-
1354 searching behavior. *Current Biology* **18** (23): 1865-1871.
1355 https://doi.org/10.1016/j.cub.2008.10.050.

1356 81. Matsuura T, Sato T, and Shingai R (2005). Interactions between *Caenorhabditis elegans* individuals
1357 during chemotactic responses. *Zoological Science* **22** (10): 1095-1103.
1358 https://doi.org/10.2108/zsj.22.1095.

1359 82. Gray J, and Lissmann HW (1964). The locomotion of nematodes. *Journal of Experimental Biology*
1360 **41**: 135-154. https://doi.org/10.1242/jeb.41.1.135.

1361 83. Croll NA (1975). Behavioural analysis of nematode movement. *Advances in Parasitology* **13**: 71-122.
1362 https://doi.org/10.1016/s0065-308x(08)60319-x.

1363 84. Croll NA (1975). Components and patterns in the behavior of the nematode *Caenorhabditis*
1364 *elegans*. *Journal of Zoology* **176** (2): 159-176. https://doi.org/10.1111/j.1469-
1365 7998.1975.tb03191.x.

1366 85. You Y-j, Kim J, Raizen DM, and Avery L (2008). Insulin, cGMP, TGF-beta signals regulate food
1367 intake and quiescence in *C. elegans*: A model for satiety. *Cell Metabolism* **7** (3): 249-257.
1368 https://doi.org/10.1016/j.cmet.2008.01.005.

1369 86. Prevedel R, Yoon Y-G, Hoffmann M, Pak N, Wetzstein G, Kato S, Schrödel T, Raskar R,
1370 Zimmer M, Boyden ES, and Vaziri A (2014). Simultaneous whole-animal 3D imaging of
1371 neuronal activity using light-field microscopy. *Nature Methods* **11**: 727=730.
1372 https://doi.org/10.1038/nmeth.2964.

1373 87. Nguyen JP, Shipley FB, Linder AN, Plummer GS, Liu M, Setru SU, Shaevitz JW, and Leifer AM
1374 (2015). Whole-brain calcium imaging with cellular resolution in freely behaving *Caenorhabditis*
1375 *elegans*. *PNAS* **113** (8): E1074-E1081. https://doi.org/10.1073/pnas.1507110112.

1376 88. Venkatachalam V, Ji N, Wang X, Clark C, Mitchell JK, Klein M, Tabone CJ, Florman J, Ji H,
1377 Greenwood J, Chisholm AD, Srinivasan J, Alkema M, Zhen M, and Samuel ADT (2015).
1378 Pan-neuronal imaging in roaming *Caenorhabditis elegans*. *PNAS* **113** (8): E1082-E1088.
1379 https://doi.org/10.1073/pnas.1507109113.

1380 89. Voleti V, Patel KB, Li W, Perez Campos C, Bharadwaj S, Yu H, Ford C, Casper MJ, Yan RW,
1381 Liang W, Wen C, Kimura KD, Targoff KL, and Hillman EMC (2019). Real-time volumetric
1382 microscopy of *in vivo* dynamics and large-scale samples with SCAPE 2.0. *Nature Methods* **16**
1383 (10): 1054-1062. https://doi.org/10.1038/s41592-019-0579-4.

1384 90. Hallinen KM, Dempsey R, Scholz M, Yu X, Linder AN, Randi F, Sharma AK, Shaevitz JW, and
1385 Leifer AM (2021). Decoding locomotion from population neural activity in moving *C.*
1386 *elegans. eLife* **10**: e66135. https://doi.org/10.7554/eLife.66135.

1387 91. Davidson JD, and El Hady A (2019). Foraging as an evidence accumulation process. *PLoS*
1388 *Computational Biology* **15** (7): e1007060. https://doi.org/10.1371/journal.pcbi.1007060.

1389 92. Labrousse A, Chauvet S, Couillault C, Kurz CL, and Ewbank JJ (2000). *Caenorhabditis elegans* is a
1390 model host for *Salmonella typhimurium. Current Biology* **10** (23): 1543-1545.
1391 https://doi.org/10.1016/S0960-9822(00)00833-2.

1392 93. Quach KT, Hughes GA, and Chalasani SH (2024). Interdependence between SEB-3 and NLP-
1393 49 peptides shifts across predator-induced defensive behavioral modes in *Caenorhabditis*
1394 *elegans. eLife* **13**: RP98262. https://doi.org/10.7554/eLife.98262.1.

1395 94. Morse JM (1995). The Significance of saturation. *Qualitative Health Research* **5** (2): 147-149.
1396 https://doi.org/10.1177/104973239500500201.

1397 95. Sulston JE, and Brenner S (1974). The DNA of *Caenorhabditis elegans. Genetics* **77** (1): 95-104.
1398 https://doi.org/10.1093/genetics/77.1.95.

1399 96. Silverman BW. (1986). Density Estimation for Statistics and Data Analysis (Chapman & Hall).

1400 97. Saravanan V, Berman GJ, and Sober SJ (2020). Application of the hierarchical bootstrap to
1401 multi-level data in neuroscience. *Neurons, Behavior, Data analysis, and Theory* **3** (5).
1402

Figures

Figure 1: *C. elegans* forage in a patchy environment with an explore-then-exploit strategy.

(A) An example animal's midbody location (colored to represent time in the experiment) as it forages in an environment bounded by a large (30 mm diameter) arena containing 19 small (~1.8 mm diameter) bacterial patches (gray). Each patch was made by pipetting ~0.5 μL of OP50 *E. coli* diluted to OD_{600} ~10 and grown at room temperature for ~1 hour. (B) Distance between the example animal's midbody position and the nearest patch edge (positive indicates inside patch) is plotted (black) for every time point. Putative encounters with a bacterial patch are indicated (gray). (C) Patch encounters (colored to represent the duration of the encounter) for 50 individuals foraging in these environments are plotted. (D) The number of total and unique patch encounters for each animal are shown. (E) Duration for each patch encounter was computed and classified as either short (0-2 minutes) or long (2-60 minutes) using a Gaussian mixture model. The distributions of all observed short and long encounters are plotted with duration binned logarithmically. (F) The observed start time of each patch encounter is shown for all short and long duration encounters. Long duration encounters occur significantly later (one-tailed Mann-Whitney U-Test). (G) The probability of residing on patch was computed for all worms across time (black) and compared to the probability of residing on patch if patch locations were semi-randomly permuted (pink). Smoothed median values are plotted with bootstrap-derived 2.5% and 97.5% quantiles shown in shaded regions. Time points where observed probabilities of residing on patch significantly exceed permuted probabilities are indicated by a black line (one-tailed Fisher's exact test with Benjamini-Hochberg correction). (H) The track of the example animal in (A) is replotted with color used to represent the animal's instantaneous velocity at each time point. (I) Velocity of the example animal over time is plotted (black) alongside patch encounters (gray) as previously identified in (B). Example encounters – one early, short duration (green) and one late, long duration (blue) – are indicated. (J,K) A 60-second time window surrounding the start of these example encounters is enlarged. (L) Velocity trajectories were aligned to patch entry for every encounter. Mean encounter-aligned (black/gray) and randomly-aligned (pink) trajectories are plotted for each animal (light) and across all animals (dark). (M) Deceleration upon encounter with the patch edge is plotted for every encounter and grouped by duration type. Deceleration was significantly lower for encounter-aligned as compared to randomly-aligned trajectories (pink) for all duration types (one-tailed Mann-Whitney U-Tests with Bonferroni Correction). (N) Mean velocity as a function of the distance from the edge of bacterial patches (computed for 50 μm bins) is shown for every animal (gray) and across all animals (black). (O) Each animal's mean velocity during time spent on and off (midpoint at least -0.46 mm from patch edge) patch is shown. Velocity on patch was significantly slower than off patch (one-tailed paired-sample *t*-test). Sample data for one animal (worm #1) are shown in (A-C,H-K). Summary data for all animals (N = 50 worms) and encounters (N = 419 total encounters) are shown in (D-G,L-O). Violin plots in (D,F,M,O) give the KDE and quartiles for each measure. Asterisks denote statistical significance (***$p<0.001$). See also Figure 1 – supplement 1-5 and Video 1-4.

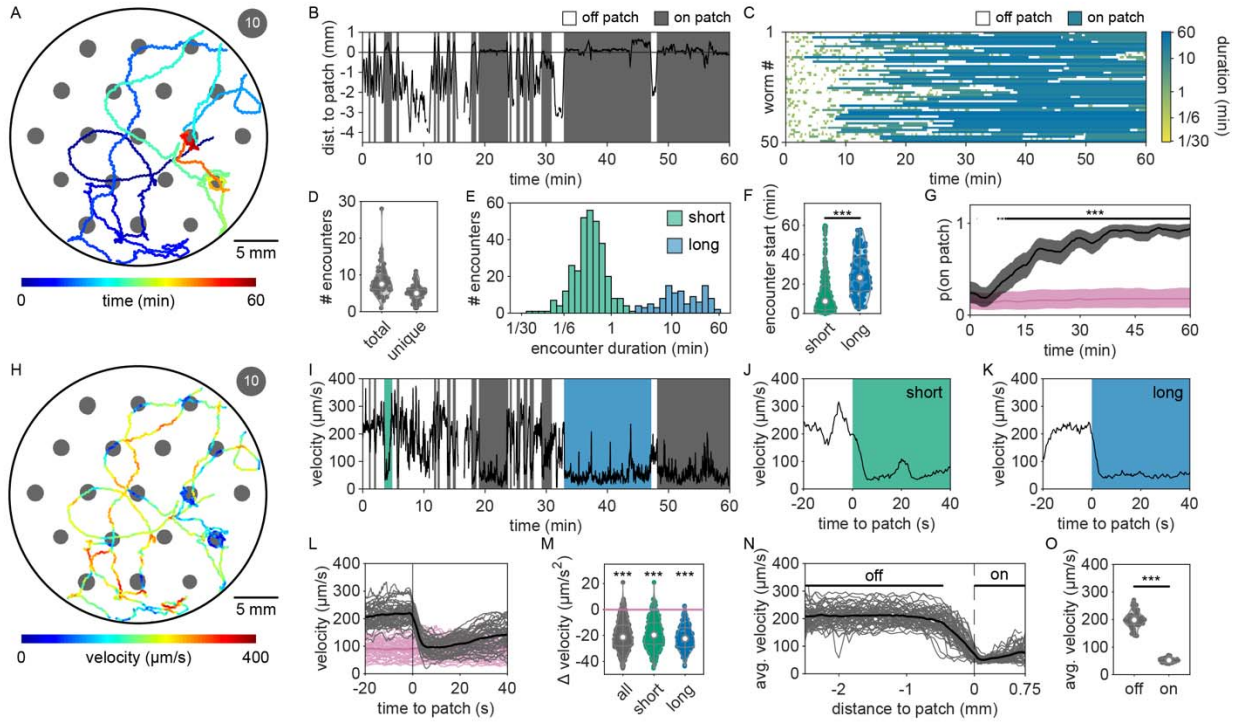
A
10
5 mm
0
time (min)
60
B
off patch
on patch
dist. to patch (mm)
time (min)
C
off patch
on patch
worm #
duration (min)
time (min)
D
encounters
total
unique
E
encounters
short
long
encounter duration (min)
F
encounter start (min)
short
long
G
p(on patch)
time (min)
H
10
5 mm
0
velocity (µm/s)
400
I
velocity (µm/s)
time (min)
J
short
velocity (µm/s)
time to patch (s)
K
long
velocity (µm/s)
time to patch (s)
L
velocity (µm/s)
time to patch (s)
M
Δ velocity (µm/s²)
all
short
long
N
off
on
avg. velocity (µm/s)
distance to patch (mm)
O
avg. velocity (µm/s)
off
on

1444 **Figure 2: The timing of the switch from explore-to-exploit is density-dependent.**
1445
1446 (A) The relative density (as estimated by fluorescently-labeled OP50-GFP) is shown for small (~1.8
1447 mm diameter) bacterial patches made by pipetting ~0.5 μL droplets of OP50 *E. coli* diluted in LB to
1448 a range of optical densities (OD_{600} = {0, 0.05, 0.1, 0.5, 1, 2, 3, 4, 5, 10} and controlling growth time
1449 at room temperature (hours = {1, 12, 48}). For (A-G,L-O), gray-scale color saturation is
1450 proportional to the relative density of each condition and corresponds to labels in (A). (B) The
1451 mean velocities of animals foraging in environments containing patches matching one of the 12
1452 bacterial densities are plotted as a function of the distance from the edge of bacterial patches
1453 (computed for 50 μm bins). (C) Animals' average on-patch velocity is plotted as a function of the
1454 relative density of bacteria. Compared to animals foraging amongst bacteria-free patches containing
1455 only LB (relative density 0), animals foraging on bacterial patches with relative density of 0.5 or
1456 greater display significantly slower on-patch velocities (one-tailed Mann-Whitney U-Tests with
1457 Bonferroni Correction). (D) The midbody location (colored to represent time in the experiment) of
1458 example animals foraging in environments containing patches (gray) of relative density 0, 1, 5, 10,
1459 and 200 are shown. (E) The total time each animal spent on patch is plotted as a function of the
1460 relative density of bacteria. Time on patch increased monotonically with increasing bacterial density
1461 (Kendall's τ correlation, $p<0.001$) following a sigmoidal trend. (F) Smoothed median values of the
1462 probability of worms residing on patch over time for each density condition are plotted. Time
1463 points where observed probabilities of residing on patch either match (pink) or significantly exceed
1464 (gray) the probability of residing on patch if patch locations were semi-randomly permuted are
1465 indicated (one-tailed Fisher's exact test with Benjamini-Hochberg correction). (G) A KDE of the
1466 distribution of encounter durations is plotted for each density condition. (H) For each encounter,
1467 the average velocity of the animal during the encounter and the duration of that encounter are
1468 plotted on a double-logarithmic plot with color representing the probabilities of clustering
1469 classification as *search* (orange), *sample* (green), or *exploit* (blue). Contours showing the first, second,
1470 and third standard deviation of the GMM used to classify *explore* and *exploit* encounters are shown as
1471 shaded ellipses with saturation corresponding to standard deviation. KDEs for distributions of
1472 average on-patch velocity and encounter duration are plotted for each encounter type. (I) For each
1473 encounter, the minimum on-patch velocity and maximum change in velocity are plotted. Contours
1474 showing the separation of *sensing* and *non-responding* encounters as estimated by semi-supervised
1475 QDA are indicated. A KDE for the distribution of the maximum change in velocity is plotted for
1476 each encounter type. (J) Features used to classify encounters as *search*, *sample*, or *exploit* are
1477 summarized. (K) KDEs of the distributions of animals' velocities are shown for all timepoints
1478 during search off and on patch as well as during sample and exploit encounters. (L) Ethograms of
1479 patch encounters (colored to represent the probability of classification as *search*, *sample*, and *exploit*)
1480 are shown for 443 individuals. (M) The average proportion of each encounter type over time is
1481 plotted. (N) Time elapsed and (O) number of encounters occurring prior to the first *exploitation*
1482 event are plotted for every animal (blue). In the event that no *exploitation* event occurred, the
1483 maximum observed time and encounters are plotted (red-orange). Both time and encounter number
1484 before *exploitation* decrease monotonically with increasing patch density (Kendall's τ correlation,
1485 $p<0.001$) following a sigmoidal trend. Summary data for all animals (N = 443 total worms; N = 20-
1486 50 worms per condition) and encounters (N = 6,560 total encounters; N = 46-876 encounters per
1487 condition) are shown in (A-C,E-I,K-O). Asterisks denote statistical significance (***$p<0.001$). See
1488 also Figure 2 – supplement 1-8 and Video 5-6.

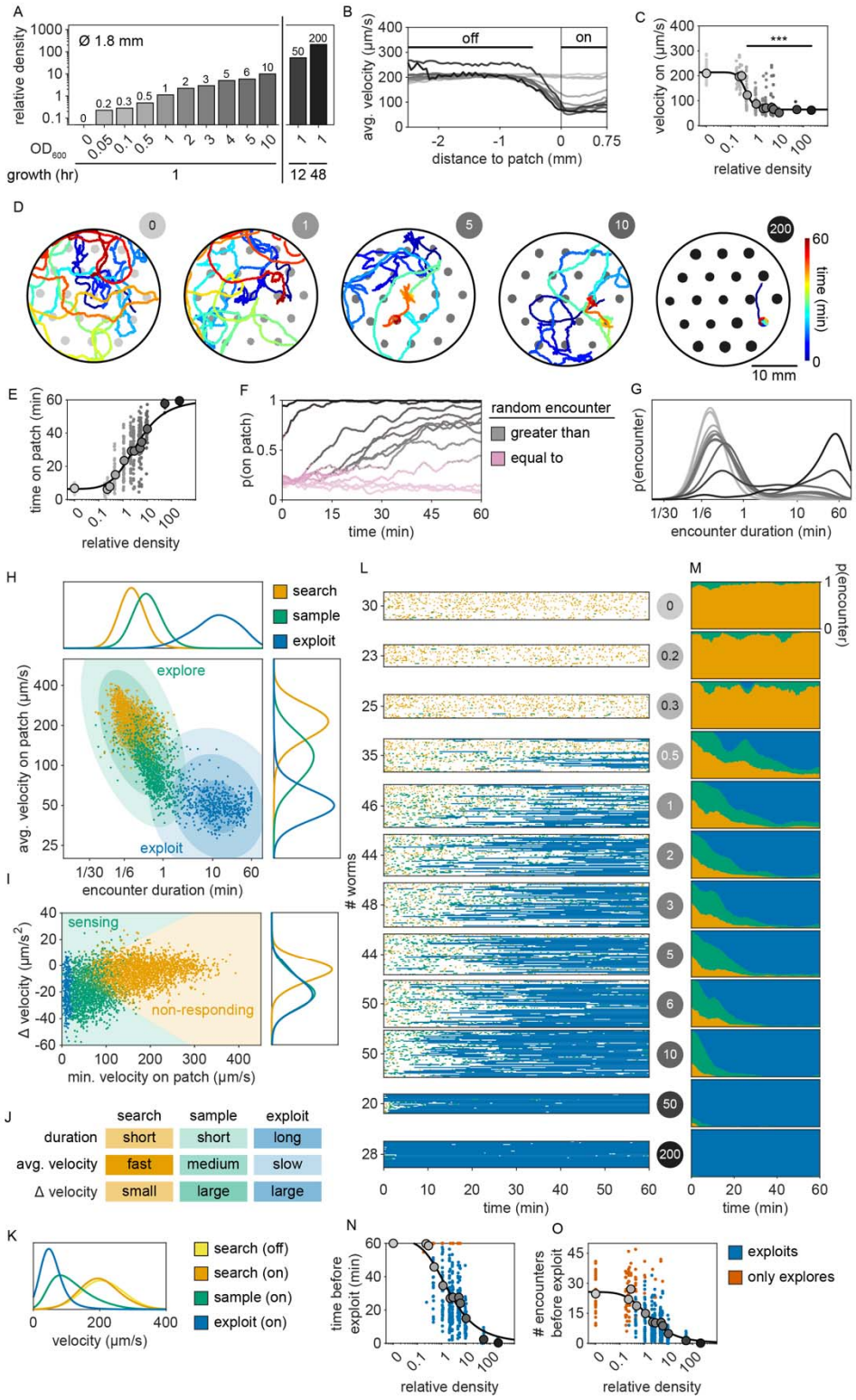
A
relative density
Ø 1.8 mm
OD600
growth (hr)
B
avg. velocity (µm/s)
off
on
distance to patch (mm)
C
velocity on (µm/s)
relative density
D
time (min)
10 mm
E
time on patch (min)
relative density
F
p(on patch)
random encounter
greater than
equal to
time (min)
G
p(encounter)
encounter duration (min)
H
search
sample
exploit
explore
avg. velocity on patch (µm/s)
encounter duration (min)
I
sensing
non-responding
Δ velocity (µm/s²)
min. velocity on patch (µm/s)
J
search
sample
exploit
duration
avg. velocity
Δ velocity
short
short
long
fast
medium
slow
small
large
large
K
velocity (µm/s)
search (off)
search (on)
sample (on)
exploit (on)
L
worms
time (min)
M
p(encounter)
time (min)
N
time before exploit (min)
relative density
O
encounters before exploit
relative density
exploits
only explores

1491 **Figure 3: *C. elegans* explore first even when only one patch is available.**
1492
1493 (A) Relative density of large (~8.3 mm diameter) and (B) small (~1.8 mm diameter) bacterial patches
1494 was varied by pipetting 20 μL and 0.5 μL, respectively, droplets of OP50 *E. coli* diluted in LB to a
1495 range of optical densities (OD_{600} = {0, 0.05, 0.1, 0.5, 1, 2, 3, 4, 5, 10} and controlling growth time at
1496 room temperature (hours = {1, 48}). (C) Large patches were formed in the center of 30 mm arenas
1497 while small patches were formed in the center of 9 mm arenas. (D-E) The midbody location
1498 (colored to represent time in the experiment) of example animals foraging in environments
1499 containing a single (D) large or (E) small patch (gray) are shown. (F-G) Ethograms of patch
1500 encounters (colored to represent the probability of classification as *search*, *sample*, and *exploit*) for (F)
1501 144 individuals (8-15 per condition) foraging on a single large patch and (G) 191 individuals (27-38
1502 per condition) foraging on a single small patch are shown. (H-I) Time elapsed prior to the first
1503 *exploitation* event (blue) for animals foraging on (H) large and (I) small patches is plotted for every
1504 animal. When *exploitation* was not observed, time elapsed in the experiment is plotted (red-orange).
1505 Animals in large and small patch environments *exploited* higher density patches significantly earlier
1506 (Kendall's τ correlation, $p < 0.001$) following a sigmoidal trend. See also Figure 3 – supplement 1-2.

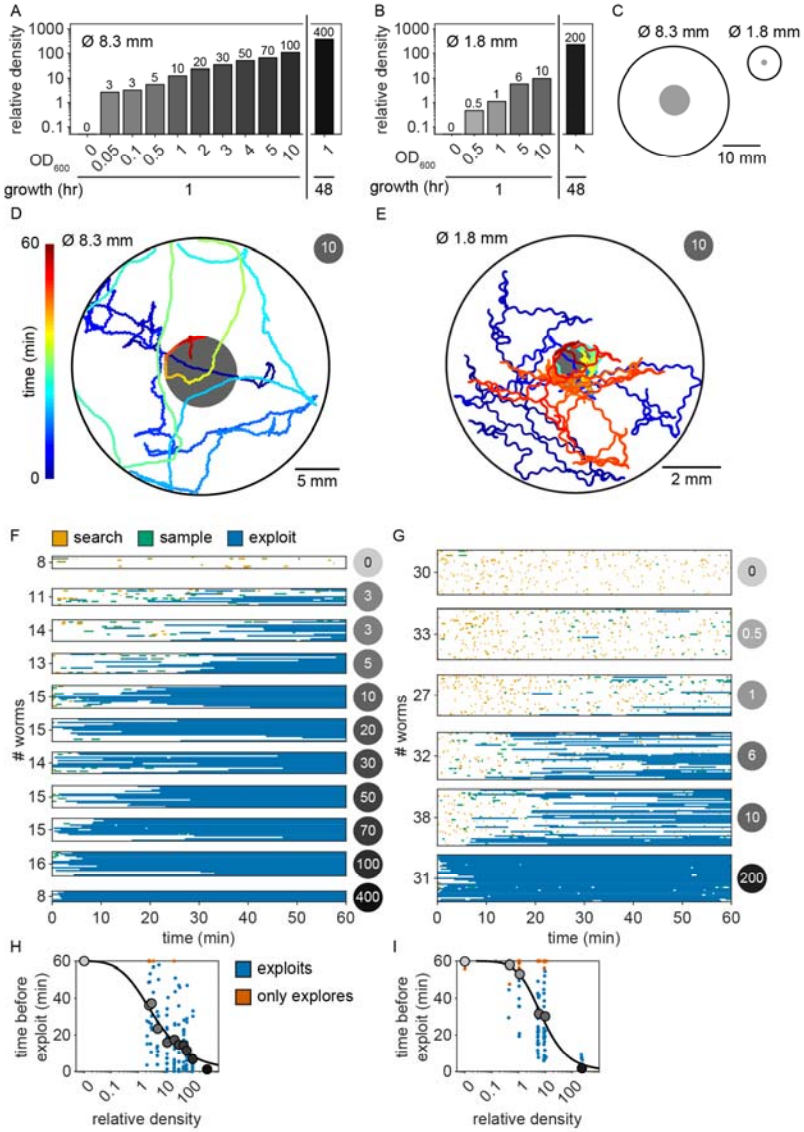
A
relative density
Ø 8.3 mm
OD600
growth (hr)
B
Ø 1.8 mm
C
Ø 8.3 mm
Ø 1.8 mm
10 mm
D
Ø 8.3 mm
time (min)
5 mm
E
Ø 1.8 mm
2 mm
F
search
sample
exploit
worms
time (min)
G
H
time before exploit (min)
relative density
exploits
only explores
I

1507
1508

Figure 4: Exploitation decisions are driven by available sensory information, satiety, and prior experience.

(A) Schematic of the covariates $\boldsymbol{x}_k$ used in our logistic regression model to predict the probability of *exploiting* a patch upon any given encounter $p(y_k = 1|\boldsymbol{\beta} \cdot \boldsymbol{x}_k)$. $\boldsymbol{x}_k$ includes the relative density of the encountered patch k (ρ_k), the duration of time spent off food since departing the last *exploited* patch (τ_s), the relative density of the patch encountered immediately before encounter k (ρ_h), and the relative density of the last *exploited* patch (ρ_e). (B) To account for uncertainty in our classification of sensation, we produced 100 sets of observations wherein we probabilistically included *sensed* encounters ($v_k = 1$) estimated from the distribution $v_k|\boldsymbol{w}_k \sim \mathrm{Bern}(p(v_k = 1|\boldsymbol{w}_k))$ where $p(v_k = 1|\boldsymbol{w}_k)$ is the probability that the patch was *sensed* as estimated in Figure 2I. To account for uncertainty in our classification of *exploitation*, we substitute the response variable y_k with our estimate of the probability that the patch was *exploited* $p(y_k = 1|\boldsymbol{z}_k)$ as estimated in Figure 2H, a procedure analogous to including *exploitations* ($y_k = 1$) estimated from the distribution $y_k|\boldsymbol{z}_k \sim \mathrm{Bern}(p(y_k = 1|\boldsymbol{z}_k))$. A schematic of these procedures is shown (see Models of exploitation probability). (C) Coefficient values for each covariate in the GLM were estimated across 50000 replicates (500 replicates of hierarchically bootstrapped animals in combination with 100 sets of probabilistically *sensed* encounters). All coefficients are significantly greater than or less than 0 (two-tailed, one-sample bootstrap hypothesis tests with Bonferroni correction). (D) Using observed $p(y_k = 1|\boldsymbol{z}_k)$ and estimated $p(y_k = 1|\boldsymbol{\beta} \cdot \boldsymbol{x}_k)$ probabilities of *exploitation*, *exploitation* events were simulated from a Bernoulli distribution. Distributions of the probability of first *exploiting* as a function of the number of encounters as estimated by the model with covariates added one-by-one and as observed are shown for animals foraging in single-density, multi-patch environments of relative density 1 or 10. (E) A schematic of multi-density, multi-patch assays where animals foraged in environments containing small (~1.8 mm diameter) bacterial patches (gray) of varying combinations of OP50 *E. coli* with relative densities 1, 4, and 7 is shown. (F) The probability of exploitation as estimated with ($p(y_k = 1|\beta_0 + \beta_k\rho_k + \beta_s\tau_s + \beta_h\rho_h + \beta_e\rho_e)$) and without ($p(y_k = 1|\beta_0 + \beta_k\rho_k + \beta_s\tau_s)$) the history-dependent terms and as observed $p(y_k = 1|\boldsymbol{z}_k)$ is shown for every pairing of current patch density (ρ_k) combined with the density of recently encountered (ρ_h) or *exploited* (ρ_e) patches. Heat maps for observed values were interpolated between the 9 patch density pairings tested. (G) *Exploitation* events were simulated from the distribution $y_k|\boldsymbol{z}_k \sim \mathrm{Bern}(p(y_k = 1|\boldsymbol{z}_k))$ and used to calculate the probability of observing *exploitation* for the first time as a function of the number of encounters for N2, *mec-4*, and *osm-6* animals foraging in single-density, multi-patch environments of relative density 1 or 10. (H) Coefficient values for each covariate were estimated using ridge regression models for each strain across 50000 replicates. A subset of these coefficients significantly varied between wild-type and mutant strains (mean of differences tests with Benjamini-Hochberg correction). Summary data for all animals (N = 443 total worms; N = 20-50 worms per condition) and encounters (μ = 2659.8, σ = 15.9) in the single-density, multi-patch assay are shown in (C,D). Summary data for all animals (N = 198 total worms; N = 20-40 worms per condition) and *sensed* encounters (μ = 1,724.6, σ = 9.9) in the multi-density, multi-patch assay are shown in (F). Summary data for all wild-type and mutant animals (N = 221 total worms; N = 14-44 worms per condition) and encounters (N = 1,352 total encounters) in a single-density, multi-patch assay are shown in (G,H). Violin plots in (C,H) show the KDE and quartiles for each measure. Asterisks denote statistical significance († $p_{unadjusted}$<0.05; *p<0.05; **p<0.01; ***p<0.001). See also Figure 4 – supplement 1-5.

-

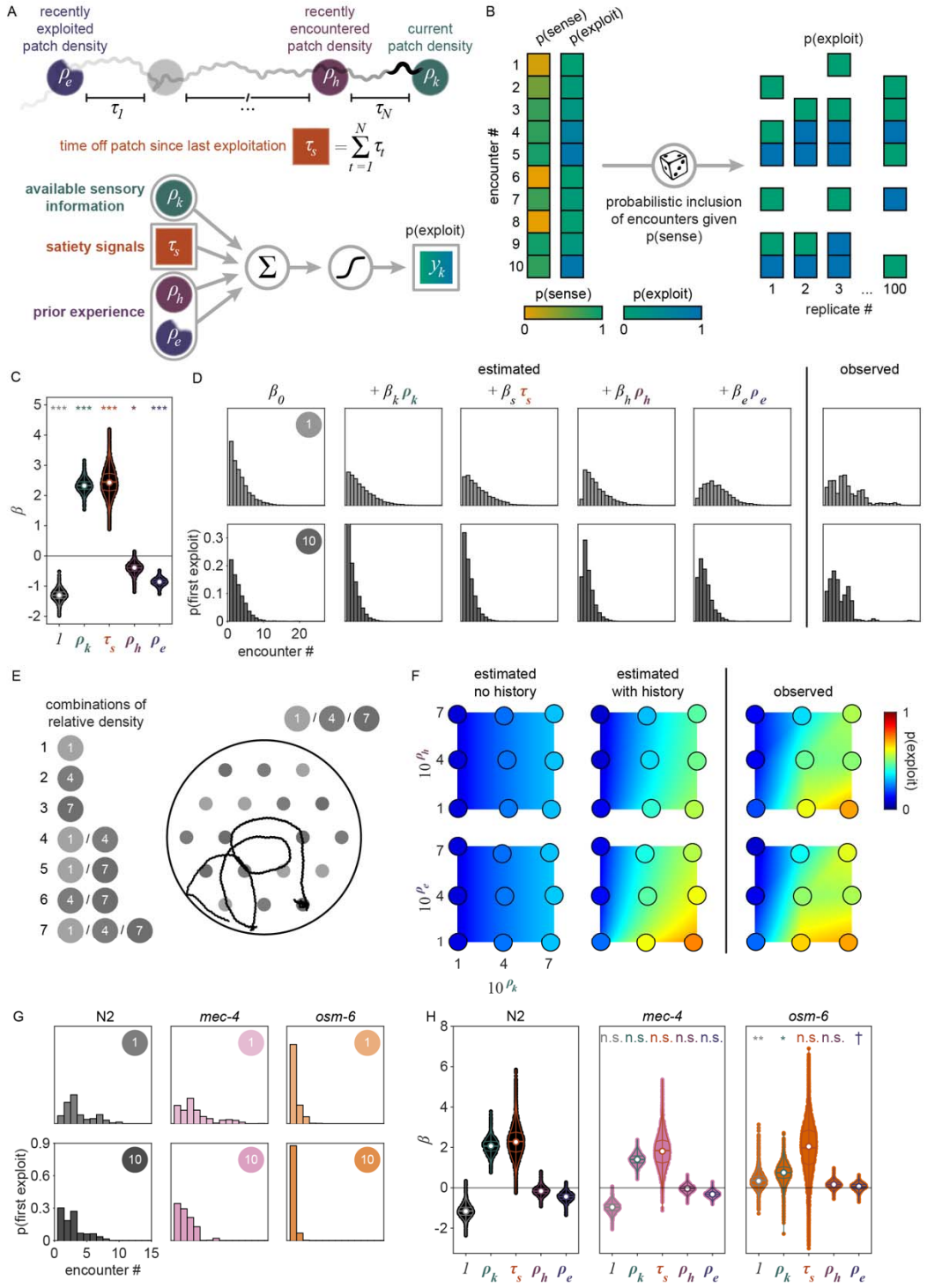
A
recently exploited patch density
recently encountered patch density
current patch density
time off patch since last exploitation
available sensory information
satiety signals
prior experience
p(exploit)
B
p(sense)
p(exploit)
encounter #
probabilistic inclusion of encounters given p(sense)
replicate #
C
D
estimated
observed
p(first exploit)
encounter #
E
combinations of relative density
F
estimated no history
estimated with history
observed
p(exploit)
G
N2
mec-4
osm-6
H

Figure Supplements

Figure 1 – supplement 1: Assay preparation, arena and patch detection, and behavioral tracking.

(A) Graphic describing the steps to prepare assay plates. Created with BioRender. (B) Example frames from a "contrast video" showing how a piece of dark cardstock passed between the light source and the assay plate enables visualization of dilute bacterial patches. (C) An image of the bacterial patches is generated from the "contrast video". (D) Masks of the arena (black) and bacterial patches (gray) were constructed using image processing techniques and, when applicable, subsequent manual corrections (see Bacterial patch location detection). Arena masks were used to calculate the image scale in pixels/mm. (E) Example frame from a behavior video containing four adult *C. elegans* is shown. (F) WormLab was used to identify the midbody location of animals in each frame (see Behavioral tracking). An inset shows detection of one of the four worms. (G) An example animal's tracked location as it forages in this environment is plotted with color used to represent time (dark blue = 0 mins; dark red = 60 mins).

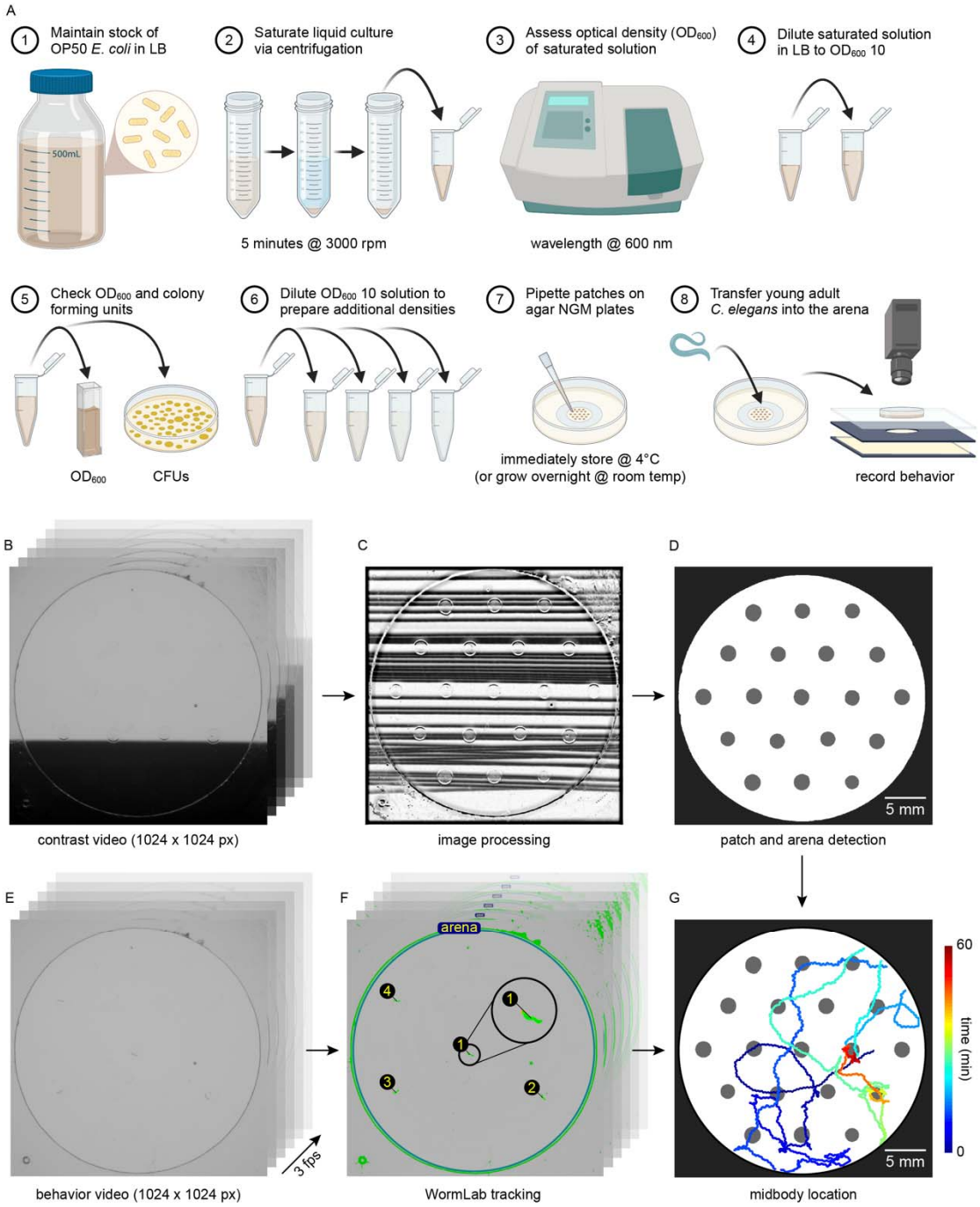
A
1 Maintain stock of OP50 E. coli in LB
500mL
2 Saturate liquid culture via centrifugation
5 minutes @ 3000 rpm
3 Assess optical density (OD600) of saturated solution
wavelength @ 600 nm
4 Dilute saturated solution in LB to OD600 10
5 Check OD600 and colony forming units
OD600
CFUs
6 Dilute OD600 10 solution to prepare additional densities
7 Pipette patches on agar NGM plates
immediately store @ 4°C
(or grow overnight @ room temp)
8 Transfer young adult C. elegans into the arena
record behavior
B
contrast video (1024 x 1024 px)
C
image processing
D
5 mm
patch and arena detection
E
3 fps
behavior video (1024 x 1024 px)
F
arena
WormLab tracking
G
60
time (min)
0
5 mm
midbody location

1572

Figure 1 – supplement 2: Defining a patch encounter using high resolution behavioral recordings.

(A) Example frame from a behavior video containing one adult *C. elegans* is shown. (B) WormLab was used to track the body of the animal in each frame (see Behavioral tracking). (C) An example image showing the center spline of the example animal as well as the location of the bacterial patch (gray) and arena (black). The inset shows the animal's center spline and bacterial patch superimposed on top of the raw image. (D) Example body postures/orientations (black) of an animal during frames when its head is on the patch edge. The distance (blue lines) between the head (black dot) and midpoint (blue dot) of the animal was calculated. A histogram of this head-to-midpoint distance is plotted, and the median value (blue) is indicated (sample size: 220 animals; 74839 frames). The median head-to-midpoint distance was subsequently used as a threshold for detection of patch encounter and leaving events. For one example animal, the distance between the head (black) or midbody (blue) position and the nearest patch edge (positive = inside patch; negative = outside patch) is plotted for every time point. The edge of the patch (solid black line) and threshold for encounter detection (dashed -.- black line) are indicated. Putative patch encounter (green) and leaving (red) events are shown. (E) Example body postures/orientations of an animal when its head is on the patch. The distance between the midpoint of the animal and the patch edge (blue lines) was calculated. A histogram of this midpoint-to-patch distance is plotted, and the 1st percentile (blue) is indicated (sample size: 220 animals; 1571163 frames). This value is used as a threshold for excluding putative encounters where the animal's midpoint never comes within 0.28768 mm of the patch edge. A 1.5 minute time window of the example animal's position in (D) is shown. The edge of the patch (solid line), threshold for encounter detection (dashed -.- line), and threshold for encounter exclusion (dashed – line) are indicated. Example putative encounters are shown. The first two sets of enter and exit events were excluded. The third set shown was included. The included encounter is shaded in gray. (F) The standard deviation of the distance between the location of the patch edge and the midpoint of the animal was calculated for every putative on-patch encounter and off-patch event (sample size: 220 animals; 2945 putative on-patch events; 2725 putative off-patch events). A subset of putative off-patch events had low standard deviations matching those of on-patch events. A one-dimensional Gaussian mixture model was fit to the off-patch standard deviation values and a threshold was set where the posterior probability of events falling in the high or low variance cluster was 0.5. A 1.5 minute time window of the example animal's position in (D) is shown. Examples of two excluded off-patch events and one included event are shown.

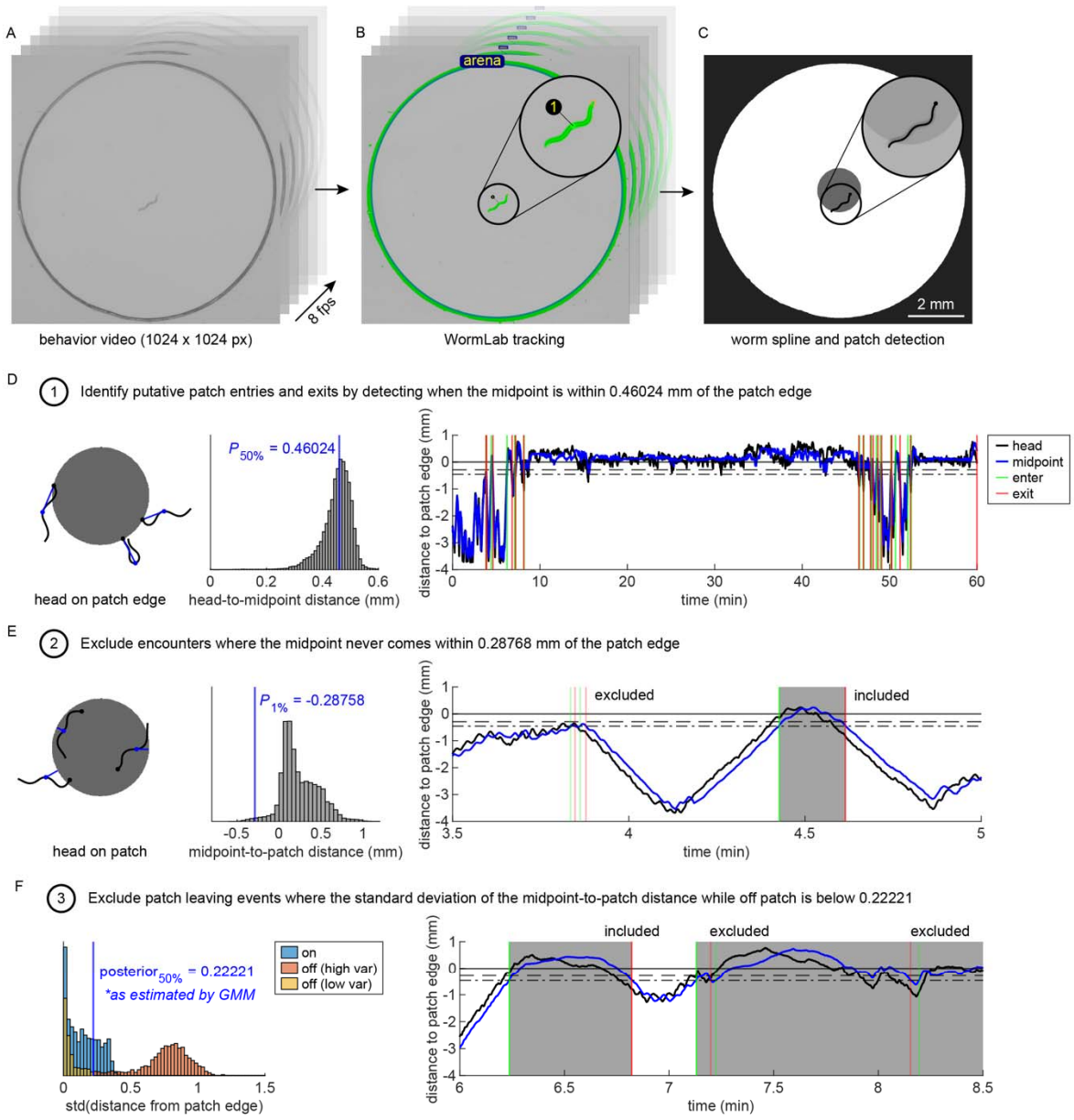
A
B
C
arena
8 fps
2 mm
behavior video (1024 x 1024 px)
WormLab tracking
worm spline and patch detection
D
1 Identify putative patch entries and exits by detecting when the midpoint is within 0.46024 mm of the patch edge
P50% = 0.46024
head on patch edge
head-to-midpoint distance (mm)
distance to patch edge (mm)
time (min)
head
midpoint
enter
exit
E
2 Exclude encounters where the midpoint never comes within 0.28768 mm of the patch edge
P1% = -0.28758
head on patch
midpoint-to-patch distance (mm)
excluded
included
F
3 Exclude patch leaving events where the standard deviation of the midpoint-to-patch distance while off patch is below 0.22221
posterior50% = 0.22221
*as estimated by GMM
on
off (high var)
off (low var)
std(distance from patch edge)
included
excluded
excluded

1606

Figure 1 – supplement 3: Classifying encounters based on duration using a Gaussian mixture model.

(A) As in Figure 1E, duration for each patch encounter (N = 419 events; 50 worms) was computed and classified as either short or long using a Gaussian mixture model (GMM). The distributions of all observed short and long encounters are plotted with duration binned logarithmically. The probability density functions for the two component Gaussians are shown. (B) The posterior probabilities for classification as short or long are sorted for all encounters, highlighting the low posterior variance of the GMM. (C) Given that some patch encounters were not fully observed (i.e., ~22% of animals were already on patch at the start of the recording and ~96% of animals were on patch when the recording ended), we identified that ~14% of observed patch durations were left-censored (i.e., having actual duration ≥ observed duration). Thus, to confirm findings in Figure 1E-F, we re-classified only non-censored observations where both the entry and exit of a patch encounter were observed. As in Figure 1C, patch encounters for 50 individuals foraging in these patchy environments are plotted across time. Encounters that were uncensored (pink) and censored (gray) are indicated. (D) The distribution of the duration of only fully observed (uncensored) encounters (N = 360 events; 50 worms) is plotted. The component Gaussians for a GMM fitting this subset of data are shown. (E) Sorted posterior probabilities for the uncensored model are shown. (F) The observed start time of each uncensored patch encounter is shown for all short and long duration encounters. Long duration encounters occur significantly later (Mann-Whitney U-Test, ***p<0.001). Violin plots show the KDE and quartiles for each duration type. (G) Posterior probabilities for classification in the long duration cluster are shown for the two models. The uncensored data model results in a slight increase in posterior probabilities of long duration classification but ultimately affected classification of only one of the 419 encounters.

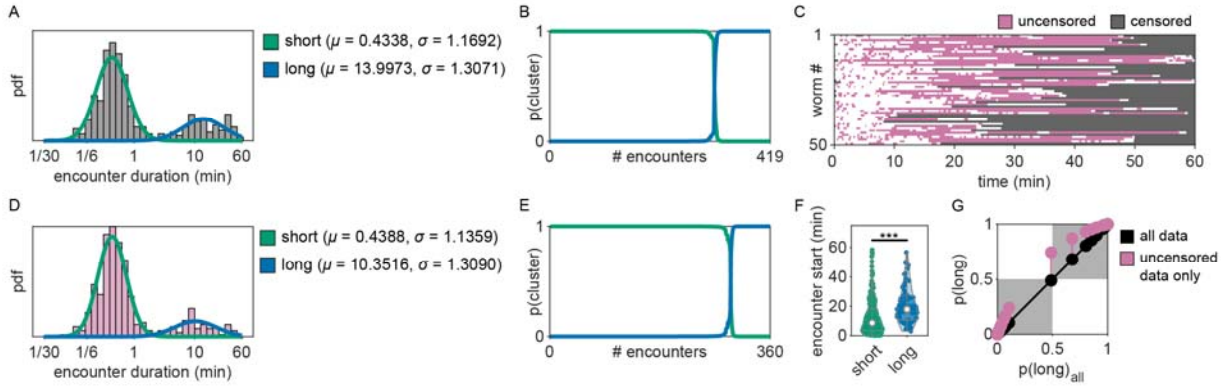

1634 **Figure 1 – supplement 4: Permuting patches to test for significance of the observed time-**
1635 **dependent increase in patch residence.**
1636
1637 (A) Locations of bacterial patches (dark gray) are shown with the threshold for putative encounters
1638 (light gray) set at 0.46024 mm (as described in Figure 1 – supplement 2 and Patch encounter
1639 detection). (B) Patches were permuted via randomized rotation and translation with the restriction
1640 that patches could not overlap with other patches nor with the arena. (C,D) Midbody location of the
1641 animal over time was overlaid on the original and semi-randomly permuted patches. (E,F) On patch
1642 events were subsequently identified. This permutation procedure was repeated for 1000 replicates
1643 for every worm tested. Smoothed median values of the probability of worms residing on patch over
1644 time was compared for every time point in Figure 1G, 2F and Figure 2 – supplement 5.
1645

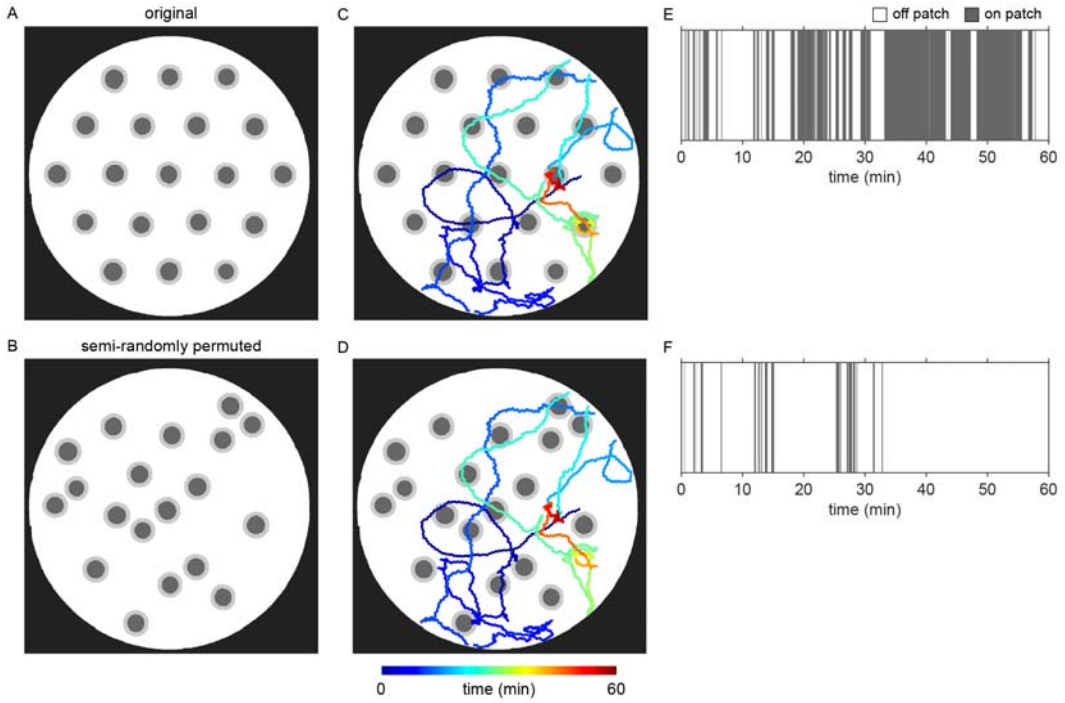

1646

1647 **Figure 1 – supplement 5: Analyzing deceleration upon encounter with a patch.**
1648
1649 (A) To quantify the magnitude of slow-down upon encounter with the patch edge, we averaged the
1650 velocity trajectories across encounters (black) and found the velocity reached a maximum at 1.5
1651 seconds before (green) and a minimum at 6 seconds after (red) the start of the encounter (gray).
1652 (B,C) Subsequently, for every encounter, a line (blue) was fit to the animal's velocity (black) for that 8
1653 second time window surrounding the start of the encounter. Deceleration was defined as the slope
1654 of this line. Examples matching (B) the short duration encounter in Figure 1J and (C) the long
1655 duration encounter in Figure 1K are shown.
1656

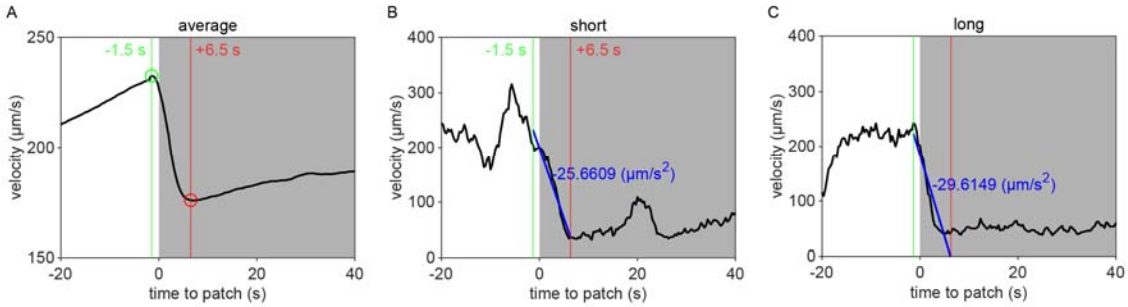

1657

1658 **Figure 2 – supplement 1: Obtaining intensity profiles for fluorescent bacterial patches.**
1659
1660 (A) Fluorescently labeled OP50-GFP bacterial patches were seeded onto agar plates under
1661 conditions matching those in the experimental assay. Small patches (0.5 μL) were pipetted in an
1662 isometric grid (6 mm center-to-center spacing) on a 16 x 25 mm rectangular template comparable to
1663 the one used in behavioral assays. Large patches (20 or 200 μL) were seeded directly onto agar plates.
1664 Brightfield and fluorescence images were acquired for every condition at multiple time points of
1665 bacterial growth. The fluorescence intensity profile of these images was obtained. (B) Due to
1666 uneven illumination within the field-of-view of our imaging system, matched fluorescence images of
1667 an empty agar plate were acquired at each time point. These "background" images were smoothed
1668 using a two-dimensional averaging filter to remove noise. (C) Fluorescence images of the bacterial
1669 patches were normalized to these background images. (D) Locations of bacterial patches within the
1670 template were automatically detected using image processing techniques. Each patch was then
1671 radially segmented in bins of equal area. The mean pixel intensity value for each bin was computed
1672 and used to create an intensity profile of the patch. (E) The patch border and peak were detected
1673 using signal processing techniques. Specifically, the patch border was identified by finding a peak in
1674 the curvature κ of the edge profile. Border amplitude was defined as the magnitude of the
1675 difference between the patch border and peak. Relative border amplitude was defined as the border
1676 amplitude divided by the exposure time. A line was fit to the values of relative border amplitude
1677 across numerous time points and experiment days (5 replicates shown as varying color points).

A

1 Brightfield and fluorescence images were acquired of OP50-GFP bacterial patches seeded uniformly using a template.

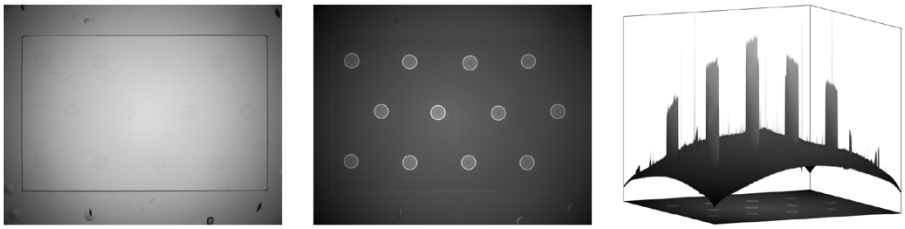

brightfield (2208 x 2752 px) fluorescence (3000 ms exposure) fluorescence intensity profile

B

2 As the diffusion of light in our imaging system resulted in uneven illumination of the field-of-view, matched fluorescence images of an empty agar plate were acquired for each time point. This "background" image was smoothed using a 2D averaging filter.

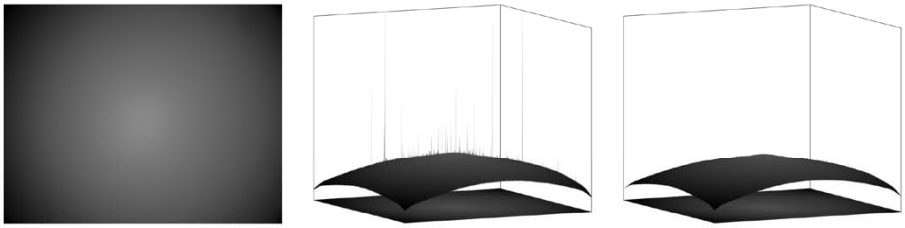

fluorescence background fluorescence intensity profile smoothed fluorescence background

C

3 Fluorescence images of the OP50-GFP bacterial patches were normalized to the smoothed background, removing the majority of the illumination-dependent spatial variance in signal intensity.

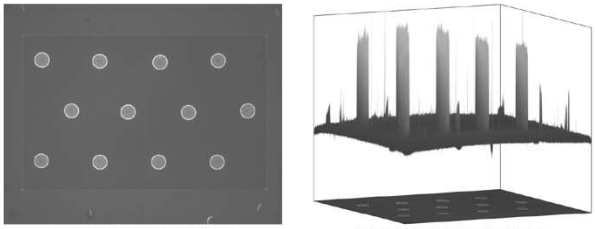

fluorescence normalized normalized intensity profile

D

4 Arena (16 x 25 mm) and bacterial patch locations were automatically detected via image processing techniques. Each patch was radially segmented in bins of equal area to compute an intensity profile of the patch.

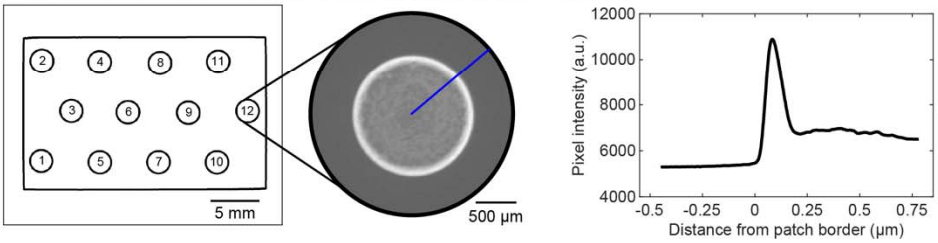

E

5 Using the profiles curvature and maximum value, the patch border and peak were detected. Border amplitude was defined as the difference in magnitude between the peak and border pixel intensities. Border amplitude was divided by exposure time to compute a relative border amplitude that could be compared across time points and patch densities.

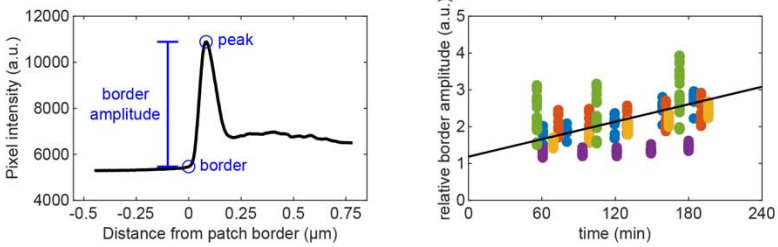

1678

1679 **Figure 2 – supplement 2: Example fluorescence profiles of bacterial patches under varied**
1680 **growth conditions.**
1681
1682 Fluorescently-labeled OP50-GFP bacterial patches were imaged (as described in Figure 2 –
1683 supplement 1 and Bacterial patch density estimation). Inverted images (darker saturation = more
1684 bacteria) are shown here to highlight the range of bacterial densities tested in these experiments. All
1685 patches are shown on the same spatial scale and using one of the two linear saturation scales: 1)
1686 regular – normalized to show variance in high density patches; 2) augmented (~22x) – normalized to
1687 show variance in low density patches). Each patch shown is labeled with the optical density (OD_{600})
1688 at time of seeding and the approximate amount of time bacteria was grown for at room temperature
1689 (i.e., 1, 12, or 48 hours). (A) An example large (200 μL) bacterial patch of the type that animals
1690 experienced immediately prior to the assays in this paper. (B) Example small (0.5 μL) bacterial
1691 patches of greatest density. (C) Example small (0.5 μL) bacterial patches of lower density. The
1692 saturation of each image has been uniformly augmented to ~22x darker to the extent that the OD_{600}
1693 10 (1H) bacterial patch is the same patch as the one in B. (D) Example small (0.5 μL) bacterial
1694 patches of lower density seeded on NGM agar plates lacking peptone. (E) Example medium (20 μL)
1695 bacterial patches of greater density. (F) Example medium (20 μL) bacterial patches of lowest density.
1696 The OD_{600} 1 (1H) bacterial patch is the same patch as the one shown in E, but ~22x darker.

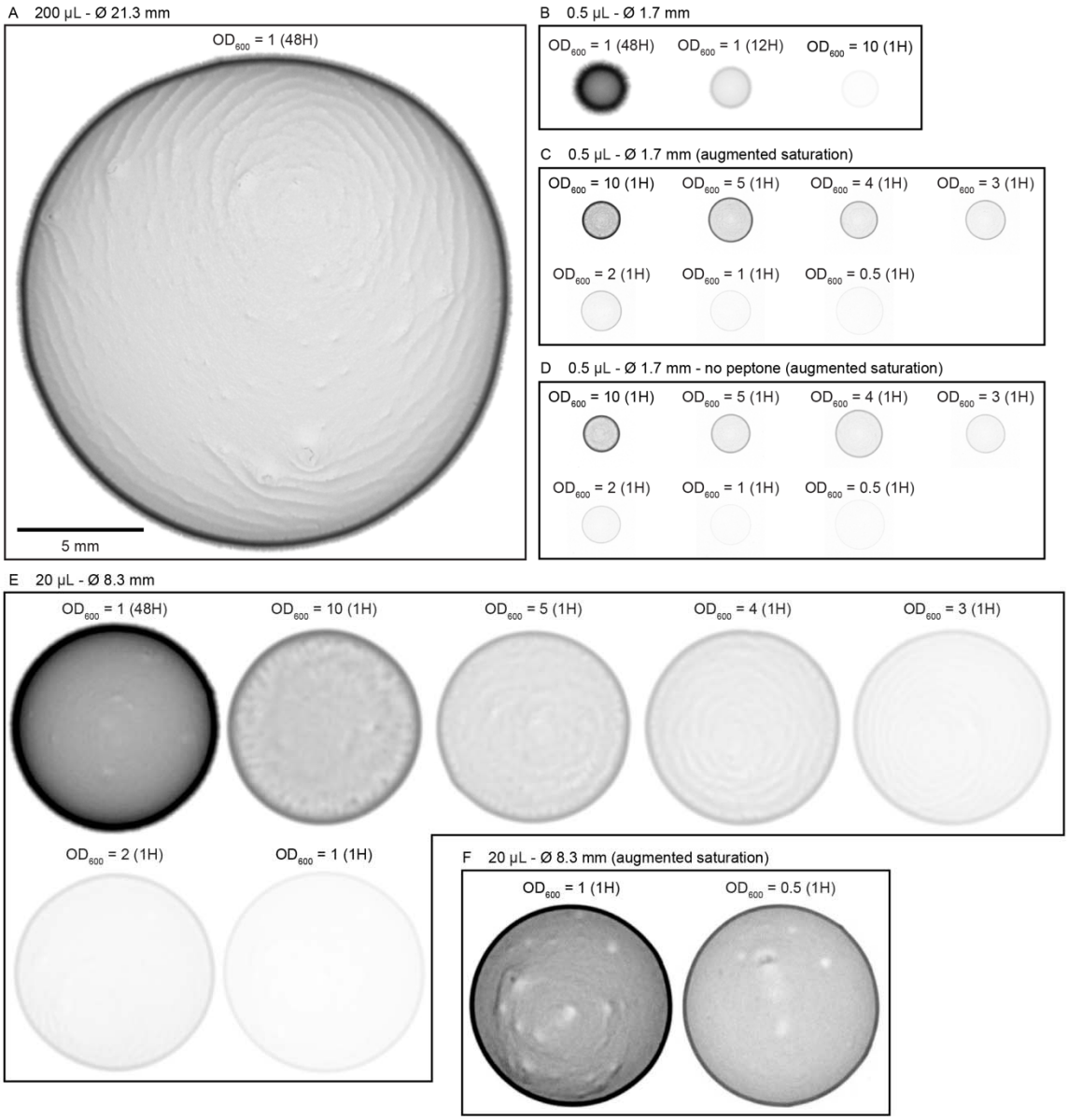
A 200 µL - Ø 21.3 mm
OD600 = 1 (48H)
5 mm
B 0.5 µL - Ø 1.7 mm
OD600 = 1 (48H)
OD600 = 1 (12H)
OD600 = 10 (1H)
C 0.5 µL - Ø 1.7 mm (augmented saturation)
OD600 = 10 (1H)
OD600 = 5 (1H)
OD600 = 4 (1H)
OD600 = 3 (1H)
OD600 = 2 (1H)
OD600 = 1 (1H)
OD600 = 0.5 (1H)
D 0.5 µL - Ø 1.7 mm - no peptone (augmented saturation)
OD600 = 10 (1H)
OD600 = 5 (1H)
OD600 = 4 (1H)
OD600 = 3 (1H)
OD600 = 2 (1H)
OD600 = 1 (1H)
OD600 = 0.5 (1H)
E 20 µL - Ø 8.3 mm
OD600 = 1 (48H)
OD600 = 10 (1H)
OD600 = 5 (1H)
OD600 = 4 (1H)
OD600 = 3 (1H)
OD600 = 2 (1H)
OD600 = 1 (1H)
F 20 µL - Ø 8.3 mm (augmented saturation)
OD600 = 1 (1H)
OD600 = 0.5 (1H)

1699 **Figure 2 – supplement 3: Quantifying the relative density of bacterial patches across**
1700 **conditions and time points.**
1701
1702 (A) Relative density of OP50-GFP bacterial patches matched to all assay conditions in this paper are
1703 shown. Relative density represents the relative border amplitude (as defined in Figure 2 –
1704 supplement 1 and Bacterial patch density estimation) normalized to the mean density of patches
1705 seeded with 0.5 μL of OD_{600} = 10 grown for 1 hour on plates with peptone (blue asterisk). In this
1706 manner, the bacterial patches experienced by animals in Figure 1 have been set to an average relative
1707 density of 10. Violin plots show the KDE and quartiles for each condition. (B) Linear fits for the
1708 relative density of bacterial patches in each condition as a function of time are plotted. Saturation of
1709 each line corresponds to the relative density as depicted in (A). For each experimental plate, the
1710 relative density of bacterial patches was estimated by applying the coefficients from these linear
1711 regressions to the total amount of time the bacteria was grown at room temperature.
1712

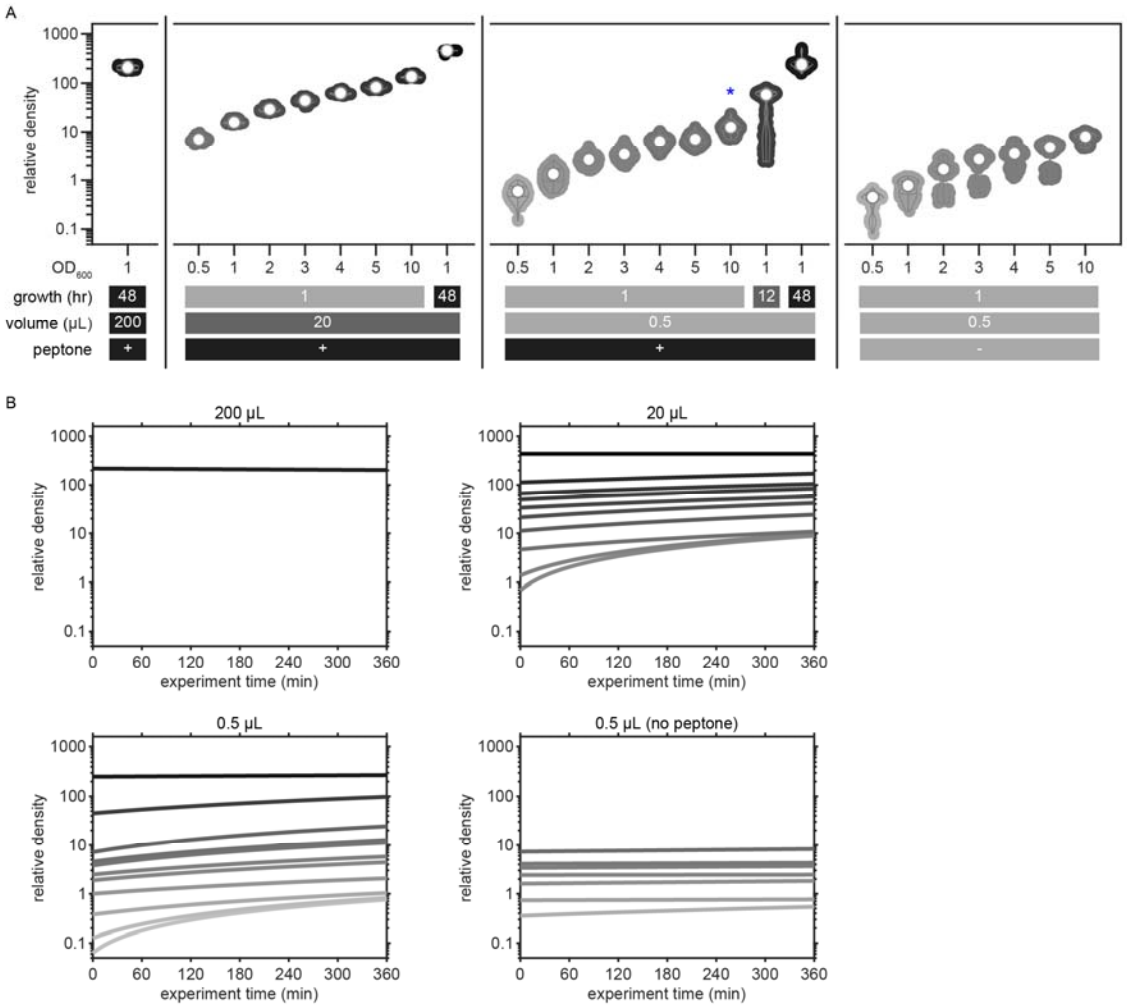

1713

Figure 2 – supplement 4: Example traces of animals foraging in environments with varying bacterial density.

Traces showing the midbody location of 12 example animals as they forage within a 30 mm arena are plotted with color used to represent time (dark blue = 0 mins; dark red = 60 mins). Locations of bacterial patches are indicated in gray. The relative density of bacterial patches in each environment is noted. Animals shown foraging on relative density 0, 1, 5, 10, and 200 are the same as those in Figure 2D.

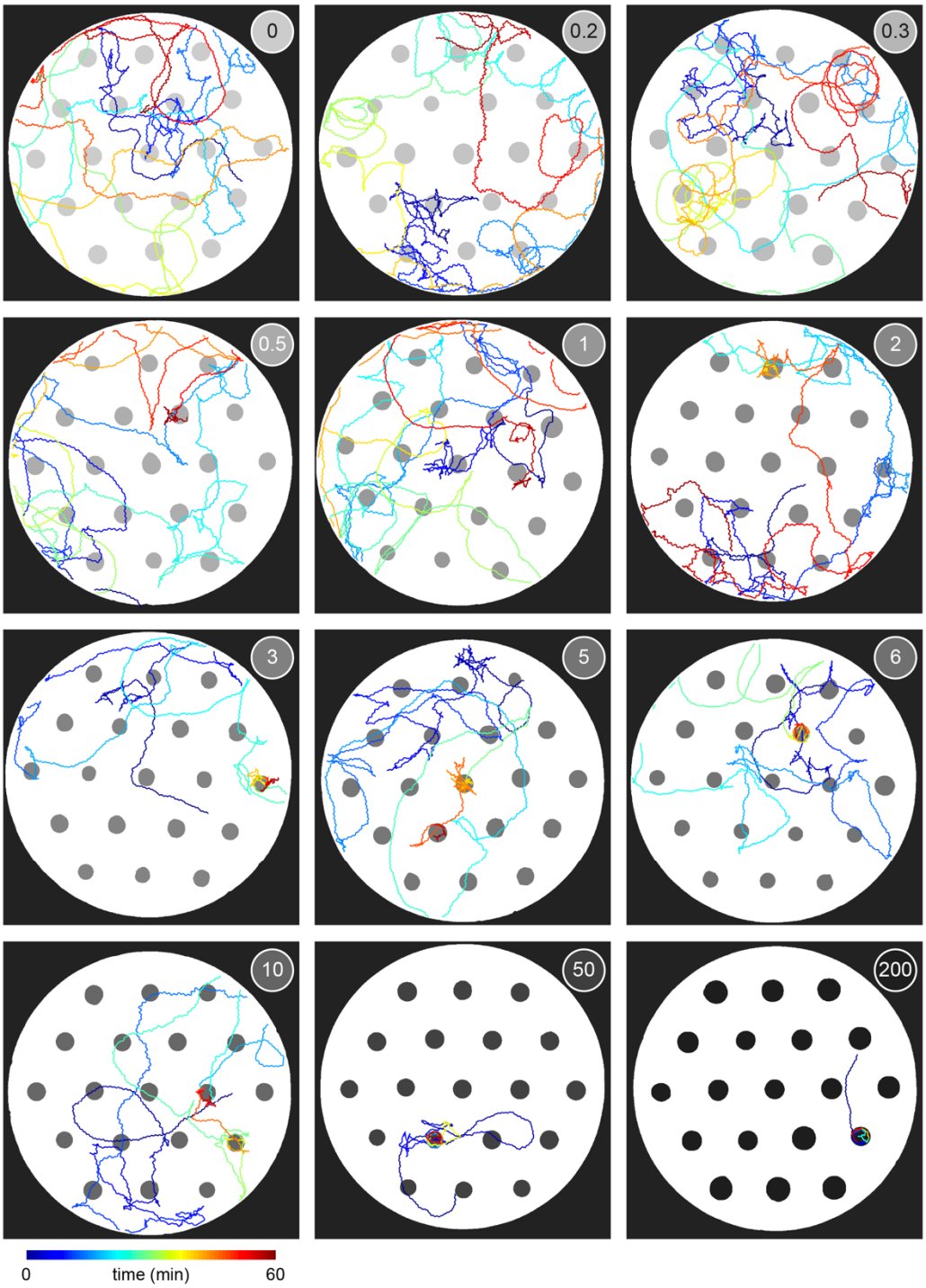

1722

Figure 2 – supplement 5: Time- and density-dependent increase in patch residence.

Probability of residing on patch was computed for all worms across time (black) and compared to the probability of residing on patch for semi-randomly permuted patch locations (pink) (as described in Figure 1 – supplement 4). Smoothed median values are plotted with bootstrap-derived 2.5% and 97.5% quantiles shown in shaded regions. Time points where observed probabilities of residing on patch significantly exceed permuted probabilities are indicated by a black line (one-tailed Fisher's Exact Tests with Benjamini-Hochberg correction, ***p < 0.001). The smoothed median values for observed data are shown in Figure 2F. Data for relative density 10 match those in Figure 1G.

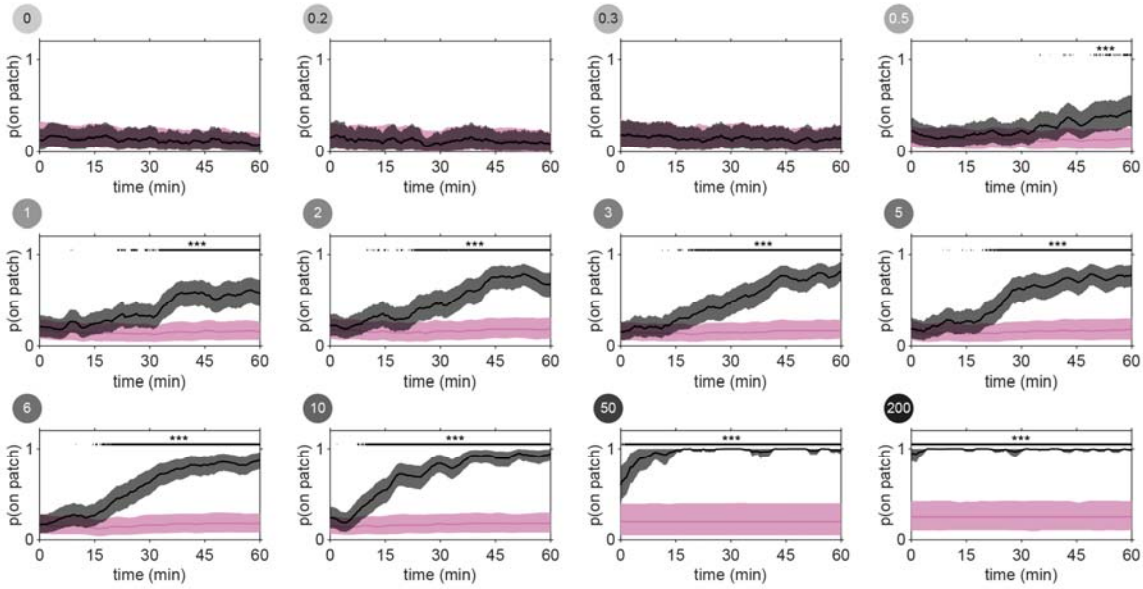

Figure 2 – supplement 6: Classifying encounters as exploration or exploitation.

(A) A two-dimensional histogram shows the frequency of events for given pairs of values for the average velocity of the animal during an encounter and the duration of that encounter for all encounters in the paper. Probabilities are represented as a heat map of color. (B) The first principal component (PC1) for these two metrics was computed. The distribution of projections of the data onto PC1 is given by a histogram (gray). Kernel density estimates (KDE) were computed using the bandwidth $\hat{h}$ defined by Silverman's Rule of Thumb (blue) and using the critical bandwidth h^* (red-orange) at which the KDE is at the threshold between uni- and bi-modal (see Patch encounter classification as exploration or exploitation). (F) Critical bandwidth values were computed across 2000 smoothed bootstrap resamples. The distribution of these bootstrapped critical values is given as a histogram and compared against the critical bandwidth of the original data set (red-orange). (D) The average velocity of the animal during an encounter and the duration of that encounter are plotted for each encounter as visualized on a double-logarithmic plot. Contours showing the first, second, and third standard deviation of the two-dimensional Gaussian mixture model (GMM) are shown as shaded ellipses with saturation corresponding to standard deviation. Encounters for all data in the paper are individually plotted as in Figure 2H but with color representing the posterior probability of clustering classification as *explore* (green) or *exploit* (blue). (E) Posterior variance of the data as defined in Patch encounter classification as *exploration* or *exploitation* was calculated for 1000 replicates of GMMs with varied regularization value α. The classifier with minimum posterior variance (i.e., $\alpha = 0.025$) was used. (F) The posterior probabilities for classification as *explore* (green) or *exploit* (blue) are sorted for all encounters, highlighting the low posterior variance of the GMM. (G) Posterior probabilities for only the data in Figure 2 are shown.

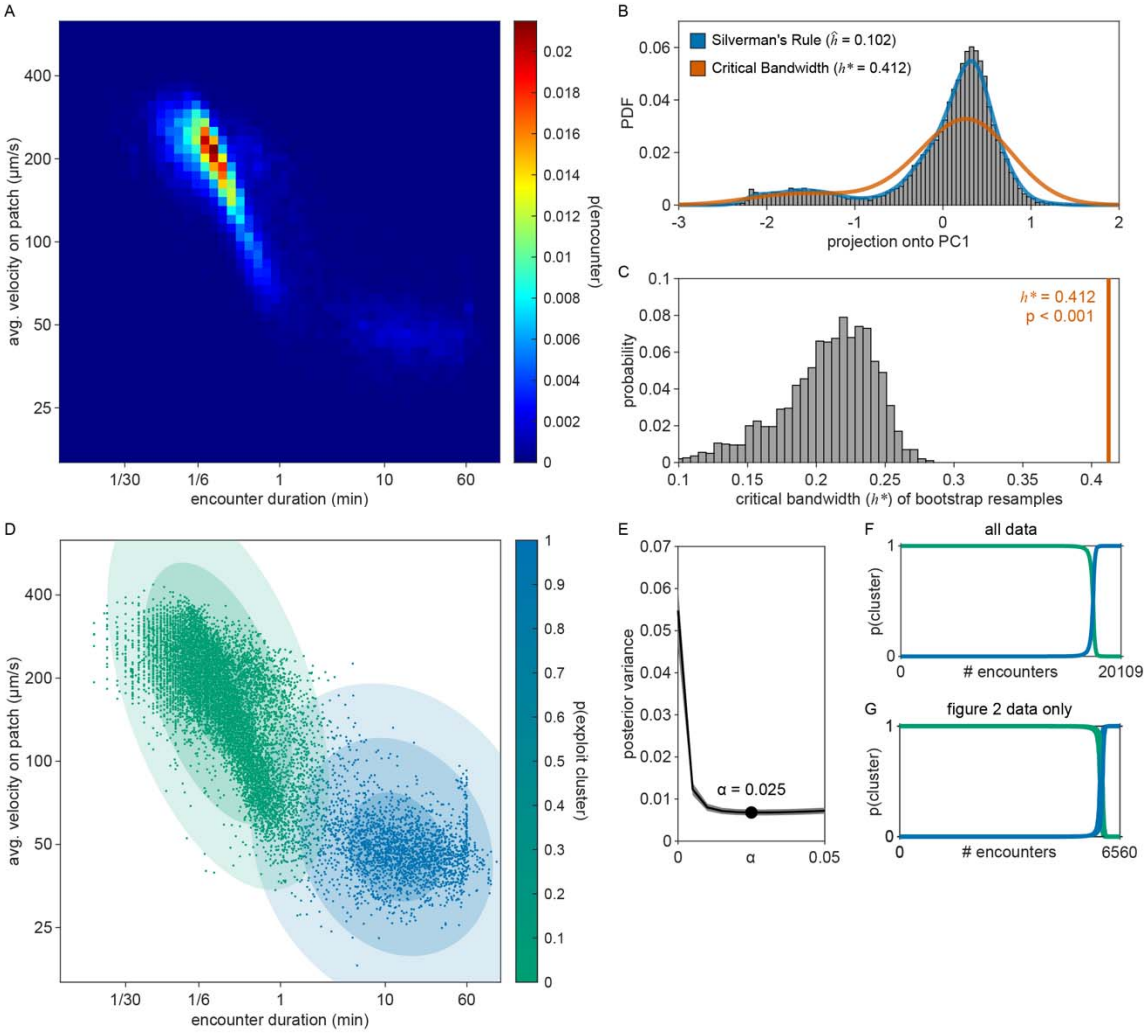
A
avg. velocity on patch (μm/s)
encounter duration (min)
p(encounter)
B
Silverman's Rule ($\hat{h}$ = 0.102)
Critical Bandwidth (h^* = 0.412)
PDF
projection onto PC1
C
h^* = 0.412
p < 0.001
probability
critical bandwidth (h^*) of bootstrap resamples
D
avg. velocity on patch (μm/s)
encounter duration (min)
p(exploit cluster)
E
posterior variance
α = 0.025
α
F
all data
p(cluster)
# encounters
20109
G
figure 2 data only
p(cluster)
# encounters
6560

1759

Figure 2 – supplement 7: Classifying encounters as sensing or non-responding.

(A) Minimum velocity (min. velocity on patch), maximum change in velocity (max. Δ velocity), and deceleration (Δ velocity) were calculated (as described in Patch encounter classification as sensing or non-responding). (B) Maximum change in velocity for every density condition is shown. Violin plots show the KDE and quartiles for each condition. Two-dimensional histograms show the frequency of events for given pairs of values for (C) deceleration and minimum on-patch velocity and for (D) maximum change in velocity and minimum on-patch velocity for all encounters in the paper. Probabilities are represented as a heat map of color. (E) The first principal component (PC1) for these three metrics was computed. The distribution of projections of the data onto PC1 is given by a histogram (gray). Kernel density estimates (KDE) were computed using the bandwidth $\hat{h}$ defined by Silverman's Rule of Thumb (blue) and using the critical bandwidth h^* (red-orange) at which the KDE is at the threshold between uni- and bi-modal (see Patch encounter classification as sensing or non-responding). (F) Critical bandwidth values were computed across 2000 smoothed bootstrap resamples. The distribution of these bootstrapped critical values is given as a histogram and compared against the critical bandwidth of the original data set (red-orange).

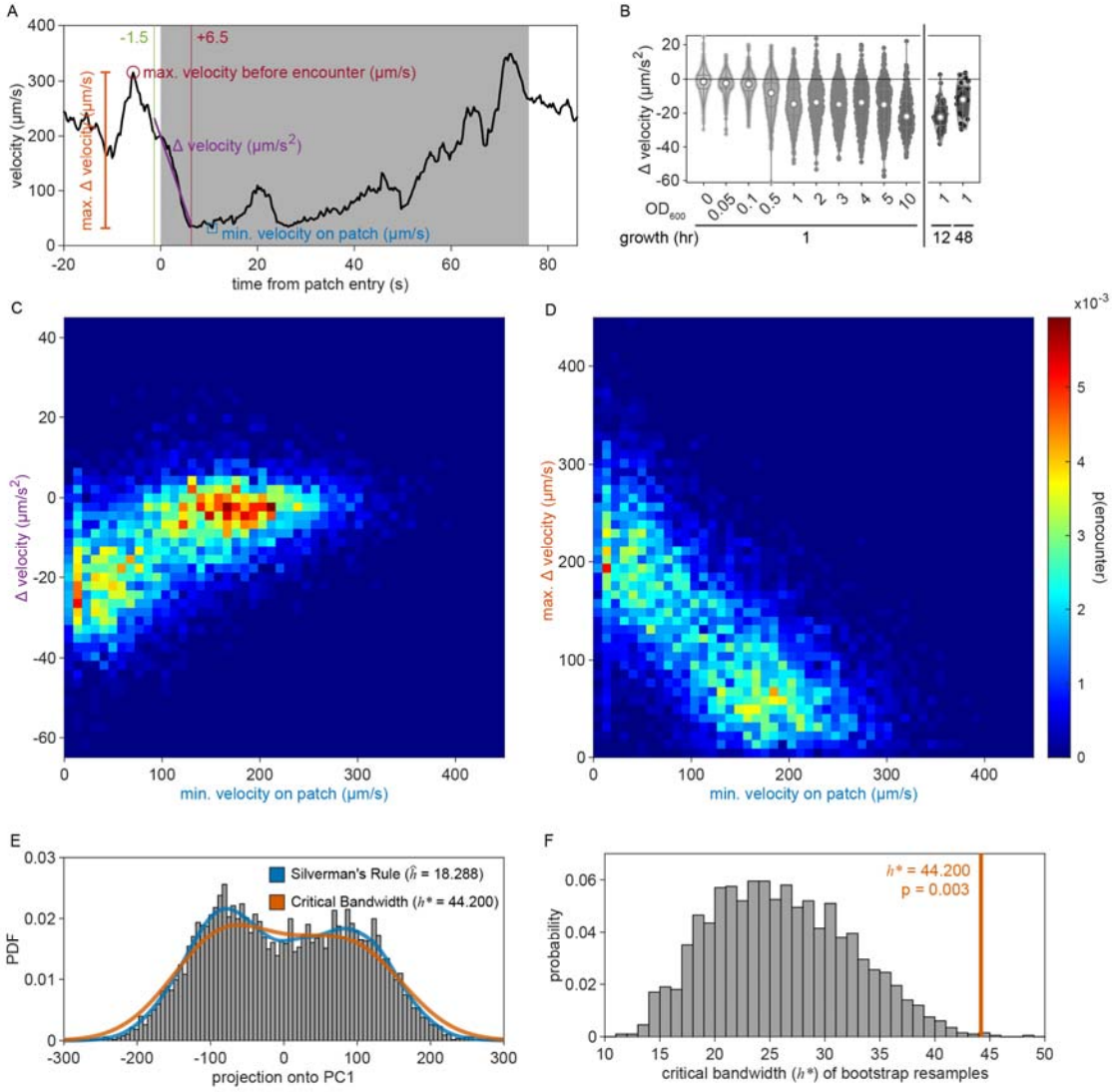
A
-1.5
+6.5
max. velocity before encounter (μm/s)
max. Δ velocity (μm/s)
Δ velocity (μm/s²)
min. velocity on patch (μm/s)
velocity (μm/s)
time from patch entry (s)
B
Δ velocity (μm/s²)
OD600
0 0.05 0.1 0.5 1 2 3 4 5 10
1 1
growth (hr)
1
12 48
C
Δ velocity (μm/s²)
min. velocity on patch (μm/s)
D
x10⁻³
max. Δ velocity (μm/s)
min. velocity on patch (μm/s)
p(encounter)
E
Silverman's Rule (ĥ = 18.288)
Critical Bandwidth (h* = 44.200)
PDF
projection onto PC1
F
h* = 44.200
p = 0.003
probability
critical bandwidth (h*) of bootstrap resamples

1777
1778

Figure 2 – supplement 8: Classifying encounters as sensing or non-responding.

(A) Deceleration upon encounter and minimum on-patch velocity during the encounter are plotted for each encounter. A three-dimensional parabolic boundary between *sensing* and *non-responding* clusters was fit using semi-supervised QDA and a subset of labeled data (blue circles = sensing, dark orange circles = non-responding). Regions identified by the classifier as *non-responding* or *sensing* are indicated by colored contours (orange = *non-responding*, green = *sensing*). Encounters for all data in the paper are individually plotted as in Figure 2I but with color representing the conditional probability of clustering classification as *non-responding* (orange) or *sensing* (green). (B) Maximum change in velocity and minimum on-patch velocity during the encounter are plotted for each encounter in the paper as in (A). (C) Minimum velocity on patch, maximum change in velocity, and deceleration are shown for every encounter in the paper. See Video 5 for three-dimensional rotation of this plot. (D) The probabilities for classification as *sensing* (green) or *non-responding* (orange) are sorted for all encounters. (E) Probabilities for only the data in Figure 2 are shown. (F) For a subset of encounters that were censored (i.e., recording did not observe animals entering the patch), probabilities of *sensing* were estimated using the semi-supervised QDA approach as well as via marginalization over the conditional probabilities using only the observed minimum velocity on patch. Marginalized probabilities were used for these values (see Patch encounter classification as sensing or non-responding).

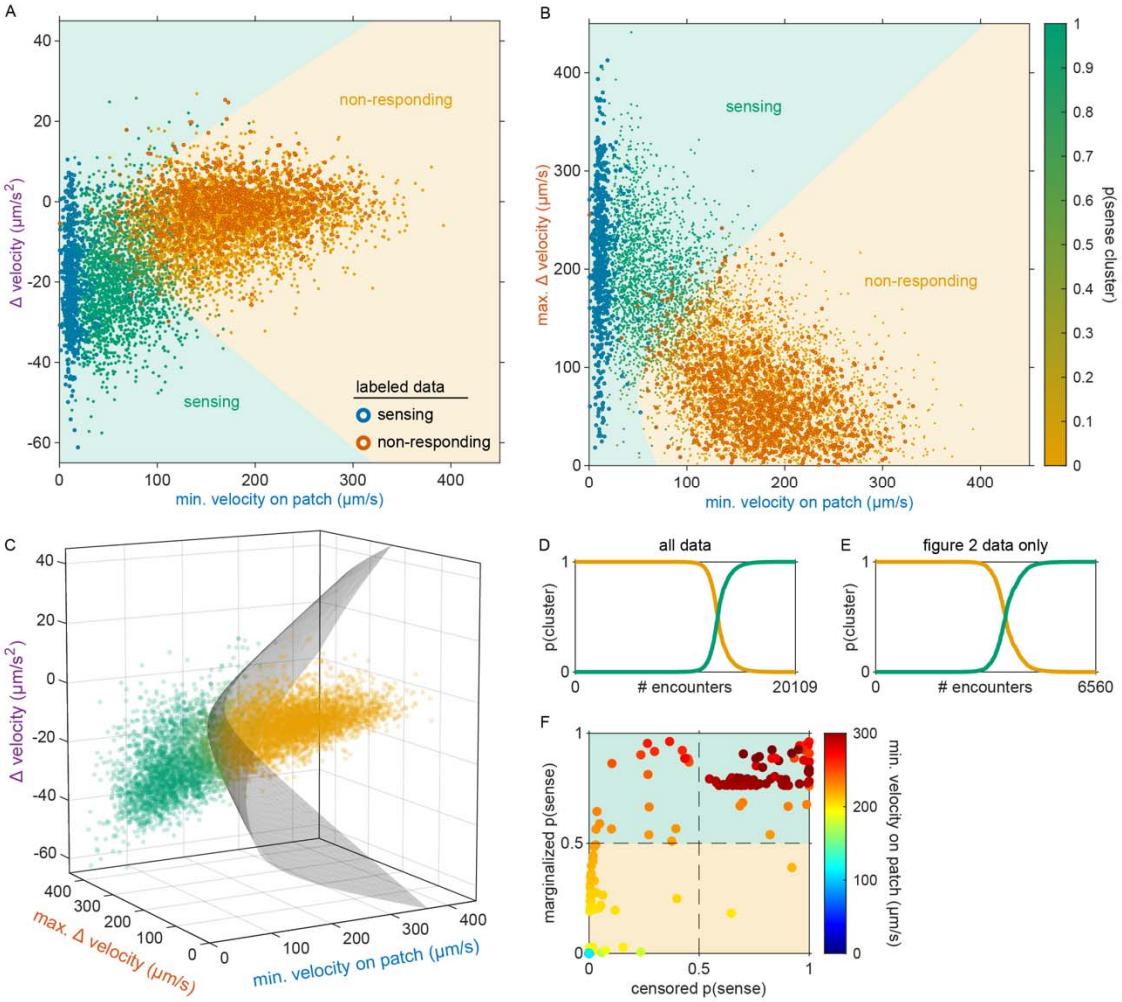
A
non-responding
sensing
labeled data
sensing
non-responding
Δ velocity (μm/s²)
min. velocity on patch (μm/s)
B
sensing
non-responding
max. Δ velocity (μm/s)
min. velocity on patch (μm/s)
p(sense cluster)
C
Δ velocity (μm/s²)
max. Δ velocity (μm/s)
min. velocity on patch (μm/s)
D
all data
p(cluster)
# encounters
20109
E
figure 2 data only
p(cluster)
# encounters
6560
F
marginalized p(sense)
censored p(sense)
min. velocity on patch (μm/s)

Figure 3 – supplement 1: Example traces of animals foraging in environments with one large bacterial patch.

Example traces showing the midbody location of 11 animals as they forage within a 30 mm arena are plotted with color used to represent time (dark blue = 0 mins; dark red = 60 mins). Location of bacterial patches are indicated in gray. The relative density of bacterial patches in each environment is noted. The animal shown foraging on relative density 10 is the same as that in Figure 3D.

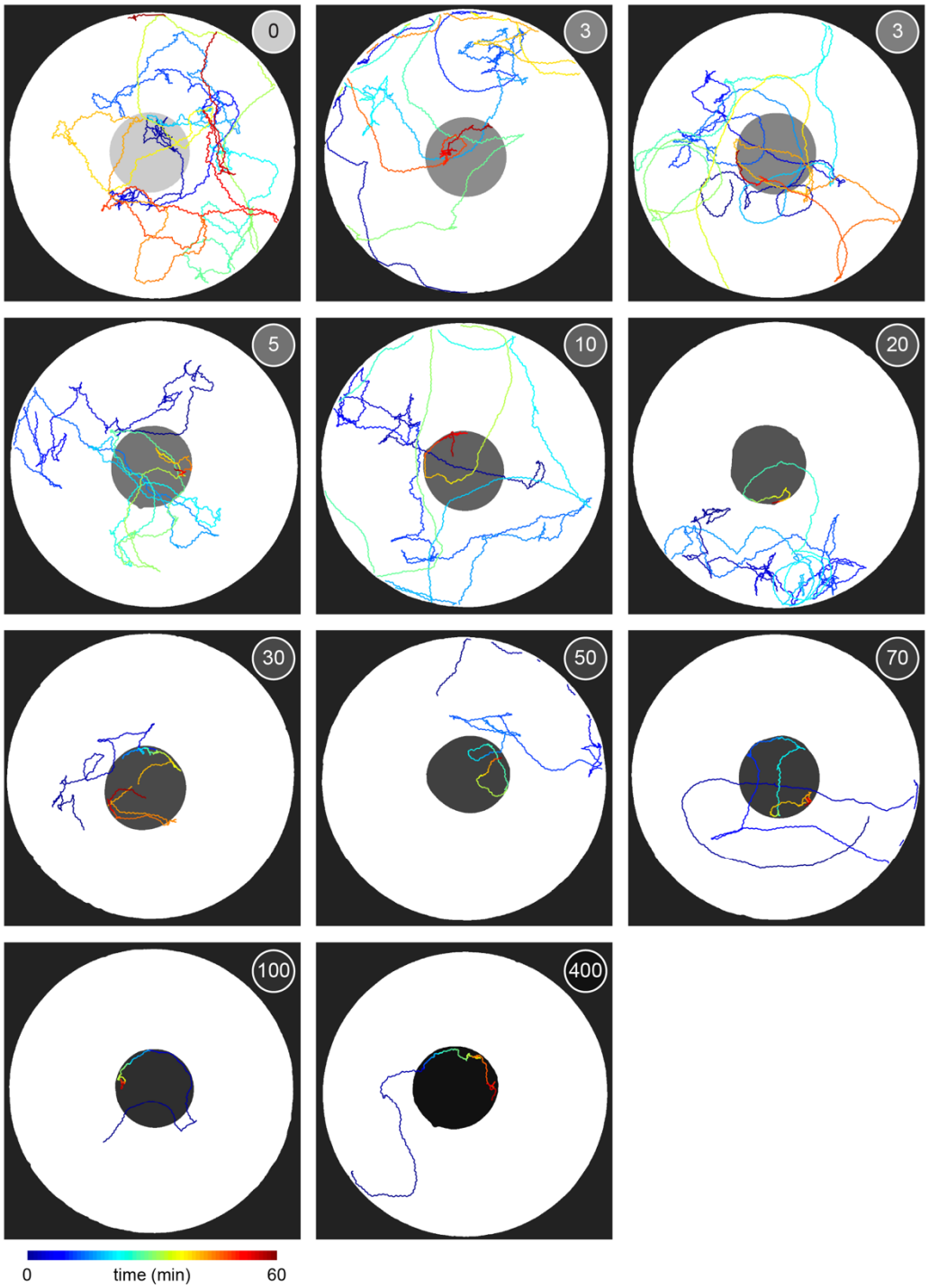

Figure 3 – supplement 2: Example traces of animals foraging in environments with one small bacterial patch.

Example traces showing the midbody location of 6 animals as they forage within a 9 mm arena are plotted with color used to represent time (dark blue = 0 mins; dark red = 60 mins). Location of bacterial patches are indicated in gray. The relative density of bacterial patches in each environment is noted. The animal shown foraging on relative density 10 is the same as that in Figure 2E.

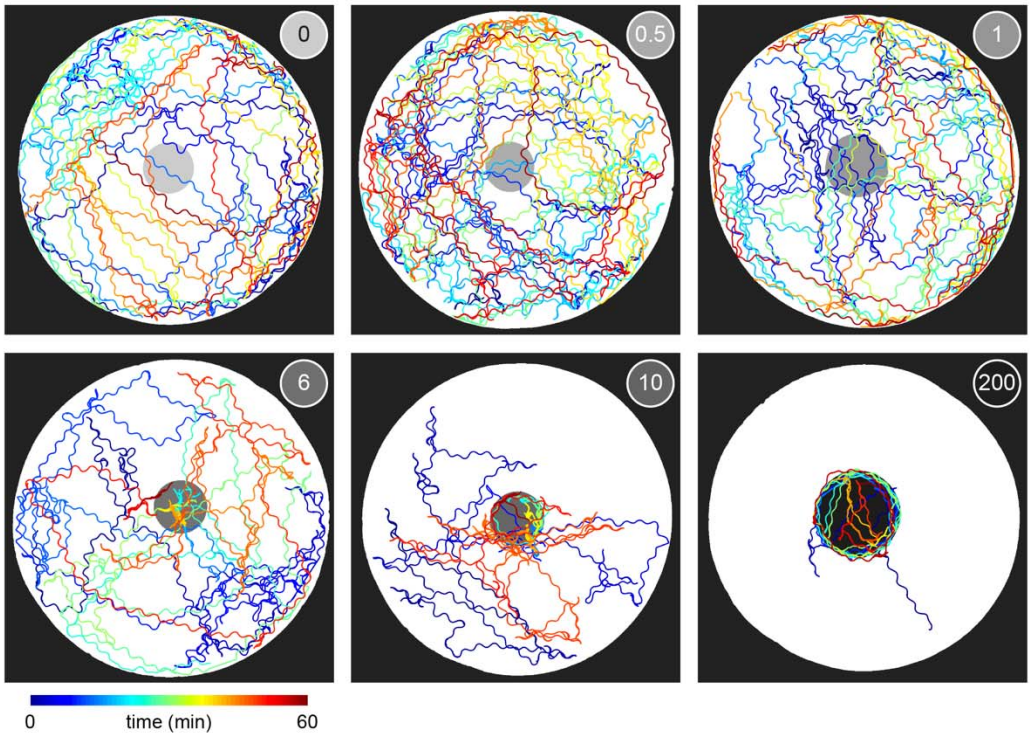

Figure 4 – supplement 1: Model selection for nested GLMs.

(A) Values of log-likehood, Aikake Information Criterion (AIC), and Bayesian Information Criterion (BIC) were computed for 50,000 replicates of the linear regression model described in Models of exploitation probability. The replicate-by-replicate difference in value of these metrics between the full model (i.e., $\boldsymbol{\beta} \cdot \boldsymbol{x}_k = \beta_0 + \beta_k \rho_k + \beta_s \tau_s + \beta_h \rho_h + \beta_e \rho_e$) and every combination of covariate subsets is plotted here. Log-likelihood values less than zero and AIC or BIC values greater than zero indicate worse model performance of the partial term models as compared to the full model. Percentages indicate the proportion of replicates where the model performed best according to that criterion. Even using BIC, the strictest model criterion, the full model performs better than any other model on the majority of replicates. (B) To illustrate the replicate-by-replicate variance, log-likelihood, AIC, and BIC are plotted across all 100 replicates of "encounter samples" (i.e., we removed encounters where the animal likely did not *sense* the encounter $v_k = 0$ as estimated from the distribution $v_k | \boldsymbol{w}_k \sim \mathrm{Bern}\big(p(v_k = 1 | \boldsymbol{w}_k)\big)$) and 500 replicates of hierarchically bootstrapped "worm samples" (i.e., we resampled animals with replacement and included all encounters of the resampled animals). Values for each metric at each replicate are colored to match their respective color bar. Metrics are shown for this subset of models to illustrate the addition of each covariate to the model. Lower AIC and BIC values for the full model (i.e., $\boldsymbol{\beta} \cdot \boldsymbol{x}_k = \beta_0 + \beta_k \rho_k + \beta_s \tau_s + \beta_h \rho_h + \beta_e \rho_e$), represent better model performance even with penalization for increasing the number of parameters. (C) Coefficients $\boldsymbol{\beta}^*$ for the null distribution (i.e., observations of the response variable $p(y_k = 1 | \boldsymbol{z}_k)$ shuffled relative to the covariates $\boldsymbol{x}_k$) are plotted. Only β_0 was significantly greater than or less than 0 (two-tailed, one-sample bootstrap hypothesis tests with Bonferroni correction). These $\boldsymbol{\beta}^*$ represent the null distribution for the $\boldsymbol{\beta}$ in Figure 4C. Violin plots in (A,C) show the KDE and quartiles for each covariate across the 50,000 replicates. Asterisks denote statistical significance (*p<0.05; **p<0.01; ***p<0.001).

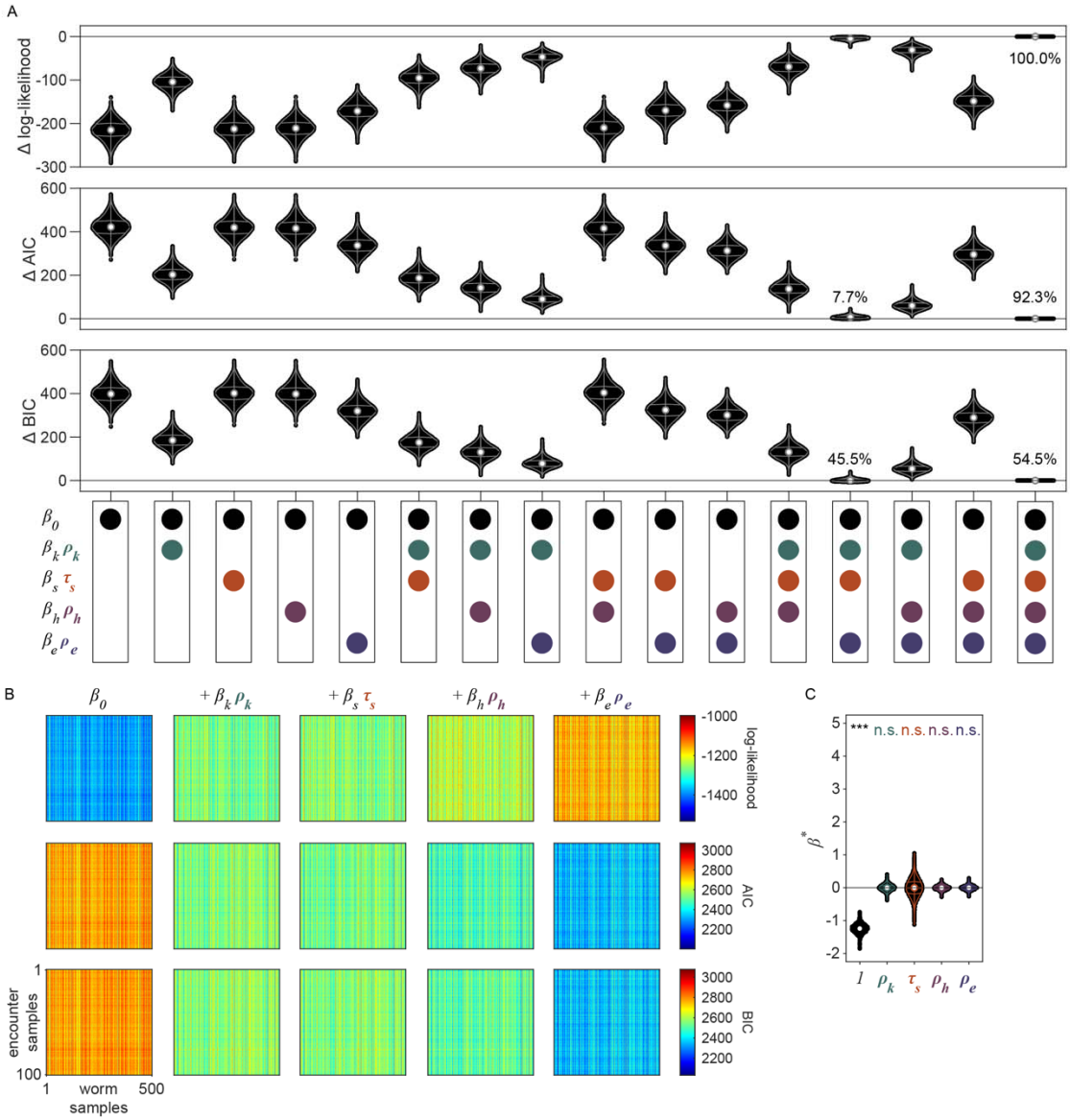
A
Δ log-likelihood
Δ AIC
Δ BIC
100.0%
7.7%
92.3%
45.5%
54.5%
B
log-likelihood
AIC
BIC
encounter samples
worm samples
C
*** n.s. n.s. n.s. n.s.

1844

Figure 4 – supplement 2: Probability of first exploitation as a function of the number of encounters.

Histograms of the probability of first *exploiting* as a function of the number of encounters as estimated by the models and as observed are shown for animals foraging in single-density, multi-patch environments of all 12 density conditions. *Exploitation* events were simulated from a Bernoulli distribution with probability estimated by the model $y_k \,|\boldsymbol{x}_k \sim \mathrm{Bern}\big(p(y_k = 1|\boldsymbol{\beta} \cdot \boldsymbol{x}_k)\big)$ where covariates were added one at time as well as from the observed probabilities estimated by the Gaussian mixture model classification $y_k|\boldsymbol{z}_k \sim \mathrm{Bern}\big(p(y_k = 1|\boldsymbol{z}_k)\big)$ in Figure 2H. Histograms for relative density 1 and 10 are the same as those in Figure 4D.

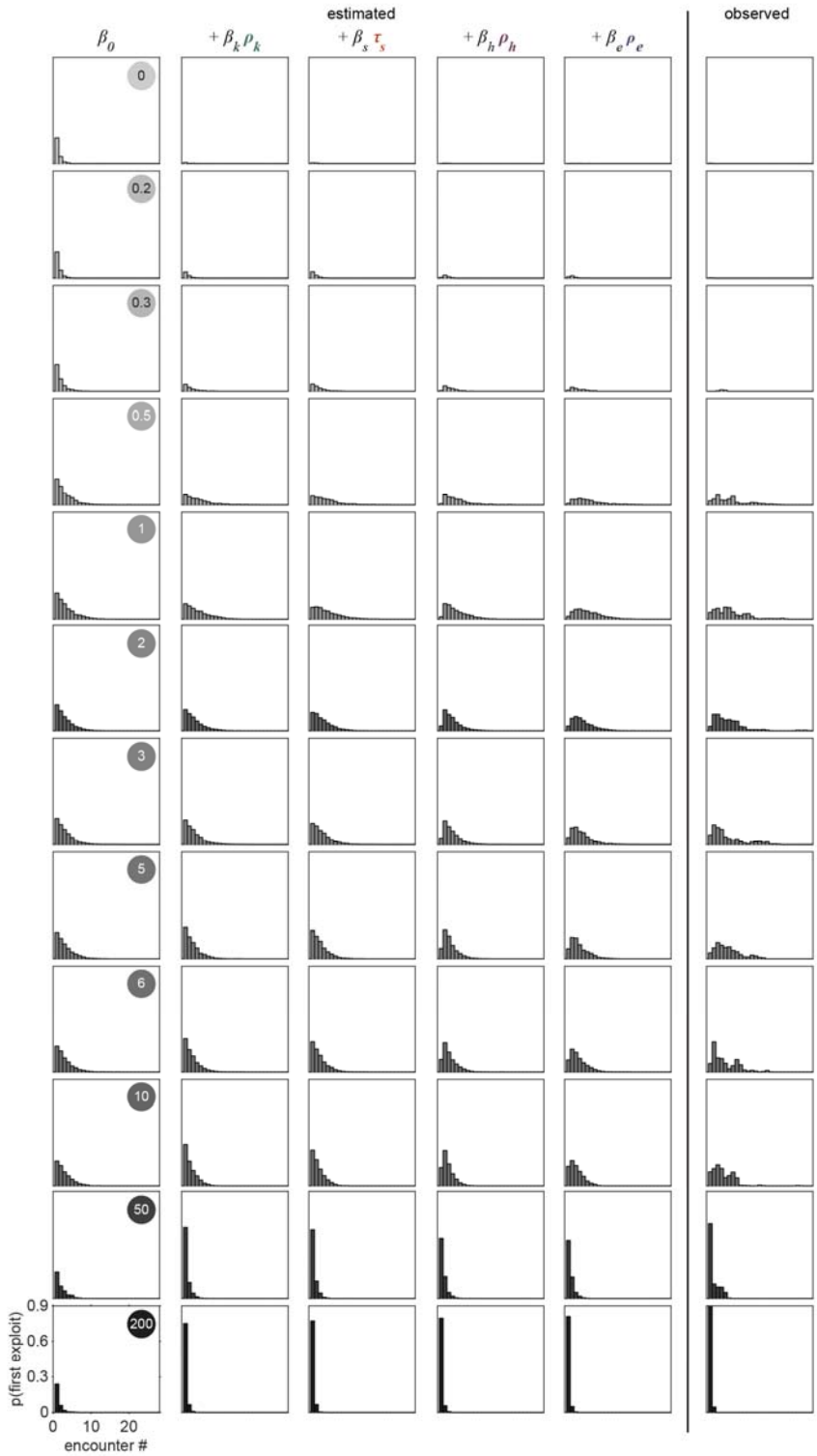
estimated
observed
β_0
$+\beta_k \rho_k$
$+\beta_s \tau_s$
$+\beta_h \rho_h$
$+\beta_e \rho_e$
0
0.2
0.3
0.5
1
2
3
5
6
10
50
200
p(first exploit)
0.9
0.6
0.3
0
0
10
20
encounter #

1855

Figure 4 – supplement 3: Exploitation decision of food-deprived animals is well-predicted by the model.

(A) Schematic of experiments used to test satiety's influence on the decision to *exploit*. As in all experiments, animals were acclimated to high density (relative density ~200) patches for ~24 hours. Well-fed animals were then removed from these acclimation plates, cleaned of bacteria, and then immediately transferred to the assay plate with relative density 5. Food-deprived animals moved about a bacteria-free arena for 3 hours prior to the assay. Examples of animal behavior while foraging in acclimation-like, bacteria-free, and single-density, multi-patch environments of relative density 5 are shown. (B) Patch encounters for 28 food-deprived and 28 well-fed individuals are plotted across time. Each encounter is colored to match its probability of classification as *search* (orange), *sample* (green), and *exploit* (blue). (C) Coefficient values were re-estimated across 50000 replicates as in Figure 4C for a model with the satiety term removed (i.e., $p(y_k = 1|\beta_0 + \beta_k\rho_k + \beta_h\rho_h + \beta_e\rho_e)$). All coefficients are significantly greater than or less than 0 (two-tailed, one-sample bootstrap hypothesis tests with Bonferroni correction; ***p<0.001). Violin plots show the KDE and quartiles for each measure. (D) Histograms of the probability of first *exploiting* as a function of the number of encounters are shown for food-deprived and well-fed animals. Model predictions of *exploitation* events were simulated from a Bernoulli distribution $y_k|\boldsymbol{x}_k \sim \mathrm{Bern}\big(p(y_k = 1|\boldsymbol{\beta}\cdot\boldsymbol{x}_k)\big)$ where the coefficient values $\boldsymbol{\beta}$ corresponded to those previously estimated for our linear regression model with (Figure 4C) and without (Figure 4 – supplement 3C) the satiety term using the data set shown in Figure 2 (i.e., the 443 well-fed animals foraging in one of 12 density conditions). Observed *exploitations* were simulated from a Bernoulli distribution using the probability of *exploitation* estimated by our GMM classifier $y_k|\boldsymbol{z}_k \sim \mathrm{Bern}\big(p(y_k = 1|\boldsymbol{z}_k)\big)$ in Figure 2H. Summary data for all animals (N = 56 total worms; N = 28 worms per condition) and encounters (N = 277 total encounters; N = 42-235 encounters per condition) are shown in (B,D).

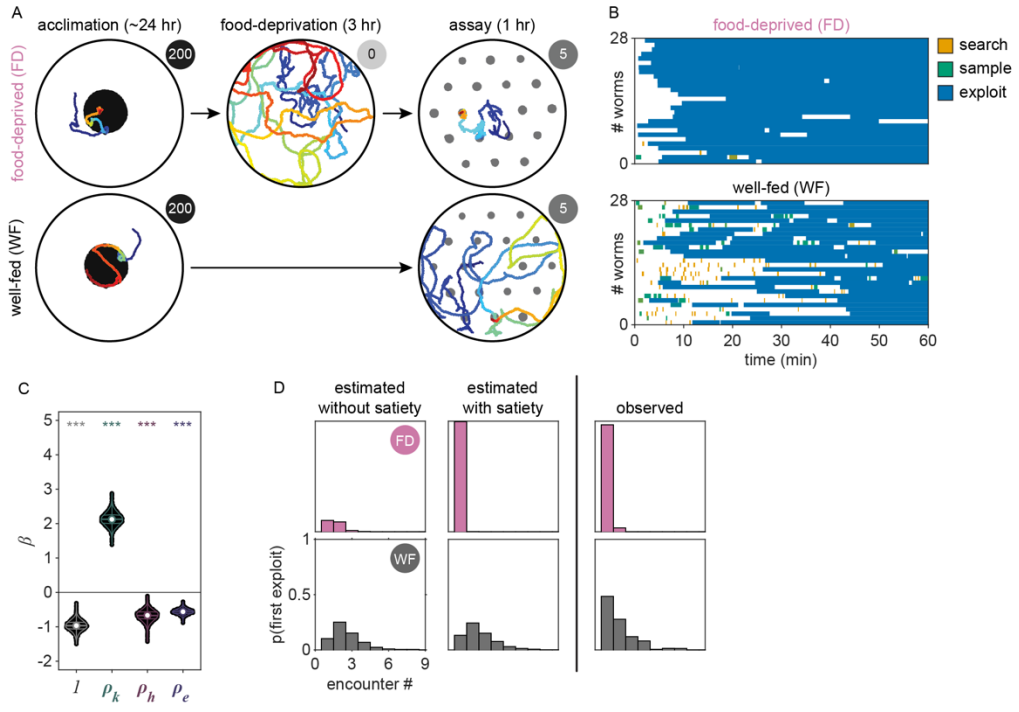

Figure 4 – supplement 4: Example traces and classified behavior of animals foraging in environments with multiple patch densities.

(A) Example traces showing the midbody location of 7 animals as they forage within a 30 mm arena are plotted with color used to represent time (dark blue = 0 mins; dark red = 60 mins). Locations of bacterial patches are indicated in gray with saturation indicating the relative density. Environments contained combinations of patches with relative density 1, 4, and 7 as noted. (B) Patch encounters for 200 individuals (20-40 per condition) are plotted across time. Each encounter is colored to match its relative density. (C) Patch encounters are colored to match their probability of classification as *search* (orange), *sample* (green), and *exploit* (blue). (D) Coefficient values were estimated across 50000 replicates for the multiple density data set for models containing only the satiety-related covariate (i.e., $\boldsymbol{\beta} \cdot \boldsymbol{x}_k = \beta_0 + \beta_k \rho_k + \beta_s \tau_s + \beta_h \rho_h + \beta_e \rho_e$), only the transfer-related covariate (i.e., $\boldsymbol{\beta} \cdot \boldsymbol{x}_k = \beta_0 + \beta_k \rho_k + \beta_t \tau_t + \beta_h \rho_h + \beta_e \rho_e$), and for both the satiety and transfer covariates (i.e., $\boldsymbol{\beta} \cdot \boldsymbol{x}_k = \beta_0 + \beta_k \rho_k + \beta_s \tau_s + \beta_t \tau_t + \beta_h \rho_h + \beta_e \rho_e$). All coefficients are significantly greater than or less than 0 (two-tailed, one-sample bootstrap hypothesis tests with Bonferroni correction) with the exception of β_t in the satiety and transfer model. (E) Coefficient values were re-estimated across 50000 replicates for the original single density data set as in Figure 4C for a model with the history-dependent terms removed (i.e., $p(y_k = 1 | \beta_0 + \beta_k \rho_k + \beta_s \tau_s)$). All coefficients are significantly greater than or less than 0 (two-tailed, one-sample bootstrap hypothesis tests with Bonferroni correction; **p<0.01; ***p<0.001). Violin plots show the KDE and quartiles for each measure. Summary data for all animals (N = 198 total worms; N = 20-40 worms per condition) and encounters (N = 3,493 total encounters; N = 282-795 encounters per condition) are shown in (B,C).

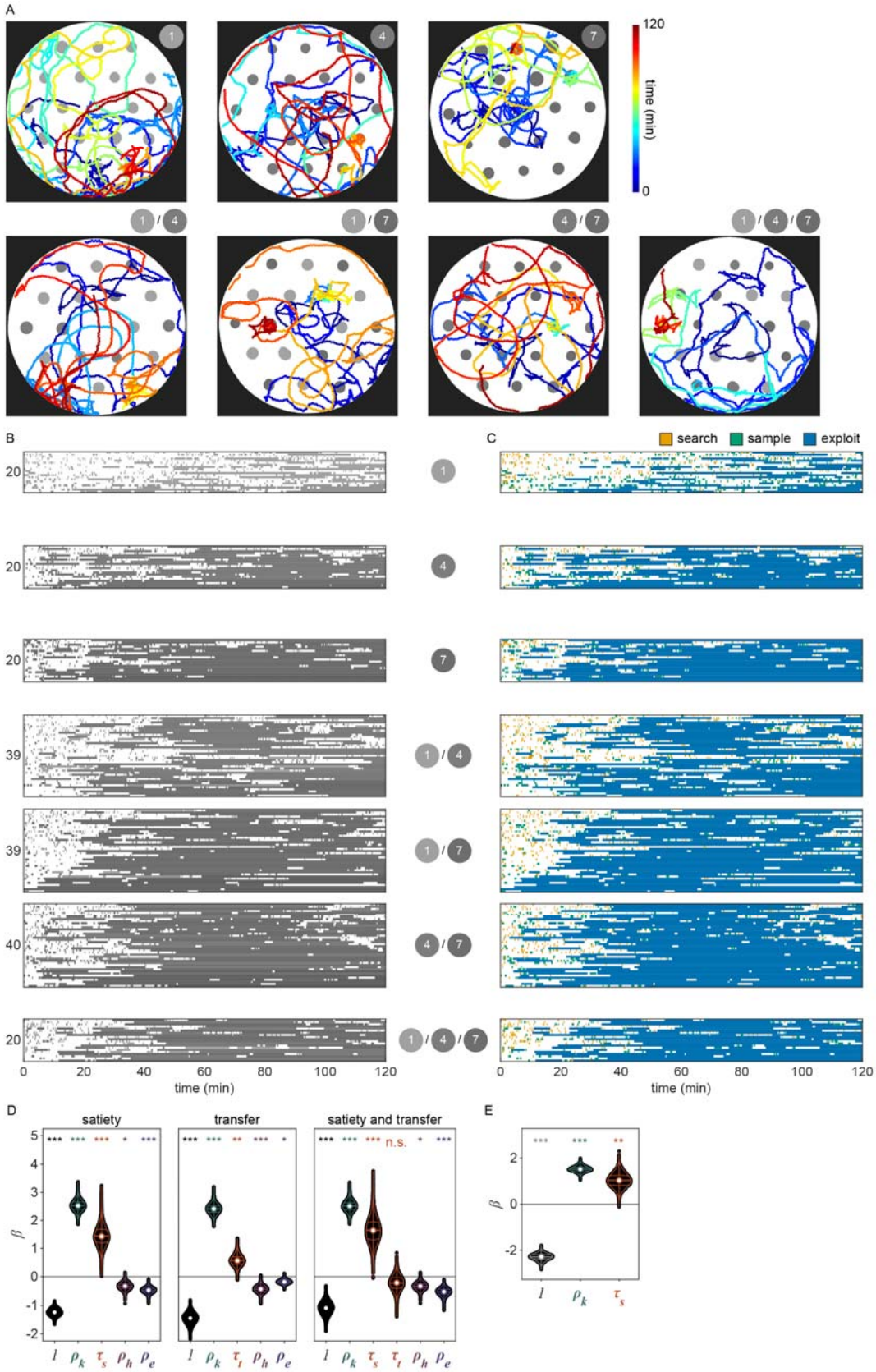
A
120
time (min)
0
B
C
search
sample
exploit
time (min)
D
satiety
transfer
satiety and transfer
n.s.
E

1905

Figure 4 – supplement 5: Example traces and classified behavior of animals with chemosensory or mechanosensory deficiencies.

(A) Example traces showing the midbody location of 9 animals as they forage within a 30 mm arena are plotted with color used to represent time (dark blue = 0 mins; dark red = 60 mins). Location of bacterial patches are indicated in gray. The relative density of bacterial patches in each environment is noted. 3 strains of *C. elegans* were tested (grey = N2, pink = *mec-4*, orange = *osm-6*) across 3 conditions of relative density (1, 5, and 10). (B) Patch encounters for 76 individuals (16-44 per density condition) of each strain are plotted across time. Each encounter is colored to match its probability of classification as *search* (orange), *sample* (green), and *exploit* (blue). (C) Histograms of the probability of first *exploiting* as a function of the number of encounters are shown for each strain and density condition. Observed *exploitations* were simulated from a Bernoulli distribution using the posterior probability of *exploitation* defined by our GMM classifier $y_k|\boldsymbol{z}_k \sim Bern\big(p(y_k = 1|\boldsymbol{z}_k)\big)$ in Figure 2H. Histograms of each strain for relative density conditions 1 and 10 are the same as those in Figure 4G. (D) Coefficients $\boldsymbol{\beta}^*$ for the null distribution (i.e., observations of the response variable $p(y_k = 1|\boldsymbol{z}_k)$ were shuffled relative to the covariates $\boldsymbol{x}_k$) are plotted. Violin plots show the KDE and quartiles for each covariate across the 50,000 replicates. These $\boldsymbol{\beta}^*$ represent the null distribution for the $\boldsymbol{\beta}$ in Figure 4H. (E) The ridge regression parameter λ was optimized for each strain to maximize the mean log-likelihood of the model. Summary data for all animals (N = 221 total worms; N = 14-44 worms per condition) and encounters (N = 1,352 total encounters; N = 27-193 encounters per condition) are shown in (B,C).

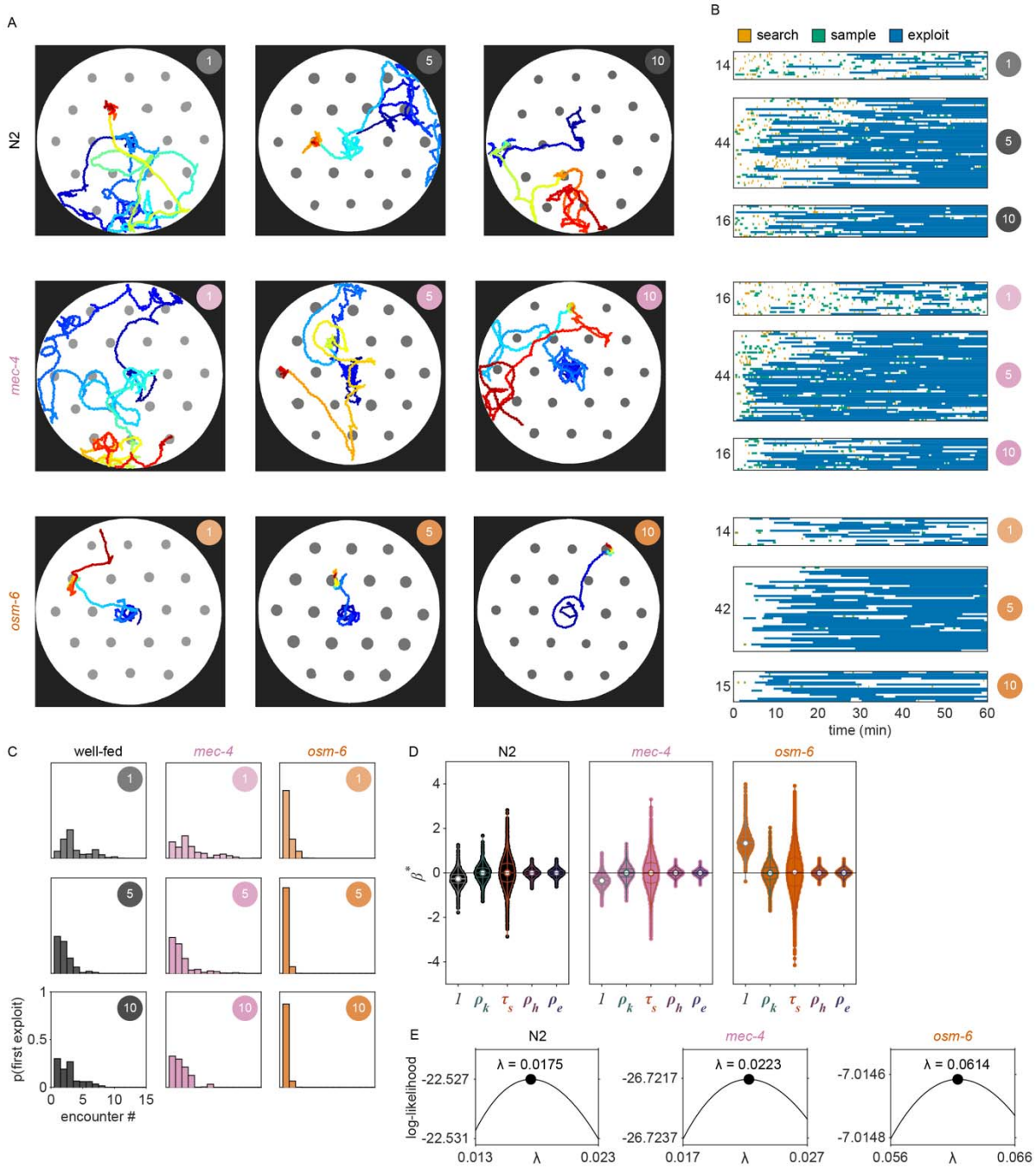
A
N2
mec-4
osm-6
B
search
sample
exploit
time (min)
C
well-fed
mec-4
osm-6
p(first exploit)
encounter #
D
N2
mec-4
osm-6
E
N2
mec-4
osm-6
log-likelihood
λ = 0.0175
λ = 0.0223
λ = 0.0614

Video Legends

Video 1. *C. elegans* foraging in a patchily distributed environment.
Four adult *C. elegans* forage for one hour in a 30 mm arena containing an isometric grid of small, low density bacterial patches.

Video 2. Visualizing dilute bacterial patches using diffraction of light.
A piece of dark cardstock passed between the light source and the assay plate enables visualization of dilute bacterial patches.

Video 3. Tracking the midbody location of an animal foraging in a patchily distributed environment.
The midbody location of one of the four animals shown in Video 1 is shown as the animal forages for one hour in a 30 mm arena containing an isometric grid of small, low density bacterial patches. The animal shown corresponds to the example animal observed in Figure 1A-B,H-K.

Video 4. Tracking the entire body of a foraging animal.
The position of the entire body of an animal is shown as the animal forages for one hour in a 9 mm arena containing one small, low density bacterial patch. The head is indicated by a small dot. The animal shown corresponds to the example animal observed in Figure 3D.

Video 5. Classifying encounters as *sensing* based on quantification of slow-down.
Three metrics quantifying the magnitude of slow-down upon patch encounter were computed. A semi-self-supervised quadratic discriminant analysis was trained on a subset of labeled data and used to classify all encounters as *sensing* (green) or *non-responding* (orange). Data correspond with Figure 2I and Figure 2 – supplement 8A-C.

Video 6. Foraging behavior of an animal with encounters labeled as *search*, *sample*, or *exploit*.
The midbody location of the animal in Video 3 is shown and labeled by the probability of classification as *searching* (i.e., off patch *exploration* and patch encounters lacking a slow-down response), *sampling* (i.e., patch encounters that were *sensed*, but not *exploited*), and *exploiting* at every time point. The animal shown corresponds to the example animal observed in Figure 1A-B,H-K.

Source Data Files

Figure 1 – source data 1. Number of total and unique patch encounters in Figure 1D.

Figure 1 – source data 2. Duration of patch encounters in Figure 1E.

Figure 1 – source data 3. Start time of patch encounters in Figure 1F.

Figure 1 – source data 4. On patch residence in Figure 1G.

Figure 1 – source data 5. Velocity of animals upon encounter with patch edge in Figure 1L.

Figure 1 – source data 6. Deceleration of animals upon encounter with patch edge in Figure 1M.

Figure 1 – source data 7. Velocity of animals upon encounter with patch edge in Figure 1N.

Figure 1 – source data 8. Velocity on and off patch in Figure 1O.

Figure 2 – source data 1. Relative density of bacterial patches in each condition in Figure 2A.

Figure 2 – source data 2. Velocity of animals upon encounter with patch edge in Figure 2B.

Figure 2 – source data 3. Velocity on patch in Figure 2C.

Figure 2 – source data 4. Time on patch in Figure 2E.

Figure 2 – source data 5. On patch residence in Figure 2F.

Figure 2 – source data 6. Duration of patch encounters in Figure 2G.

Figure 2 – source data 7. Encounter classification as explore or exploit using a Gaussian Mixture Model (GMM) in Figure 2H.

Figure 2 – source data 8. Encounter classification as sense or no response using semi-supervised Quadratic Discriminant Analysis (QDA) in Figure 2I.

Figure 2 – source data 9. Velocity during search, sample, and exploit behaviors in Figure 2K.

Figure 2 – source data 10. Encounter classification as explore or exploit and sense or no response in Figure 2L.

Figure 2 – source data 11. Probability of an encounter type over time in Figure 2M.

Figure 2 – source data 12. Time before first exploitation in Figure 2N.

Figure 2 – source data 13. Number of encounters before first exploitation in Figure 2O.

Figure 3 – source data 1. Relative density of large (20 μL) bacterial patches in Figure 3A.

Figure 3 – source data 2. Relative density of small (0.5 μL) bacterial patches in Figure 3B.

Figure 3 – source data 3. Encounter classification as explore or exploit and sense or no response in Figure 3F.

Figure 3 – source data 4. Encounter classification as explore or exploit and sense or no response in Figure 3G.

Figure 3 – source data 5. Time before first exploitation in Figure 3H.

Figure 3 – source data 6. Time before first exploitation in Figure 3I.

Figure 4 – source data 1. Coefficients of linear regression model in Figure 4C.

Figure 4 – source data 2. Probability of exploitation occuring for the first time as a function of the number of encounters in Figure 4D.

Figure 4 – source data 3. Observed and predicted (with and without history-dependence) posterior probabilities of exploitation in Figure 4F.

Figure 4 – source data 4. Probability of exploitation occurring for the first time as a function of the number of encounters for animals with sensory mutations in Figure 4G.

Figure 4 – source data 5. Coefficients of linear regression model in Figure 4H.